END-OF-LIFE MATERIALS BASED LIGHTWEIGHT GEOPOLYMER MORTARS SUITABLE FOR ADDITIVE MANUFACTURING

EKLEMELİ İMALATA UYGUN ÖMRÜNÜ TAMAMLAMIŞ MALZEME BAZLI HAFİF JEOPOLİMER BAĞLAYICILI HARÇLAR

MEHMET ÖZKAN EKİNCİ

PROF. DR. MUSTAFA ŞAHMARAN

Supervisor

Submitted to

Graduate School of Science and Engineering of Hacettepe University

as a Partial Fulfillment to the Requirements

for be Award of the Degree of Master of Science

in Civil Engineering

2023

ABSTRACT

END-OF-LIFE MATERIALS BASED LIGHTWEIGHT GEOPOLYMER MORTARS SUITABLE FOR ADDITIVE MANUFACTURING

Mehmet Özkan EKİNCİ

Master of Science, Department of Civil Engineering

Supervisor: Prof. Dr. Mustafa ŞAHMARAN

July 2023, 114 pages

Traditional Portland cement is extensively employed in the building industry to satisfy the housing and transportation need of the rising human population. However, the production of Portland cement contributes to greenhouse gasses released into the atmosphere, accounting for 5-7% of global CO_2 emissions. The development of a sustainable, low-carbon, and eco-friendly binder, namely geopolymer as an alternative to Portland cement is essential to ensure a sustainable built environment. Furthermore, the reuse of end-of-life materials is of vital importance for the construction of a sustainable future and the transition to a circular economy. Approximately 800 million tons of construction waste is generated annually in Europe. The employment of generated end-of-life construction and demolition waste in the production of "green" geopolymer binders is considered to be a viable methodology to minimize multiple environmental impacts sourced from CO_2 emissions and ineffective disposal of end-of-life materials. Similarly, insulative construction materials play a crucial role in modern sustainable building design and construction. The main attribute of these construction materials is providing thermal insulation, which is essential for maintaining comfortable indoor temperatures and reducing energy consumption resulting in significant energy savings

and reduced environmental impact. 40% of the global energy consumption is attributed to buildings. Lightweight aggregates are broadly used in the development of thermal insulative, low-density, lightweight, and energy-efficient construction materials. Another important point in the construction sector is the automation of the construction processes. 3-dimensional (3D) additive manufacturing technology is an emergent innovative automation system in the construction industry providing faster construction, reduced material waste, low energy use, and cost savings compared to traditional construction methods. The layer-by-layer production technique of 3D additive manufacturing technology enables design freedom for complex structures. With the widespread use of 3D-printing technology in the construction industry, safe and uniquely designed structures can be built without the use of formworks in a more economical, faster, and reliable way.

The aim of this thesis is to develop end-of-life materials-based lightweight geopolymer mortars suitable for additive manufacturing. An entirely end-of-life construction demolition waste-based alkali-activated lightweight insulative geopolymer mortars are produced for 3D printing applications in this study. The fresh state open-time rheological properties, fresh and dry densities, mechanical properties at 7, 14, and 28 days, thermal insulation properties, as well as elevated temperature resistance of geopolymer mortars were determined. Finally, 3D-printing performance and the 3D-printing quality of the mortars were visually assessed. As a result, it is believed that developed geopolymer mortars will offer an innovative, viable, sustainable, and green solution to the multiple issues confronted in the construction industry, such as greenhouse gas emissions, management of construction and demolition wastes, high construction costs and thermal energy loss in buildings.

Keywords: End-of-life Material, Construction and Demolition Waste, Geopolymer, Lightweight Mortar, Thermal Insulation, Additive Manufacturing, 3D Printing

ÖZET

EKLEMELİ İMALATA UYGUN ÖMRÜNÜ TAMAMLAMIŞ MALZEME BAZLI HAFİF JEOPOLİMER BAĞLAYICILI HARÇLAR

Mehmet Özkan EKİNCİ

Yüksek Lisans, İnşaat Mühendisliği Bölümü

Tez Danışmanı: Prof. Dr. Mustafa ŞAHMARAN

Temmuz 2023, 114 sayfa

Geleneksel Portland çimentosu, artan insan nüfusunun konut ve ulaşım ihtiyacını karşılamak amacıyla inşaat sektöründe yaygın olarak kullanılmaktadır. Fakat, Portland çimentosu üretimi atmosfere sera gazı salınımına sebep olarak küresel CO_2 emisyonlarının %5-7'sinden sorumludur. Portland çimentosuna alternatif olarak sürdürülebilir, düşük karbonlu ve çevre dostu bir bağlayıcının, yani jeopolimerlerin geliştirilmesi, sürdürülebilir yapılı bir çevre sağlamak için çok önemlidir. Ayrıca ömrünü tamamlamış malzemelerin yeniden kullanılması, sürdürülebilir bir geleceğin inşası ve döngüsel ekonomiye geçiş için hayati önem taşımaktadır. Avrupa'da yılda yaklaşık 800 milyon ton inşaat yıkıntı atığı oluşmaktadır. "Yeşil" jeopolimer bağlayıcıların üretiminde ömrünü tamamlamış inşaat yıkıntı atıklarının kullanılması, CO_2 emisyonlarından ve ömrünü tamamlamış malzemelerin efektif olmayan şekilde bertaraf edilmesinden kaynaklanan birçok çevresel etkiyi en aza indirmek için geçerli bir metodoloji olarak kabul edilmektedir. Ayrıca, yalıtkan yapı malzemeleri de modern ve sürdürülebilir yapıların tasarımı ve inşasında çok önemli bir rol oynamaktadır. Bu yapı malzemelerinin temel özelliği, konforlu iç mekân sıcaklıklarını korumak için gerekli olan ısı yalıtımı sağlayarak enerji tüketimini azaltmaktır. Bu sayede önemli ölçüde enerji tasarrufuyla

beraber çevresel etkilerin azalmasını sağlar. Küresel enerjinin %40'ı binalar tarafından kullanılmaktadır. Hafif agregalar; yalıtkan, düşük yoğunluklu, hafif ve enerji tasarrufu sağlayan yapı malzemelerinin üretilmesinde yaygın olarak kullanılmaktadır. İnşaat sektöründe bir diğer önemli nokta ise inşa süreçlerinin otomasyonudur. İnşaat sektöründe gelişen 3 boyutlu (3B) eklemeli imalat teknolojisi, geleneksel inşaat yöntemlerine kıyasla daha hızlı inşa, daha az malzeme israfı, düşük enerji kullanımı ve maliyet tasarrufu sağlayan yenilikçi bir otomasyon sistemidir. 3B eklemeli imalat teknolojisinin katman katman üretim tekniği, karmaşık yapılar için tasarım özgürlüğü sağlar. 3B baskılama teknolojisinin inşaat sektöründe yaygınlaşması ile güvenli ve özgün tasarımlı yapılar, kalıp kullanılmadan daha ekonomik, hızlı ve güvenilir bir şekilde inşa edilebilmektedir.

Bu tezin amacı, eklemeli imalata uygun ömrünü tamamlamış malzeme bazlı hafif jeopolimer bağlayıcılı harçlar geliştirmektir. Bu çalışmada 3B baskılama uygulamalarında kullanılabilir, tamamıyla ömrünü tamamlamış inşaat yıkıntı atığı bazlı, alkali aktive edilmiş, hafif ve yalıtkan jeopolimer harçlar üretilmiştir. Jeopolimer harçların taze hal açık zaman reolojik özellikleri, taze ve kuru yoğunlukları, 7, 14 ve 28 günlük mekanik özellikleri, ısı yalıtım özellikleri ve yüksek sıcaklık dayanımları belirlenmiştir. En sonunda, harçların 3B baskılanma performansı ve 3B baskı kalitesi de görsel olarak değerlendirilmiştir. Sonuç olarak, geliştirilen jeopolimer bağlayıcılı harçların, sera gazı emisyonları, inşaat ve yıkıntı atıklarının yönetimi, yüksek inşaat maliyetleri ve binalarda ısıl enerji kaybı gibi inşaat sektöründe karşılaşılan birçok soruna yenilikçi, uygulanabilir, sürdürülebilir ve yeşil bir çözüm sunacağına inanılmaktadır.

Anahtar Kelimeler: Ömrünü Tamamlamış Malzeme, İnşaat ve Yıkıntı Atığı, Jeopolimer, Hafif Harç, Isı Yalıtımı, Eklemeli İmalat, 3B Baskılama

ACKNOWLEDGEMENT

First and foremost, I would like to express my deep gratitude to my esteemed advisor, Prof. Dr. Mustafa ŞAHMARAN. Without his inspiration, motivation, guidance, knowledge, and most importantly holistic support, this study would not have been possible.

Secondly, I would like to thank my thesis committee members Prof. Dr. İlhami DEMİR, Assoc. Prof. Dr. Gürkan YILDIRIM, Assoc. Prof. Dr. Mustafa Kerem KOÇKAR, Asst. Prof. Dr. Hüseyin ULUGÖL provided me with the opportunity to defend my thesis and insightful comments.

I am sincerely grateful for the academic assistance and intellectual support of Anıl KUL, Hüseyin İLCAN, Emircan ÖZÇELİKCİ, and Oğuzhan ŞAHİN. Also, I would like to thank my colleagues in the Civil Engineering Department, Nazım Çağatay DEMİRAL, Utku BELENDİR, Eray TEKSİN, Furkan KARA, and Atakan OSKAY as well as Yakup KUŞ and Mehmet Burak UZUN for their genuine friendship and support in laboratory studies.

The author gratefully acknowledges the financial assistance of the Scientific and Technical Research Council (TUBITAK) of Turkey provided under Project: 119N030.

Finally, I would like to extend my deep gratitude to my beloved father, mother, and sister. Without their encouragement and support in all of my pursuits, I would not succeed. I always knew that you had endless belief in me and wanted the best for me throughout my life.

MEHMET ÖZKAN EKİNCİ

July 2023, Ankara

TABLE OF CONTENTS

LIST OF TABLES

LIST OF FIGURES

1. INTRODUCTION

1.1 General

The increasing global population has led to a growing demand for heating and cooling in buildings, resulting in a significant rise in energy consumption. Therefore, the importance of thermal insulation properties of building materials has become essential in the modern construction industry, as they play a vital role in creating thermally comfortable, sustainable, and energy-efficient buildings. The residential buildings account for a sizeable amount of the world's electrical consumption, while climate control systems account for about 60% of the overall demand. Around 40% of the annual global energy usage is attributed to buildings [1]. Additionally, the energy needed to power climate control systems generate a significant quantity of emissions into the atmosphere. The low thermal resistance of buildings caused by their limited thermal energy storage capacity, which results in thermal exchange between the ambient and enclosure of the building elements is one of the primary causes of the high energy consumption in building climate control activities [2]. It is difficult to achieve sustainable climate control due to the large energy loss through the building components in structures, which greatly raises energy consumption. Insulation materials are highly effective in reducing heat loss in buildings. These insulation materials significantly reduce the requirement for continuous heating using fossil fuels or natural gas and cooling operations using air conditioning systems in such buildings, hence, provide energy efficiency. The utilization of thermal insulative building materials enables the construction of environmentally friendly residential, commercial, and public buildings that consume less energy while ensuring indoor comfort.

It is considered unsustainable for the construction sector to continue depending on traditional techniques in a world characterized by significant developments in industries. Conventional manufacturing methods fall short in terms of efficiency, safety, and cost-effectiveness. By adopting automation, the construction industry has the potential to implement sustainable, innovative, safe, and cost-efficient manufacturing methods [3]. In the present state of the industry, numerous initiatives have the potential to take the place of outdated production methods. The implementation of 3-dimensional additive manufacturing (3D-AM) has been a significant advancement in the construction industry,

facilitating the integration of automation technologies. One of the best alternatives to automation in this industry is 3D-AM, reduces errors in traditional applications, lowers labor costs, speeds up manufacturing, lowers the risk of work accidents, and eliminates the need for formwork [4–6]. 3D-AM offers the potential to create innovative and sustainable structures while achieving cost and time efficiency. A previous study indicated that 3D-AM could potentially reduce construction completion time by 50-70%, material waste by 30-60%, and labor costs by 50-70% [7]. Based on another study, formwork contributes to approximately 33% of the overall costs and accounts for 50% of the completion time in construction projects [6]. By implementing additive manufacturing techniques and eliminating the requirement for traditional formwork technologies, labor costs can be reduced by up to 80% [8,9]. Furthermore, the adoption of these innovative methods decreases construction time from 35% to 60% [6,10,11]. Furthermore, the types of designs constrained by conventional techniques are considerably broadened by 3D-AM. The 3D-AM enables manufacture without formwork, allowing architectural concepts to go beyond the limits of current structures. The widespread use of 3D-AM in buildings is also expected to result in significant post-production carbon dioxide (CO_2) emissions reductions due to the factors like 30% less waste material, minimized energy use, in-situ manufacturing, and fewer resource requirements with freedom of design. [12–14]. Given the numerous benefits listed, 3D-AM can be crucial in the development of emergent and sustainable construction solutions.

The growth of the global population and the rapid pace of urbanization have led to a significant rise in the generation of construction and demolition waste (CDW) arising from various urban development works such as restoration, reconstruction, and demolition. Concrete, roof tiles and bricks and glasses are some of well-known CDW materials. Annual CDW produced by Europe (EU28) is around 800 million tons [15–17]. 45 million tons of CDW are produced annually in Turkey [18]. By the year 2050, it is predicted that the amount of CDW produced by the global construction sector will climb from 12.7 billion tons in 2000 to 27 billion tons [19]. Natural catastrophes like earthquakes, storms, or fires can cause significant structural damage or complete destruction. In these circumstances, CDW is produced and dispersed throughout the impacted region. The 7.3-magnitude Kahramanmaraş earthquake that hit Turkey in 2023 caused a large quantity of CDW, which is predicted to be between 450 and 920 million

tons [20]. Nevertheless, only approximately 20 to 30% of end-of-life CDW is recovered globally, huge part of the CDW is disposed of primarily in landfills [21].

Portland cement is extensively employed in the building industry due to its superior durability and strength. Nevertheless, the production of Portland cement contributes to greenhouse gasses released into the atmosphere, as it accounts for 5-7% of global CO_2 emissions [22,23]. The release of enormous amounts of greenhouse gases during the manufacturing process has negative implications for the environment. In light of these environmental challenges, there is a growing interest in alternative binders that can serve as an alternative to Portland cement. One promising alternative is geopolymer binders, which are known for their numerous environmental benefits [24]. Geopolymer binders are produced through the chemical reaction of aluminosilicate-based materials, such as mostly blast furnace slag (GGFBS) and fly ash (FA), with alkali activators including sodium silicate (Na_2SiO_3), sodium hydroxide (NaOH), potassium hydroxide (KOH) and calcium hydroxide ($Ca(OH)_2$). However, in the past decade, there has been a significant advancement in utilizing CDW-based materials for geopolymer production. Utilization of end-of-life CDW in the production of geopolymer binders enables effective upcycling of CDW materials which is a crucial environmental issue across the world. Incorporating CDW as a raw material in geopolymer systems contributes to establishing a circular economy by promoting resource efficiency and waste reduction. Besides, geopolymer binders and Portland cement exhibit comparable characteristics such as high strength and durability [25–28]. By reducing the reliance on Portland cement and its associated CO_2 emissions, the utilization of geopolymer binders can contribute to the development of a more environmentally friendly and sustainable built environment.

Modern building techniques have become increasingly dependent on lightweight building materials, which provide plenty of benefits and handle key industry difficulties. Lightweight mortars, which are possibly produced by utilizing lightweight aggregates are mostly known for their low density. The importance of lightweight mortars originates from their capacity to enable quicker building processes, lower material transportation costs, and minimize the stress on foundations and load-bearing components by decreasing the overall dead load of structures [29,30]. Reducing the mass of a structure not only decreases its overall weight but also lessens the potential risks of earthquake-induced damages. This is explained by the fact that the forces exerted by earthquakes on structures

and buildings are directly related to their mass. Thereby structural resilience of the buildings can be improved by reducing the earthquake proneness of the structures [31]. Another advantage of low-density lightweight mortars is high thermal insulation properties that are preventing the transfer of heat, reduce the energy consumption for heating and cooling systems, and enhance occupant comfort [32]. Buildings can achieve optimal energy performance, minimize their ecological impacts, and improve their sustainability through the utilization of lightweight mortars.

1.2 Research Objectives and Scope

The main objective of this thesis is to develop 3D printable lightweight CDW-based thermal insulative geopolymer mortars. Within this scope, an entirely end-of-life CDW-based green geopolymer binder is produced by alkali-activating red clay brick (RCB), hollow brick (HB), roof tile (RT), concrete (C), and glass (G). The produced geopolymer binder serves as a substitute for Portland cement, aiming to minimize greenhouse gas emissions linked to Portland cement production while simultaneously reducing the environmental impacts of CDW and enhancing resource efficiency through the upcycling of CDWs. Geopolymer mortar mixtures were produced by adding recycled concrete aggregate (RCA) and lightweight, porous expanded perlite aggregate (EPA) to the developed alkali-activated geopolymer binder containing 100% CDW. Lightweight, low thermal conductivity 3D printable geopolymer mortars were developed by replacing the RCA in the mortar mixture with EPA.

The developed 3D printable lightweight geopolymer mortars underwent tests to determine their fresh state open-time rheological properties, fresh state and dry densities, mechanical properties, thermal insulation properties, and resistance to elevated temperatures. The selected mixtures among the developed geopolymer mortars were used in laboratory-scale 3D printing trials, and the printing quality of the mixtures with different characteristics was assessed visually. The thermal conductivity coefficients of molded and 3D printed thermal plates created from the geopolymer mortar with the lowest density were compared as well to uncover additional insights into the effect of the 3D printing technique on the thermal insulation capability of thermal plates.

The green, innovative and applicable objectives that the study aims to reach are listed below:

- Developing a cutting-edge, green, and eco-friendly geopolymer binder that can be used as an alternative to Portland cement, which uses fossil fuels and generates significant amounts of CO_2 during its production.

- Minimizing the environmental impact caused by CDWs such as RCB, HB, RT, C, and G through upcycling in 100% CDW-based geopolymer binder production and contributing to sustainable development.

- Producing 3D printable low thermal conductivity lightweight geopolymer mortars by utilizing low-density and porous aggregates.

- Determining the fresh state open-time rheological properties, fresh state and dry densities, mechanical properties at various ages, thermal insulation properties, and elevated temperature resistance of developed lightweight geopolymer mortars.

- 3D printing demonstrations and visual investigations of printing quality of selected lightweight geopolymer mortars as well as examining the effect of 3D printing technique on thermal insulation.

1.3 Thesis Outline

The thesis is divided into five chapters. Contents covered in each chapter are as follows:

An overview of the present situation is given in the first chapter, "Introduction," which is followed by a thorough description of the identified challenges and why their solutions are essential.

The second chapter, "Literature Review," first provides a broad overview of the mechanism of geopolymer binders before delving into the evolvement of 3D-AM technology throughout history. Then the chapter goes into more detail on the development of 3D-AM in the construction sector, outlining its present state and going through the benefits it provides. This chapter also discusses the application of geopolymers combined with 3D-AM technology and studies on geopolymers as insulation materials in academic literature.

In the third chapter, "Materials and Methodology," particular details are provided regarding the precursor materials and aggregates utilized in the production of geopolymer mortar, including their oxide compositions and crystal structures. Additionally, the geopolymer mortar mixing ratios, mixture preparation, curing conditions, and the production of test specimens are covered. Comprehensive information about the tests that were carried out on samples are provided.

The fourth chapter of the thesis focuses on the discussion of applied flow table and buildability tests for fresh-state rheological properties, compressive and flexural strength tests for mechanical properties at various ages, thermal conductivity tests for thermal insulation characteristics, and elevated temperature resistance tests on developed entirely CDW-based 3D printable lightweight thermal insulative geopolymer mortars. Assessment of the printing quality of the chosen mixtures by visual inspections is also discussed. In addition, the 3D printed plate is compared with the conventionally molded plate in terms of thermal insulation performance.

In the concluding chapter of the study, the results and findings with explanations are succinctly reported.

2. LITERATURE RESEARCH

This section provides a detailed literature review and research about the subtopics that are in parallel with the scope of this thesis.

2.1 Geopolymerization Mechanism

A synthetic alkali aluminosilicate known as a "geopolymer," named after Davidovits, is produced when an aluminosilicate source reacts with aqueous alkali hydroxide or silicate solution [33]. Since the resultant geopolymeric binder is the product of an inorganic polycondensation reaction, or geopolymerisation, alkali activated alumino-silicate binders are referred to as inorganic geopolymeric compounds [34]. According to Davidovits [34], these reactions result in three-dimensional tecto-aluminosilitace frameworks with the fundamental equation as specified below:

$$M_n[-(SiO_2)_z - AlO_2]_n . wH_2O$$

n represents the level of polycondensation, and M is a potassium, sodium, or calcium cation in this formula. The term "polysialates" refers to the silicon-oxo-aluminate component that is used to represent the frameworks. The sialate network is made up of connected SiO_4 and AlO_4 tetrahedra that share all of the oxygen atoms. A Si-O-Al bridge may always be used to cross-link and construct new chains and rings together. Polymers of ring and chain made of Si^{+4} and Al^{+3} is called polysialates. Geopolymers are the term used to describe the three-dimensional silico-aluminate polysialate structures that range from amorphous to semi-crystalline. This structure is demonstrated in Figure 2.1.

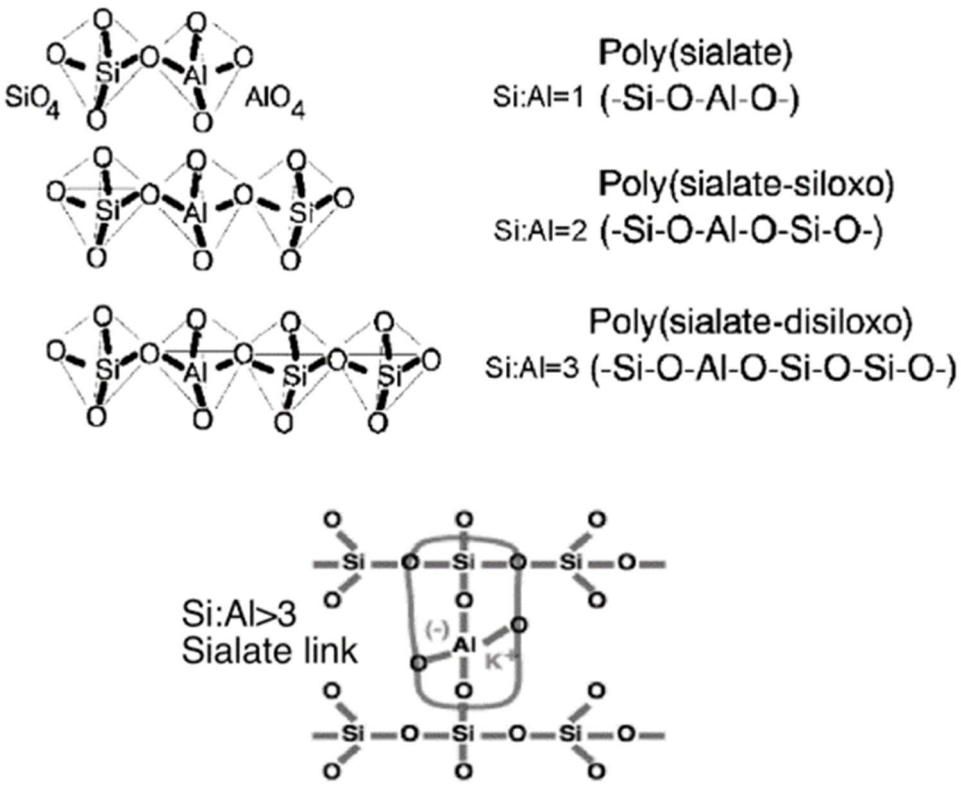

Figure 2.1 Poly-sialate structure of geopolymer [34]

Geopolymerization was examined in 4 distinct, concurrent phases in the study by Giannopoulou and Panias [35]. Aluminosilicate sourced Si and Al dissolve in highly alkaline aqueous solution in the first phase. In this phase, the aluminosilicate oxides' surface metal ions share water molecules and create hydroxylate surface sites aluminol (Al-OH) and silanol (Si-OH). In these hydroxylates assembly, alkali sourced hydroxide ions form surface species. The surface species release silicon and aluminum ions into the mixture, where hydroxide ions dissolve them. The dissolution of Si and Al can be represented by the following chemical equation where a states sodium or potassium:

$$(SiO_2, Al_2O_3) + 2aOH + 5H_2O \rightarrow Si(OH)_4 + 2Al(OH)_4^- + 2M^+$$

The formation of oligomers in the aqueous phase takes place in the second stage. Certain interactions occur between the created hydroxy complexes as concentrations of Si and Al in the aqueous phase undergoes growth through dissolution. In line with the following chemical equations, interactions lead to the creation of oligomer geopolymer precursors made up of polymeric Si-O-Al and Si-O-Si bonds:

$$Si(OH)_4 + Si(OH)_4 <=> (OH)_3Si - O - Si(OH)_3 + H_2O$$

$$Si(OH)_4 + Al(OH)_4^- <=> (OH)_3Si - O - Al^{(-)}(OH)_3 + H_2O$$

$$2Si(OH)_4 + Al(OH)_4^- <=> (OH)_3Si - O - Al^{(-)}(OH)_2 - O - Si(OH)_3 + 2H_2O$$

The oligomers' polycondensation occur to create a three-dimensional aluminosilicate structure in the third step of geopolymerization. A 3D framework involving SiO_4 and/or AlO_4 tetrahedra attached alternately through the sharing of common oxygen ions develops with increasing precursors concentration in the aqueous phase due to their polycondensation as it is shown by equations below.

$$n[(OH)_3Si - O - Si(OH)_3] \rightarrow \begin{array}{c} | \quad | \\ (-Si - O - Si - O-)_n + 3nH_2O \\ | \quad | \\ O \quad O \end{array}$$

$$n\left[(OH)_3Si - O - Al^{(-)}(OH)_3\right] \rightarrow \begin{array}{c} | \quad | \\ (-Si - O - Al^{(-)} - O-)_n + 3nH_2O \\ | \quad | \\ O \quad O \end{array}$$

Geopolymer precursors are bound together during this polycondensation reaction, commonly referred to as polymerization, while water molecules are simultaneously removed. The production of macromolecular chains and/or rings as a result of the precursors' reactions at hydroxyl ion sites assists in the creation of the three-dimensional structure.

In the last stage, solid particles bond into geopolymer structure and hardening of the system into geopolymer structure occurs. Undissolved particles are bonded together inside the final geopolymeric structure as the geopolymeric structure interacts with the

active areas of solid particles as it forms in the aqueous phase as shown in the equation below where X denotes surface sites.

$$X-OH+HO-\left(-\underset{\underset{O}{|}}{Si}-O-\underset{\underset{O}{|}}{Al}-O-\right)_n \rightarrow X-O-\left(-\underset{\underset{O}{|}}{Si}-O-\underset{\underset{O}{|}}{Al}-O-\right)_n+H_2O$$

The Si-OH and Al-OH groups present at active outer surface areas have a significant impact. The undissolved particles can be efficiently included into the geopolymeric structure by macromolecular chains or rings in the structure creating bonds of Al-O-Si and Si-O-Si with these surface locations. Therefore, polymeric matrix hardens.

According to recent study by Cong et al. [36], although it was reported that authors in the literature have different opinions about the reactions occurring during geopolymerization, geopolymerization mechanism is divided into three main steps in the study. The concentrated alkali solution dissolves the aluminosilicate components during the initial step of geopolymerization, producing free silica and alumina tetrahedron units. The dissolved components then go through a transformation and solidification process along with a condensation reaction between the hydroxyl groups of the alumina and silica. An inorganic geopolymer gel phase is created as a result of this process, and water is released as a result of hydrolysis. The geopolymer gel phase undergoes condensation processes as it hardens further, creating a three-dimensional network of silicoaluminates that eventually forms the geopolymer structure.

Another recent study by Shilar et al. [37] claims that aluminosilicate is converted into a binder using a method called geopolymerization using Si-Al-rich minerals. Sodium silicate (Na_2SiO_3), potassium silicate (K_2SiO_3), and sodium hydroxide (NaOH), well-known kinds of alkaline solutions, activate catalysts that have an impact on the geopolymerization process. Compounds like sodium aluminosilicate and calcium silicate hydrate are produced during this procedure. Gel strengthens the mechanical characteristics of the polymer and activates it, while sodium silicate hydrate creates a tetrahedral network. A complex chemical reaction is involved in the process. The

following figure is an illustration from the author's investigation of the physiochemical process of geopolymerization:

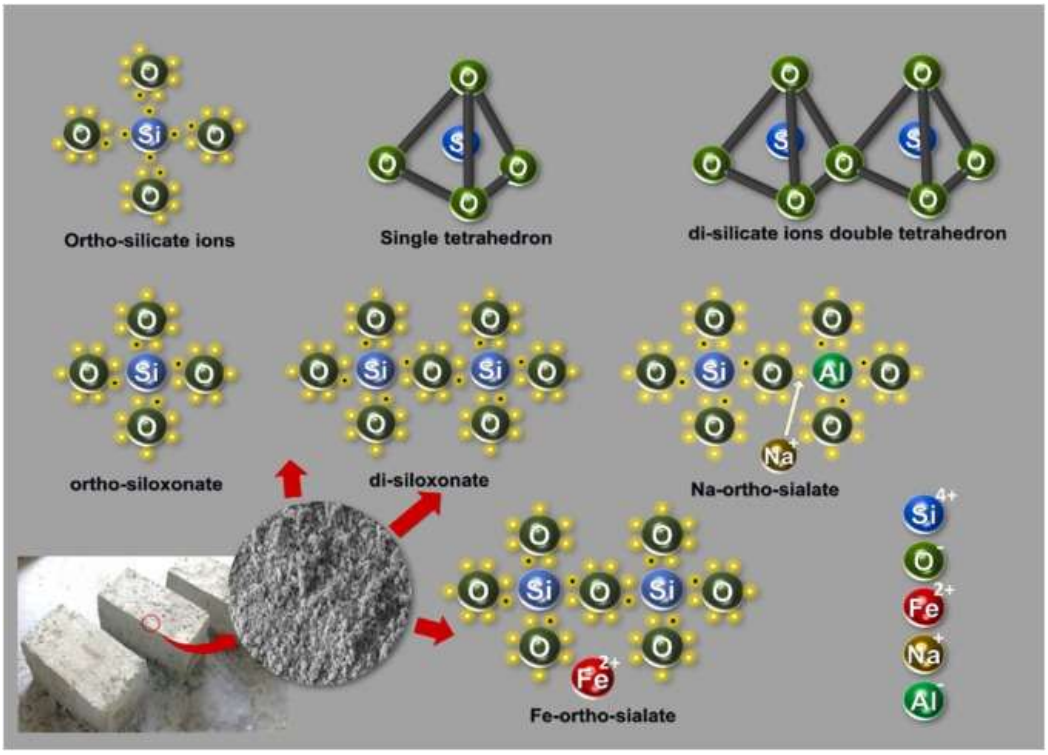

Figure 2.2 Physiochemical process of geopolymerization [37]

2.2 Utilization of End-of-Life CDW-based Materials in the Production of Geopolymers

Fly ash (FA) and ground granulated blast furnace slag (GGBFS) are two common industrial byproducts that are the main ingredients utilized in geopolymerization. In applications involving geopolymer and pozzolanic cement, these by-products have proven to have good engineering qualities [38]. The supply of FA and GGBS is having difficulties keeping up with the rising demand in the building sector for green alternatives to cement. An enormous quantity of CDW has also been generated as a result of the global manufacturing of concrete. For instance, Europe produces over 800 million tons of CDW per year [39]. Although efforts have been made to recycle building and demolition debris into aggregate, there are still barriers to widespread adoption, such as the cost-effectiveness and quality of recycled aggregate in comparison to natural aggregates [39]. Recent research has focused on using construction debris waste as a substitute for highly demanded products like GGBFS and FA in the production of geopolymer binders. This

approach intends to produce environmentally friendly geopolymer binders as Portland cement additives while also utilizing construction demolition waste into the manufacturing process.

A thorough analysis of the literature on CDW-based geopolymer development is provided below:

Vafaei and Allahverdi [40] investigated the production of glass waste based geopolymer activated with NaOH solution. Glass waste and calcium aluminate cement used in the study. Flow table, Vicat, compressive strength test, as well as FTIR, SEM, and EDS analyses are conducted for microstructural and compositional characterization. Additionally, the formation of efflorescence was examined. The results revealed that the higher content of calcium aluminate cement resulted in accelerated setting times. Moreover, by substituting 24% of calcium aluminate cement with glass waste and incorporating 10% Na_2O, the geopolymer's compressive strength was significantly enhanced, reaching approximately 90 MPa.

Tuyan et al. [41] used brick waste to produce geopolymer in their study. The influence of concentration of alkaline activator and conditions of curing on the consistency and strength of geopolymer composites are investigated. The alkali activators employed to produce geopolymer were liquid Na_2SiO_3 and NaOH. Geopolymer samples were cured for 24 hours at room temperature, followed by exposure to six different temperatures ranging from 50 to 100°C for up to 90 days. A series of tests and analyses were conducted, including compressive strength test, flow table test, TGA, Micro-CT, and FTIR analysis and porosity measurement. The results indicated that silica modulus of 1.6 and 10% Na_2O content was optimal. Curing condition of 5 days at 90°C provided maximum strength.

Rovnaník et al. [42] investigated the effect of curing conditions and various concentrations of alkaline activators on the strength of residual powder-formed clay brick and metakaolin geopolymers. As the alkaline source, Na_2SiO_3 with a silica modulus of 1.4 was employed. Geopolymer samples were allowed to cure for 4 hours at room temperature, 20 hours at 40°C, and up to 14 days in plastic bags. Shear stress and yield stresses as well as compressive and flexural strengths of geopolymer samples were tested. Additionally, SEM, XRD, FTIR, and NMR analyses were performed. The findings

demonstrated that adding more waste clay brick powder reduced plastic viscosity while having no impact on yield stress. The highest strengths were achieved with a mixture of 25% waste clay brick powder and 75% metakaolin. It was discovered that some crystalline phases took part in the geopolymerization process.

Sedira et al. [43] investigated the utilization of waste clay brick and tungsten mining waste sludge in the geopolymer composites. The alkali activators used were Na_2SiO_3 and NaOH. Produced samples were cured for 24 hours at 60°C. Following that, curing continued at room temperature for up to 28 days. The main test conducted was the compressive strength test. Various analyses such as TGA, DSC, XRD, SEM, EDS, FTIR, and MIP were performed. The findings demonstrated that compressive strength increased as waste clay brick content increased. Nevertheless, after 14 days, a loss in strength was noted. The inclusion of waste clay brick promoted the dissolution of certain phases of minerals.

Shoaei et al. [44] inspected the curing temperatures and alkaline solution to binder ratio on ceramic waste based geopolymer composites. Both Na_2SiO_3 and NaOH solution were utilized as alkali activators. The samples were first allowed to cure for 24 hours at room conditions, then for 24 hours at 60, 75, 90, and 105° C, and finally for up to 28 days at room temperature. Viscosity, compressive and flexural strength, and microstructural analysis were carried out. Research findings indicated that the flowability of the geopolymer mixture was improved by higher alkali reactivity/precursor ratio. The composites were cured at 90°C for 24 hours to reach their maximum compressive and flexural strengths.

Hwang et al. [45] studied on alkali activated ceramic and brick waste based high strength pastes. In the investigation, F-type FA and GGBS are also used. NaOH solution and liquid Na_2SiO_3 were employed as the alkali activators. Samples subjected to 24 hours of curing in plastic bags was followed by up to 56 days of curing at room conditions. The flow table, compressive strength as well as ultrasonic pulse velocity, and thermal conductivity is determined. The findings revealed that compared to ceramic waste composites, brick waste geopolymer composites had reduced workability. The blend of brick waste geopolymer that produced the highest strengths was 25% FA and 75% GGBFS. Higher compressive strength was obtained by reducing the SiO_2/Al_2O_3 ratio.

Lum Wong et al. [46] inspected the effect of utilization of brick waste and FA with high calcium as raw materials in geopolymer mortars on absorption, sorptivity, flowability and mechanical properties. As alkali activators, the researchers used NaOH and Na_2SiO_3. The produced specimens are allowed to cure until the testing days at room temperature. SEM and EDS analyses were carried out. The findings demonstrated that an increase in the brick waste content, Na_2SiO_3/NaOH ratio, and NaOH molarity led to a reduction in flowability. The highest compressive strength was 44 MPa utilizing 10% brick waste with a Na_2SiO_3/NaOH ratio of 2.5, and a 10M NaOH. Moreover, the most influential parameter for sorptivity was NaOH molarity.

Xiao et al. [47] conducted a comprehensive study to examine the effects of waste glass and C-type fly ash as raw materials of geopolymer binder, along with NaOH solution as the alkali activator. The samples were allowed to cure for up to 60 days at room conditions. On the geopolymer samples, compressive strength and evaluation of efflorescence production are examined. The study found that adding waste glass required a higher NaOH molarity. Notably, the composition that contained 75% fly ash and 25% waste glass and was cured in a 5M NaOH solution had the maximum strength, measuring 34.5 MPa.

Mahmoodi et al. [48] conducted a research to investigate the effect of utilizing C and F type FA, GGBS, and metakaolin as raw materials in waste ceramic based geopolymers on setting time and compressive strength, as well as flowability. Liquid sodium silicate and NaOH solution were employed in the alkali activation process. The samples were initially ambient cured for 1 day, followed by placing all initial mixtures in plastic bags for 28 days. Four further optimal formulations were produced and subjected to curing for 24-hour at 50°C to 100°C, followed by a 28-day curing time at ambient temperature. The findings demonstrated that a rise in the SiO_2/Al_2O_3 and Na_2O/SiO_2 ratios triggered a reduction in setting time and an improvement in flowability. Na_2O/SiO_2 ratio of 0.20, SiO_2/Al_2O_3 ratio of 11.1, and 0.3 liquid/solid ratio were observed to result in the maximum possible strength. Furthermore, strongest development of strength occurred with curing at 75°C. The study found that the best supplemental cementitious material for enhancing ceramic-based geopolymers was C-type FA.

Ouda and Gharieb [49] studied utilizing concrete waste containing dolomite aggregate on compressive strength of brick waste geopolymer. NaOH solution was employed for alkali activation of the binder. Initially, the samples were exposed to 80°C for a duration of 24 hours. Subsequently, they underwent a curing period lasting 28 days, at 40°C. Highest compressive strength is attained by employing NaOH with the concentration of 12%. The incorporation of concrete waste proved beneficial in enhancing the strength of brick based geopolymers. Additionally, the utilization of calcined concrete waste provided more compact microstructure in the brick-based geopolymer composites.

Tho-In et al. [50] investigated the influence of employing lamp and bottle glass wastes in fly ash based NaOH and sodium silicate activated geopolymers on mechanical properties and microstructure. The FA-based geopolymer specimens were ambient cured for 1-hour, then cured for 2 days at 60°C. Lastly, curing process was continued for 7 days at ambient conditions. When the mixture contained 20% waste glass content, the highest compressive strength of 48 MPa was attained.

Dadsetan et al. [51] examined the mechanical, microstructural, and rheological characteristics of geopolymer pastes made of glass powder and metakaolin. As alkali reagents, NaOH solution and Na_2SiO_3 were used. The samples then allowed to cure for up to 90 days. The results showed that waste glass geopolymers with SiO_2/Al_2O_3 ratios of 11.9, as well as $Na_2O/SiO2$ ratios of 0.26 with liquid-to-solid ratios of 0.45 had the best compressive strength. The strength of paste greatly enhanced after devitrification at 90°C for 60 minutes. The silanol groups and compressive strength were found to increase as the tridymite concentration in the waste glass increased.

Yıldırım et al. [52] conducted a comprehensive study targeted to develop and characterize alkali activated geopolymer using a combination of mixed clay based CDW units. Geopolymer samples were prepared by utilizing NaOH solutions with molarities of 10, 15, and 19 M. Subsequently, the samples were heat cured at 95 to 125 °C for durations of 1 to 3 days. The results clearly demonstrated the effectiveness of employing a completely CDW-based approach for producing alkali-activated binders with exceptional compressive strength capabilities, reaching up to 80 MPa.

Ulugol et al. [53] conducted a study focused on the development of geopolymers using CDW-based precursors, including sort of bricks and glass. The researchers investigated the impact of curing temperatures ranging from 50 to 125 °C, curing periods ranging from 24 to 72 hours, and sodium concentrations of 10, 12, and 15% of the NaOH on the compressive strength. Samples were characterized by microstructural analyses The outcomes showed that compressive strengths greater than 45 MPa could be attained by utilizing hollow brick as a precursor and curing it at 115 °C for 24 hours with a Na content of 12%. It was discovered that red clay brick and roof tiles performed similarly in terms of compressive strength. However, geopolymers using glass as a precursor showed lower compressive strength. The study underlined that CDW-based materials can be used successfully to produce geopolymer pastes and offer new insights into the effective utilization of CDWs in this field.

Ilcan et al. [54] investigated the fresh state characteristics of geopolymer mortars entirely comprising CDW. The mortars were produced employing a range of bricks as well as concrete, glass, and concrete debris aggregates. The mixes were activated by inclusion of various ratios of $Ca(OH)_2$ from 0 to 8% and NaOH with molarities ranging from 7.5 to 15. Through the use of flow curve, the rheological characteristics of the mortars were evaluated. Ram extrusion was also employed to evaluate the mixtures' extrudability. The number of alkaline activators in the mortars affects rheological characteristics, according to the study. The thixotropy tests indicated that the geopolymers' viscosity recovery capabilities ranged between 65% and 82% depending on the activator content. Ram extrusion tests revealed that when the resting time was longer than 60 minutes, some mixes displayed various forms of failures in the extrusion process. All other mixes, however, continued to be extrudable even after 120 minutes, with the exception of those that had been activated with 15M NaOH.

Ozcelikci et al. [55] conducted a research focusing on the development and characterization of mortars utilizing mixed CDW-based geopolymers cured at ambient conditions. The precursors for the mixtures included a mix of bricks, concrete and glass in some mixtures, GGBFS was used to partially substitute the CDW precursors. Durability and mechanical strengths were assessed. The findings showed that the completely CDW-based and slag-incorporated mortars attained compressive strength values of over 30 and 50 MPa at 28 days, indicating their potential usage as CDW-based

structural concretes. The results show that it is feasible to create ecologically friendly building materials with adequate strength and durability.

2.3 A Revolutionary Approach to Industrial Production with 3D-AM

2.3.1 Background and Development of 3D-AM Technology

Additive manufacturing is a procedure, defined by ISO and ASTM as adding materials layer by layer to create objects from 3D model data, in contrast to conventional subtractive manufacturing techniques [56,57]. In the 1980s, 3D additive manufacturing was launched to replace the previously used industrial subtractive manufacturing technology. The classic and most popular method of industrial solid item manufacturing involves removing material from a specific solid block until the desired shape is obtained. Tools like as lathes and milling machines are commonly employed in this approach, known as subtractive manufacturing. Sculptors extracting marble or other solid materials from a block, potters molding pots, and woodcarvers all do similar labor. In contrast to this traditional approach, additive manufacturing described as the practice of adding material layer by layer resulting a formation of a 3D object.

Instead of deleting superfluous material from an entire block, this approach allows for the creation of 3D things by beginning from scratch and adding materials in layers to each other. By analogy with a comparable technique used in inkjet printers, additive manufacturing has been termed 3D printing over time. It has been stated that over 30,000 patents relating to 3D printing have been issued in the United States alone since the 1980s [58]. Simultaneously, several open-source computer applications that contribute to the additive manufacturing process have been made available to all humanity over the internet [58,59].

Hideo Kadoma, who invented rapid prototyping in 1981, was the first to use 3D printing. Dr. Kadoma pioneered 3D printing technology by inventing rapid prototyping, a technique that prints thick layers of rapid-drying photopolymers which mimic sectional shape of a CAD design [58].

Charles Hull patented Stereolithography in technology 1984, which relies on the interactions of a UV beam with photopolymer in a liquid phase. When subjected to UV

beams, photopolymers in liquid form instantaneously change every layer into a stiff structure of plastic that mimics the computer aided design model. Stereolithography was the very first fast prototyping method, which meant the accelerated, accurate, and reproducible manufacture of objects, typically with computer assistance. Hull's enterprise, namely 3D Systems, released the Sereolithography Apparatus (SLA-1), the first ever commercially available Sereolithography Apparatus, in 1992 [59,60].

Figure 2.3 SLA-1 3D-printer [61]

Larry Hornbeck invented the Digital Light Processing (DLP) concept in 1987, which was marketed by Texas Instruments. This technology has a wide range of uses, including projector production and 3D printing. The optical semiconductor, also known as a digital microscope device or DLP chip, is at the heart of DLP technology [62]. Both DLP and SLA employ photopolymers, however their illumination sources are different. In the DLP technique, more classic lighting sources are used. The printing medium in DLP is fluid plastic resin. When exposed to a significant amount of light, resin solidifies swiftly. When compared to abovementioned technology, SLA, DLP print speed is higher. DLP produces more resilient 3D models [59].

Scott Crump, Stratasys Inc. co-founder, patented a novel application, namely Fused Deposition Modeling (FDM) in 1989. An FDM printer extrudes a resin that has been heated just over its melting temperature, placing it layer by layer, rather than curing a photopolymer resin with reflected light. This process, unlike SLA, utilizes a projector to cure the whole layer, resulting in a considerable improvement in material printing speed. FDM technology is still employed in many entry-level 3D-printers currently [63].

Several more 3D printing methods were being studied in the 1990s. William Masters' patented Ballistic Particle Manufacturing (BPM) projected micro beads of melted wax material from a jet traveling in an X-Y axis to make thin plate-like samples. In 1995, Michael Feygin submitted a patent for Laminated Object Manufacturing (LOM), which employed mechanized cross-sectional slice production from a sheet according to a virtual 3D model, then mounting and gluing the cross-sectional layers to make a solid object. Itzchak Pomerantz pioneered Solid Ground Curing (SGC), which utilizes an optical mask method to selectively treat layers of photocurable resin [64].

These new technologies, which were developed throughout the mid-1980s, 1990s, and 2000s, were mostly focused on industrial uses, frequently for prototyping. Also, advanced technology firms carried out R&D research. As a result, new terminology such as Rapid Tooling, Rapid Casting, Rapid Prototyping and Rapid Manufacturing have appeared in the literature [65]. The ASTM introduced the phrase "additive manufacturing" as a common name for abovementioned techniques in 2005. The definition of additive manufacturing is “process of joining materials to make objects from 3D model data, usually layer upon layer” [59].

Since 1984, when the 3D-printer designed, introduced and commercialized by Charles Hull of 3D Systems Corporation, 3D-printers have evolved and become more useful with the advancement of various technologies [66]. 3D-printers have become available at more affordable prices. The usage areas of 3D-printers, which currently serve humanity, are quite wide. Today, the main industries where 3D-printers are used are automotive, healthcare, construction, aerospace, military, architecture, fashion, education and more [67].

2.3.2 3D-AM Technology in Construction Industry

The construction industry presents a compelling synergy with 3D printing technology, owing to its established proficiency in computer-aided manufacturing and access to the requisite data for generating a 3D component through the design process. The utilization of diverse materials, coupled with the inherent creative liberty, empowers the production of intricate geometries both on and off-site. When integrated with the capabilities of automated and autonomous manufacturing, these attributes harmonize impeccably with the demands of the construction sector. From this perspective, the adoption of 3D printing facilitates the expedited and precise fabrication of intricate structures, thereby reducing labor costs and wasted materials. Furthermore, holds a potential to facilitate future advancements in challenging or hazardous regions, including those in outer space, where human labor is impractical or unsafe.

Dr. Behrokh Khoshnevis launched the first 3D printing initiative for the construction industry in 1995. Khoshnevis manufactured 3D ceramic components using the stereolithography method. Despite the fact that components' mechanical characteristics could not optimized, he successfully managed to create a complex-shaped ceramic [68]. In next year, Khoshnevis obtained a patent titled "Additive Manufacturing Apparatus and Method," which introduced a machine to produce 3D objects by additive manufacturing technique. The machine consists of double nozzle, as well as double feeding mechanism to deposit material. The control unit provides movement to the nozzles. Utilizing spatulas to create flat surfaces quickly and precisely is another function of the apparatus., replacing the need for various tools typically required in traditional applications. In 2001, Khoshnevis, introduced a notable advancement in 3D printing technology within the field of construction. Employing a robotic arm-mounted Fused Deposition Modeling 3D-printer, Khoshnevis successfully printed a wall by sequentially depositing layers of concrete. This novel technology was named Contour Crafting (CC). Computer-controlled additive manufacturing technique, namely CC, benefits from the trowel's exceptional capabilities of surface-forming, thereby facilitating the creation of smooth and precise planar and freeform surfaces through extruded materials [69]. CC stands as the pioneering additive manufacturing technology extensively employed in the construction industry today. According to Dr. Khoshnevis, Contour Crafting offers several key advantages.

These include unparalleled surface quality of printed components, enhanced production speed, and a wide range of material options. The prototype Contour Crafting machine operated within a working envelope measuring 5 m x 8 m x 3 m, providing a printing area of 120 m^3. Other benefits associated with this technology encompass cost reductions, minimized material waste and accidents, accelerated construction pace, and the ability to fabricate intricate architectural forms, among others. It was anticipated that Contour Crafting technology would enable the construction of concrete structures that were challenging to achieve through traditional pouring methods, facilitating efficient and environmentally friendly housing construction.

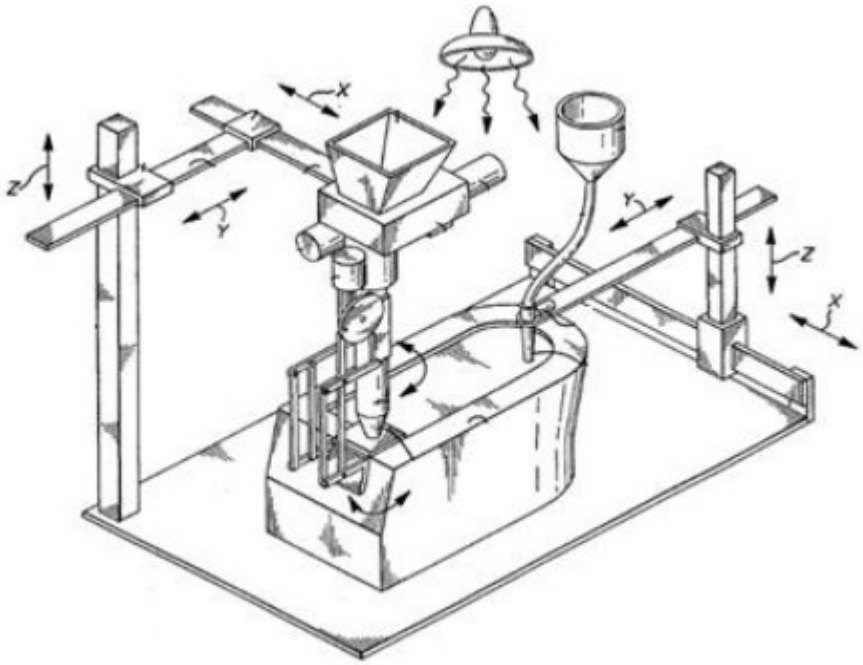

Figure 2.4 Dr. Khoshnevis's 3D-printer [59]

The 3D Concrete Printing (3DCP) system was created by academics at Loughborough University in 2003. [70]. The system employed a concrete extrusion machine equipped with a pressing extension that exclusively moved in the x-direction. This machine was mounted on a movable horizontal beam capable of movement in the y and z directions within a frame measuring 5.4×4.4 ×5.4 m. The printing speed achieved varied, reaching up to 83 mm/s depending on the printing pattern's complexity. The concrete printing process involved several stages, including data preparation, material preparation, material transmission, and the actual printing process.

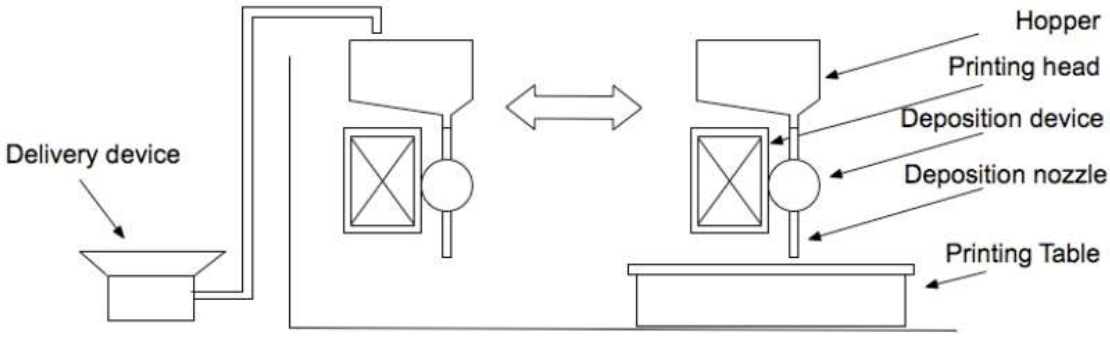

Figure 2.5 3D-printer system developed by Loughborough University [70]

The D-shape technique, introduced by Enrico Dini in 2007, involves the localized solidification of sand bed in an extensive scale by selectively depositing a type of binding agent [71]. In this method, a programmatically guided nozzle moves along a predetermined path, applying a liquid binder onto a specific portion of the sand bed along with a firm catalyst. Subsequently, a chemical reaction occurs, initiating the solidification process. Meanwhile, the surrounding sand provides structural support. This sequential layer-by-layer process continues as additional layers of sand are added. The printed item is taken out of the sand bed when the printing process is finished, while the residual sand can be easily recycled and reused for subsequent printing operations.

Figure 2.6 D-shape 3D-printer [72]

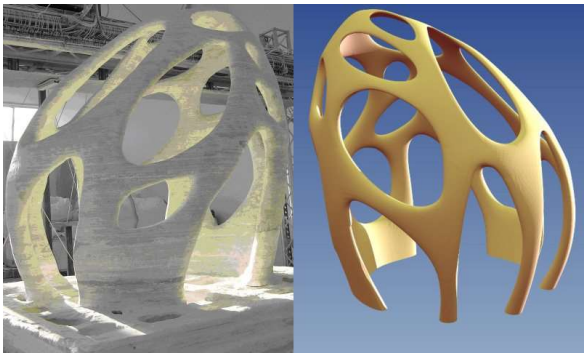

Figure 2.7 Architectural piece created by D-shape technique [72]

In summary, the different 3D printing techniques exhibit distinct characteristics [70,73–76]:

- CC technique utilizes a mold that becomes an integral part of the produced unit, whereas 3D Concrete Printing (3DCP) and D-shape techniques do not employ molds.

- CC technique employs a mixture of mortar for formwork and cementitious material for construction, while 3DCP technique utilizes printable concrete, and D-shape technique employs granular sand and stone dust.

- The nozzle diameter in CC technique is 15 mm, ranging between 9-20 mm in 3DCP technique, and as small as 0.15 mm in D-shape technique.

- The average layer thickness differs among the techniques, with CC technique having an average of 13 mm, 3DCP technique ranging from 6-25 mm, and D-shape technique ranging from 4-6 mm.

- While reinforcement can be used in both CC and 3DCP techniques, it is not suitable for utilization in the D-shape technique.

The variety of 3D printing techniques has allowed for more laboratory-scale research, but as robotic and materials science advancements have accelerated, industrial-scale applications have begun to emerge. Some of the important industrial applications are below:

In late 2015, XtreeE emerged as a pioneering firm dedicated to advancing additive manufacturing at an industrial level. With a primary focus on large-scale 3D concrete printing, the company offers rental services for large-scale printing systems, enabling clients to access and utilize such technology and assists customers in co-design and the production of large-scale prototypes. In 2015, XtreeE built a structural wall within the scope of a university project named Democrite, using additive manufacturing technique. At present, XtreeE employs a robotic arm known as Concreative for their printing

operations, which has the capability to fabricate objects up to 3 meters in height and 5 meters in length without the need for repositioning. Notably, the structures constructed using this robotic arm demonstrate enhanced concrete quality, exhibiting a reported compressive strength exceeding 80 MPa [77].

Figure 2.8 A structural wall 3D printed by XtreeE [78]

In 2016, a significant milestone was achieved in the construction industry with the inauguration of the world's first-ever 3D-printed pedestrian bridge (3DBRIDGE) in Madrid. The concept of the project was developed by Acciona, which was responsible for the design of the structure as well as development of material, and production of the printed units. Micro reinforced concrete was used to print the pedestrian bridge, which has a 1.75-meter width and a total length of 12 meters. The Advanced Architectural Institute of Catalonia carried out the architectural concept while D-Shape manufactured the 3D-printer. The dimensions of the 3D-printer that D-Shape utilizes are 6 x 6 x 3 m. The printer is fast enough to create structures of 1.2m^3 per hour from 10 mm layers. Through the use of parametric and computational design, which took into account the details inherent in natural shapes, the 3D printed bridge was made possible. A significant international milestone is being set for the construction sector by the effective application of large-scale 3D printing technology in a public context [79–81].

Figure 2.9 World's first 3D-printed pedestrian bridge [82]

Companies that aimed to advance large-scale 3D printing for construction purposes started to appear around the same time. Such a business includes Apis Cor, which was established in 2017. To enable on-site printing of entire structures, Apis Cor designed a concrete crane with a 132 m^2 printing area. Depending on the manufacturer, the printer itself has compact dimensions of about 4x1.6x1.5 m and weighs about 2 tons. The 3D printing technology employed by Apis Cor facilitates the layer-by-layer printing of an entire house using a concrete mixture, completing the construction within a remarkable timeframe. The printer has a maximum printing speed of 165 mm/s. A transportable 3D-printer and a mobile automated mixing and feeding equipment comprise the system. In addition, Craverio reported that geopolymer binders can be used in this 3D-printer as well as cementitious binders [83]. Notably, unlike many other printers that necessitate a flat concrete base, the printer developed by Apis Cor incorporates a stabilization system that allows installation on nearly any surface, even with less than a 10 cm elevation difference [84,85].

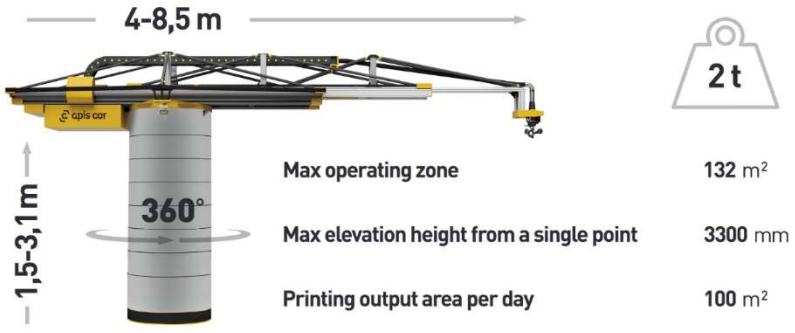

Figure 2.10 A 3D-printer designed by Apis Cor [86]

In 2018, the construction company ICON made history by obtaining the first-ever license to construct a 3D-printed home [87]. Robotics, software, and building materials are all included in the advanced construction technologies developed by Texas-based ICON. A major accomplishment for the company was their first project, which involved building a 3D-printed house in Austin, Texas. ICON initially concentrated on smaller-scale programs meant to address housing issues in regions with wildly varying building requirements or where such standards have not yet been created. Through their innovative approach and utilization of 3D printing technology, ICON has demonstrated its commitment to finding practical solutions for housing needs globally. Presently, ICON has extended its ambitions to include the construction of homes in the United States, alongside collaborating with NASA to explore potential construction methodologies for lunar habitats. ICON has developed a specialized 3D-printer known as Vulcan II. The Vulcan II 3D-printer is engineered to enable the swift and accurate construction of bigger structures and achieve a substantial printing capacity of around 600 m², with a printing area measuring approximately 2.6x8.5x 2.6m. A maximum print speed of 175 mm/s has been designed for the printer, which weighs about 1.7 tons [88].

Figure 2.11 3D-printed house in Austin, Texas [89]

PERI, a Germany-based company renowned for its expertise in manufacturing and supplying formwork and scaffolding systems within the construction sector, has recently ventured into 3D printing projects in collaboration with COBOD, a Danish technology partner specializing in concrete 3D-printers. Serving as a significant milestone for the

company, PERI successfully constructed Germany's first 3D-printed home, commencing the printing process in 2020, with is serving for residential use since 2021. Moreover, in June 2021, PERI embarked on another remarkable project by initiating the printing of a home in Tempe, Arizona. This particular undertaking holds great significance as it is a collaborative effort with Habitat for Humanity, the world's largest nonprofit home builder, known for its extensive experience in constructing nearly a million homes. The Tempe house, spanning an area of 160 m², features three bedrooms and two bathrooms, employing a hybrid model that combines traditional construction methods with 3D printing. Operating printer COBOD2 has 250 mm/s maximum printing speed and 14.6m width by 8.1m height with unlimited length of printing area. Notably, approximately 80% of the structure is 3D printed by COBOD2 printer, showcasing the innovative capabilities and potential of this technology in the construction industry [90–92]. Additionally, PERI is now working on construction of the Europe’s largest 3D printed building.

Figure 2.12 A bird's-eye view of the ongoing 3D printing of house [93]

The building sector has recently undertaken numerous projects where single and multi-story houses, offices, and other types of structures are produced utilizing 3D printing technology. In contrast to conventional construction techniques, these projects aim to construct homes more quickly, economically, and sustainably [94]. The building of 3D-printed homes is currently regarded as a developing industry, and various regulations and construction standards are currently being developed in this field [95]. Latest studies and initiatives indicate that 3D printing technology will get through these challenges and become more prevalent in the building sector in the future.

Figure 2.13 3D printed houses all around the world, a) Office of the future [96], b) World's largest 3D-printed building [97], c) Sustainable housing neighborhood [98], d) Two story 3D-printed house [99], e) Low carbon 3D housing [100], f) Two story 3D-printed family house [101]

2.3.3 Advantages of 3D-AM Technology

Additive manufacturing (AM) technology is becoming an increasingly important topic in many sectors due to its benefits. In the construction sector, AM offers an innovative approach to producing distinctive and sophisticated components that would otherwise not be feasible using conventional manufacturing techniques [11]. This creates an

opportunity for significantly increased customization without incurring additional expenses, allowing for exceptional architectural intricacies on a larger scale [102]. This technique allows design freedom for building complex structures in-situ or pre-printed [8]. García de Soto et al. [103] reported that as the complexity of the shape increases, the productivity advantage of additive manufacturing can range from 12.5% to 38% based on hours per installation values.

The construction industry is commonly recognized as being reliant on labor [104,105]. The cost of labor as a share of total construction expenses can change based the complexity of the project, the location, and the state of the labor market and more. Construction labor expenses constitute approximately 30% to 50% of the total expenditure of a construction project [103,104]. Pan et al. [94] state that labor expenses account for 60% of the entire expense of the construction projects. Labor costs can be reduced by up to 80% by implementing additive manufacturing technologies according to the studies [8,9].

The design flexibility that additive manufacturing (AM) technology offers allows for the production of since AM technology does not require any molds, it also does not need any tooling, which results in huge cost savings [14]. Varies from project to project, formwork activities account for approximately 35% to 60% of the total cost of construction projects [102]. Pan et al. [94] state that formwork labor and cost represent more than 50% of the overall cost of construction. Therefore, utilizing 3D printing technologies could potentially lead to savings of more than half of the overall cost. Similarly, Malaeb et al. [106] concluded that the utilization of 3D printing technology could result in a reduction of 35% to 60% in the overall construction expenses attributable to the elimination of formwork requirements.

In terms of speed, 3D-printing technology significantly outperforms conventional construction techniques. Traditional building involves several processes that take time and need sequential labour, such as formwork preparation, manual labor, and curing time. Contrarily, 3D printing permits the quick layer-by-layer deposition of material, enabling continuous and concurrent construction. As a result, there is no longer a need for heavy manual labor, and the whole building time is drastically decreased. Rouhana et al. [107] conducted a study where they modeled the construction of a 200 m^2 house to compare the

building speed between contour crafting technology and traditional construction methods. The results of the study revealed that utilizing contour crafting technology allowed for the construction of the same structure to be completed three times faster compared to conventional methods. Krimi et al [11] conducted an investigation into the production of singular formed walls using additive manufacturing, precast, and cast-in-place techniques. The study demonstrated a significant reduction in the construction time when utilizing 3D printing technology. Specifically, the construction process was found to be 1.7 times faster compared to prefabrication and four times faster than cast-in-place concrete.

Aside from saving money and allowing design freedom, the utilization of 3D-printer technology in the construction industry offers significant environmental benefits as it offers a more sustainable approach to construction by reducing waste generation and minimizing CO_2 emissions. Conventional building techniques generally lead to substantial material waste throughout the manufacturing and installation processes. On the contrary, 3D-printing allows for precise and controlled material deposition, bringing down material waste and optimizing resource utilization. In a study conducted by Sakin et al. [5], it was found that the employment of 3D-printing has the potency of reducing construction debris by 30-60%. Furthermore, 3D printing technology typically requires less energy compared to conventional construction techniques, resulting in lower CO_2 emissions. The ability to customize and fabricate components on-site also reduces the need for transportation, further decreasing energy consumption and associated emissions. K. Kim et al. [108] predicted in their study that additive manufacturing technology could significantly decrease CO2 emissions by 76% and construction waste by 86%.

In conclusion, the utilization of 3D printing technologies holds great promise for the construction industry. The capacity to achieve complex and specialized structures with precision and efficiency grants flexibility in design and architectural creativity. Investigations demonstrating the substantial reduction in construction duration achieved through 3D printing in comparison to traditional approaches highlights the advancements in construction speed. Furthermore, the incorporation of 3D printing techniques offers considerable potential for cost reduction, particularly concerning labor and material waste management. The environmental benefits are equally noteworthy, as 3D printing has the capability to mitigate construction waste and minimize CO_2 emissions. These

advancements in 3D printing technology pave the way for a more sustainable future and resource-efficient building approach. Ongoing research and development endeavors have the potential to transform the construction industry, encouraging improved efficiency, cost-effectiveness, and environmental sustainability.

2.4 Utilization of Geopolymer in 3D-AM Technology

The introduction of 3D printing technology has created new opportunities for innovation in the building industry. The application of geopolymers in additive manufacturing (AM) processes is one interesting area of investigation. Inorganic polymers known as geopolymers, which are produced from abundant and environmentally friendly materials, have special qualities that make them desirable for green building techniques. There are numerous investigative works in the scientific literature focused on the development of 3D printable construction materials. The following section provides an overview of the studies conducted on geopolymers produced using 3D printing technology.

Panda et al. [109] aimed to develop a geopolymeric mortar for 3D applications. Alkali sources utilized include KOH and K_2SiO_3, whereas aluminosilicate sources include FA, BBFS, and silica fume. The research emphasized the establishment of a printable thixotropic region (a range of shear stress) concerning extrudability and buildability. Moreover, study showed that the minimum threshold level for achieving the desired thixotropic behavior suitable for the 3D printing method varied depending on factors such as test apparatus and design of blend, as well as applied shear rate.

Xia & Sanjayan [110] conducted a study focusing on the impact of various curing conditions and mediums on the mechanical characteristics of geopolymers produced by 3D concrete printing method. The initial stage of post-processing was immersing 3D printed geopolymer samples for 3 or 7 days at 25 to 80 °C in saturated anhydrous sodium metasilicate solution. According to the results of tests performed on geopolymer samples that were cured in various temperatures and mediums, 60 °C curing sped up the hardening process, and the combination of 8.0 M NaOH solution and Na_2SiO_3 solution with a SiO_2/Na_2O ratio of 3.22 enhanced the strength. This is because temperature-controlled kinetics are only effective up to a specific temperature and the reaction rate of geopolymer is quicker at higher temperatures. Additionally, a highly alkaline environment enhances

the surface hydrolysis of the largely unreacted slag particles as well as dissolving of silica and alumina species.

Panda et al. [111] investigated the difference of mechanical strength between fresh and old layer of 3D printed geopolymer mortars. To evaluate the variation in bond strength of printed materials, printing intervals between layers, nozzle speed, and nozzle clearance were taken into account. FA, GGBFS, silica fume, river sand, and liquid K_2SiO_3 were all employed in this study. The specified time difference ranges from 1 minute to 6 days. In terms of mm/s, nozzle speed is described as 70, 90, and 110. Furthermore, the nozzle standoff distances are defined as 0 cm, 2 cm, and 4 cm, respectively. Test results came from three distinct cases. In the initial case, the printing time gap ranged from 1 minute to 6 days while the nozzle speed was 90 mm/s and the nozzle standoff was 0 cm. However, due to extrusion complications, 20 minutes was chosen as the top limit in this study. In the second scenario, the nozzle standoff was once again 0 cm, the time interval was 3, and the nozzle velocity ranged from 70 mm/s to 110 mm/s. In the third scenario, the nozzle standoff varied from 0 cm to 4 cm, and the nozzle speed was 90 mm/s. Rheometer was used to test the material's yield stress and viscosity. The outputs of the tests revealed that standoff distance and nozzle speed provide superior bond strength values at their lower levels, whereas time gap has an inverse relationship with bond strength. While nozzle standoff distance extended from 0 to 4 cm, the geopolymer samples' tensile bond strength reduced from 2.3 to 1.1 MPa. When the printer speed raised from 70 to 100 mm/s, the tensile strength likewise reduced, from 1.7 to 1.5 MPa.

Zhang et al. [112] investigated the structural reconstitution ability and flowability of geopolymer pastes containing GGBFS, steel slag, sodium metasilicate, and NaOH with different Si/Na ratios. The study concluded that an increase in Si/Na ratios reduces the flowability, viscosity, and structural reconstitution ability of the geopolymer paste, and slows down the development of flowability.

Panda et al. [113] investigated the mixture proportions, as well as fresh state properties of geopolymer mortar suitable for 3D printing. In the study, the characteristics of a 3D printed geopolymer binder were examined. To create the finest printable mix, five distinct mix designs were created. The raw materials utilized were FA, GGBFS, and undensified micro silica fume. As an activator, solutions of K_2SiO_3 and NaOH were utilized. In the

mix design, river sand was used as the aggregate, and the aggregate/binder ratios were adjusted to be 1.1, 1.3, 1.5, 1.7, and 1.9, respectively. To ensure the thixotropic open time feature of the geopolymer mortar, the change in yield stress over time was taken into account. In this investigation, GGBFS was used in place of 5%, 10%, and 15% fly ash to achieve a change in yield stress. The extrudability of the mixtures was shown to be strongly impacted by the addition of sand, according to test results. Lower extrudability was caused by high yield stress properties. When the amount of ground GGBFS in the mix raised, yield stress increased, caused the shape retention factor to increase. Thixotropic open time is also decreased. For seamless extrusion of geopolymer mortar, it was discovered that yield stress should be between 0.6 and 1.0 KPa.. The yield stress that enables the material to maintain its form under its own weight has been discovered to be inversely correlated with shape retention parameters. Mixtures with higher yield strengths maintained their shape better and distort less during the slump test.

Sun et al. [114] evaluated the fresh state properties of geopolymer mortars containing GGBFS, calcium carbonate powder, NaOH, and Na_2SiO_3. A series of tests, including the Vicat test for setting time, flow table test for flowability, and rheometer test to determine shear stress, apparent viscosity, flowability, and plastic viscosity values, were conducted. According to the obtained results, the mixtures with plastic viscosity ranging from 10.08 to 10.42 and flowability ranging from 32.53 to 66.71 Pa could be continuously extruded at a printing speed of 30 mm/s without any cracks, interruption, or collapse.

Panda et al. [115] investigated applicability for extrusion-based additive manufacturing of the geopolymer mixtures. As a precursor for the geopolymer paste, Class F FA and GGBFS were employed. Nano clay was used to enhance the thixotropy of the mixture. As an activator, KOH and K_2SiO_3 solutions were utilized. In the study, two molar ratio values 1.8 and 2 were used for K_2SiO_3. By mass, the geopolymer mortar was composed of 85% FA and 15% GGBFS. Using a 1.5 aggregate to binder ratio, river sand having smaller size than 2 mm were added to the mixture. Nanoclay was included in the combinations up to 0.5%. The yield stress and plastic viscosity were found to decrease significantly with raising water-to-solid ratio. When the water-to-solid ratio was increased from 0.35 to 0.40 at a molar ratio of 1.8, the yield stress decreased by 30%. The yield stress and viscosity improved as the molar ratio value increased. Due to nanoclay's flocculation capability, using a minor amount of additional nanoclay had a favorable

effect on the yield stress and viscosity. Additionally, clay inclusion improved the mixture's capacity to recover within 60 seconds. Study also reported a decrease in compressive strength by around 17% and the strength rate of the geopolymer was not accelerated by the nano clay.

Bong et al. [116] investigated the fresh and hardened properties of a 3D printable geopolymer. Several important geopolymer synthesis parameters, such as alkaline activator type, the mass ratio of activators and more were studied. In this study, geopolymer mixes were made using two different Na-based and one K-based liquid alkaline activators. The silicate solutions included one K_2SiO3 solution and two Na_2SiO_3 solutions with varying mass ratios. 8M of NaOH and KOH solutions are produced by dissolving in tap water. FA and GGBFS were combined to function as the binder in each combination. The testing on the 3D printed geopolymer mortars led to the conclusion that most crucial factors influencing the open time properties are activator type and SiO_2/Na_2O. This is explained by the fact that these variables regulate the reaction and setting time of the geopolymerization. The specimens' compressive strengths ranged from 8.5 to 16.6 MPa.

Sahin et al. [117] conducted an assessment of ambient-cured geopolymers made entirely from CDW for their rheological properties in relation to 3D-AM applications. The study used CDW-based precursors, including hollow brick, red clay brick, roof tile, and glass, activated using various ratios of NaOH concentrations (5 to 25M), $Ca(OH)_2$ contents (0 to 10%), and Na_2SiO3 with Na_2SiO_3/NaOH ratios (0 to 1). Utilizing the empirical tests, rheological characteristics were evaluated. Using a ram extruder, the extrudability of the geopolymer mixtures was examined, and one specific mixture was selected for small scale 3D printing in the laboratory. The activation of the mixtures by 6.25 M NaOH and 10% $Ca(OH)_2$ demonstrated superior performance for 3D-AM applications. The results showed that 100% CDW-based geopolymers utilized successfully for 3D printing and have the sufficient rheological and mechanical characteristics. The effectiveness of the empirical test techniques used to assess the 3D printability of geopolymers has been proven.

Ilcan et al. [118] developed geopolymer mortars entirely composed of CDW and cured at ambient conditions, with rheological properties specifically tailored for 3D-AM. The

various alkaline activator combinations of NaOH with molarities ranging from 7.5 to 15, $Ca(OH)_2$ concentrations ranging from 0 to 15%, and Na_2SiO_3 with Na_2SiO_3/NaOH ratios ranging from 0 to 1 as the alkaline activators. Compressive strength measurements and empirical testing were used to evaluate rheological parameters. The study's results showed that it is possible to effectively geopolymer mortars with appropriate rheological characteristics for 3D-AM. The designed mortars, which demonstrated adequate compressive strengths, displayed perfect extrusion during 3D-AM, preserved their original shape and completely matched the printed structure that was desired.

Demiral et al. [119] conducted an evaluation of the mechanical behavior and bonding features of totally CDW-based geopolymer mortars cured at ambient conditions and fabricated using the 3D-AM technique. Utilized materials composed of waste of clay-based bricks and tiles, also glass and concrete along with various amounts of alkali activators made up of 10 to 12.5M NaOH, as well as 0 to 8% $Ca(OH)_2$. Additionally, concrete waste was utilized for producing fine aggregate for geopolymer mortars. Anisotropic behavior was examined in three loading directions for compression, two loading directions for flexure. Additionally, splitting and direct tensile strength tests were used to examine the bond strength. The findings indicated that the content of the alkaline activator had a significant impact on the mechanical behaviour. Specifically, printed samples with 10M NaOH and 4% $Ca(OH)_2$ tested to have a maximum compressive strength exceeding 20 MPa at the 90th day. The same mixture also displayed the highest flexural strength at the 90th day, reaching 6.5 MPa. The investigation concluded that performance of the bonds between succeeding layers being one of the major determining factors of anisotropic behavior. However, when loaded perpendicular to the printing direction, the performance of the 3D-printed specimens was equal or slightly better than that of the mold-cast ones.

2.5 Geopolymer Based Insulation Materials

The literature review focuses on geopolymer based insulation materials, which have gained significant attention in recent years in the building sector owing to their potential in enhancing energy efficiency. As an alternative to conventional insulating materials, geopolymers have promise qualities like fire resistance and minimal environmental impact [120]. The goal of this section is to give a thorough overview of the ongoing

research and development efforts in geopolymer-based insulating materials, including their composition, production methods, physical properties, and mechanical characteristics.

Top et al. [121] examined utilizing NaOH and Na_2SiO_3 as alkali activators to synthesize geopolymer concrete by mixing lightweight aggregates in combination with FA wastes. The produced geopolymer concretes were examined in connection to the alkali activator concentration, solid/liquid ratio, and curing temperature. Geopolymer concretes' mechanical characteristics are also assessed. The acidic pumice to fly ash ratio increased gradually throughout experiments. The uniaxial compressive strength values of the samples that were cured at 70 °C for 24 hours and samples cured at ambient temperature were compared. Despite the uniaxial compressive strength being close to one another after 28 days, high strength was attained early on as a result of the high temperature curing process, study revealed. The samples' uniaxial compressive strength enhanced as Na_2SiO_3 concentration was raised. The specimens were easier to deal with when the acidic pumice/fly ash ratio was increased. The study found that expanded perlite aggregates absorbed 200% water by its mass. In comparison to acidic pumice aggregates, pre-wetted expanded perlite aggregates enabled the development of lighter geopolymer samples (1250 kg/m^3). Expanded perlite aggregates were prewetted, which lowered the amount of alkali solution needed by 32.5%. Lightweight concrete sample uniaxial compressive strengths varied from 10 to 50 MPa.

Safari et al. [122] investigated the properties of pumice-based geopolymers under different curing conditions, various curing times, temperatures, and molarities of alkaline solutions. In the investigation, pumice utilized as a precursor was sized down to 63 μm. Alkali solutions were made up of a mixture of Na_2SiO_3 and NaOH solutions with molarities of 8, 10, 12, 14, 16, 18 and having NaOH/Na_2SiO_3 mass ratio of 2.5. Water-reducing admixture is added to the alkali solution 2% by mass of pumice before mixing to improve workability. For all specimens, the solution to binder rate was adjusted to be 0.35. According to test results, raising the molarity from 8M to 12M enhanced the compressive strength. Nevertheless, it was noted that the compressive strength decreased after 12M and reached its lowest level (12 MPa) at 18M at 28 days. The 12M specimens

that were cured under 80°C for 120 hours had the best strength at the 28th day (72 MPa). High temperatures and rapid curing periods can produce products with high early strength, whereas low temperatures and extended curing times produce geopolymers with greater strength than short curing times at higher temperatures. Without applying heat curing, the specimens under ambient conditions achieved 27.3MPa compressive strength. The flexural strength and compressive strength were both affected in the similar ways. The findings revealed that the ideal specimens are 10-12M with curing under 60°C for 72 hours. The curing temperature, curing length, compressive strength, and flexural strength were all taken into consideration. Due to its composition and curing circumstances, pumice-based geopolymer paste may cost 3 to 8 times more per cubic meter than ordinary paste, according to cost study for the mixes. As a conclusion, the optimal blend from a compressive strength/cost perspective is 12M cured under 100°C for 24 hours.

Wang et al. [123] investigated the effect of incorporation phase changing material (PCM) to clay geopolymer on its mechanical and thermal properties. The clay geopolymers examined in the study include PCM made by a vacuum absorption technique and expanded perlite. The geopolymer mortar was produced utilizing clay, water glass, blast furnace slag, and alkaline NaOH activators. Using a ratio of 1.5 SiO_2/Na_2O and a Na_2O content of 4% by mass of clay and slag, an alkaline activator solution is created. The PCM was created using perlite that had been soaked with paraffin and a capsule composed of $CaCl_2$ and glass water to restrict the perlite from leaking paraffin. Ratios of clay/slag=0.67, activator/binder=0.1, and water/binder=0.12 used in the research. The paraffin content was 55.47% by mass in the composite. PCM was used as a 30% volume replacement for the sand in the mixture. To evaluate both liquid and solid-state conditions of PCM, specimens were tested in cold and hot condition. When saturated expanded perlite was used, the compressive strength improved from 7.7 MPa to 7.8 MPa. Compressive strength is also enhanced to 8.0 MPa after PCM is encapsulated. In comparison to cold specimens, heated specimens had moderately lower compressive strengths. Additionally, the curing period of clay geopolymers has a significant impact on their compressive strength. Both PCM-encapsulated paraffin and EP-impregnated paraffin showed comparable results.

Wongsa et al. [124] studied the propoerties of lightweight high-calcium FA-based geopolymer concrete (LWGC). In research, high-calcium content FA is activated by Na_2SiO_3 and NaOH was employed as the geopolymer binder. Clay brick and pumice were utilized as aggregates. Compressive and splitting tensile strength, density and thermal conductivity of LWGCs are examined and compared to the characteristics of the control mixtures. In the study, different type of aggregates which sized between 75 μm to 9.5 mm is employed such as pumice and clay brick aggregate, with limestone aggregate and river sand. The alkaline activator was made using a 10M solution of NaOH and a constant fly ash to mass ratio of 0.7. Na_2SiO_3/NaOH mass ratios of 0.5, 1.0, and 1.5 were used for specimens. The test findings demonstrated that the specimens' slump decreased as the Na_2SiO_3/NaOH ratio increased. Additionally, due to looser texture of clay brick aggregate and pumice aggregate, LWGC comprising these aggregates have worse mechanical characteristics than those with natural aggregates. According to the research, the highest compressive strength of LWGCs comprising pumice aggregate was 7.0 MPa and clay brick aggregate had a maximum compressive strength of 18.3 MPa. The compressive and splitting tensile strengths of the LWGCs in general are increased by the increase in the Na_2SiO_3/NaOH ratio. However, the compressive and tensile strengths decreased as the Na_2SiO_3/NaOH ratio was raised further.

Z. Su et al. [125] investigated fly ash based geopolymer composites incorporating fibers and glazed hollow beads (GHB). The study evaluated geopolymer composite preparation and identified the ideal preparation conditions. Compressive and flexural strength, porosity, thermal conductivity and other miscellaneous parameters of geopolymers are analyzed. Three types of 6 mm length fibers polypropylene, alkali-resistant, and lignin fiber with ratios of 0 to 1% by total mass were utilized in this experiment to increase crack resistance and strength. Fly ash with a high aluminum concentration and slag with a high silicon and calcium content are used to make geopolymer paste. Fly ash with a high aluminum concentration and slag with a high silicon and calcium content are used to make geopolymer paste. In geopolymer paste, there are 30% GGBFS and 70% FA. The alkali activator was made using 14.5% water and 10M each of NaOH and Na_2SiO3. Adding GHB at ratios of 0%, 5%, 10%, 15%, and 20% by mass of solid components to the combination (fly ash, slag and GHB). The test findings indicated that with increased GHB level, the compressive and flexural strength of geopolymers dropped. It was also observed

that as fiber use increased, porosity decreased. Thermal conductivity was reduced by 84% by adding 20% GHB.

Pasupathy et al. [126] evaluated mechanical and thermal characteristics of geopolymer concrete that includes readymade foam and hydrophobic expended perlite. GGBFS and FA were used to make the geopolymer binder. In this investigation, sodium metasilicate anhydrous powder with a molar ratio of $SiO_2/Na_2O=1$ was utilized as the alkali activator. Powdered sodium metasilicate was made into a solution. By using %0, %10, and %20 of the binder, hydrophobic expended perlite was added to the mixture as a porous aggregate. In the mixtures, fine sand is also utilized as an aggregate. Premade foam is incorporated into mixes during the mixing stage. Additionally, the same quantity of polyvinyl alcohol fiber was used in each mixture. Flexural and compressive strength tests were performed on specimens to determine their mechanical characteristics. The TCi thermal conductivity instrument was used to assess the geopolymer specimen's thermal conductivity. According to test results of the study, the 7-day compressive strength improved from 300 to 840 kPa (65%) and the 28-day compressive strength increased from 480 to 1380 kPa (188%) when the expanded perlite ratio was elevated from 0 to 20%. Fine air gaps also increased when used perlite and ready-made foam were added to the system, improving its mechanical and thermal performance. Utilizing hydrophobic expended perlite also helped to increase pore uniformity. The thermal conductivity of the mixes with 10% and 20% hydrophobic expended perlite addition reduced thermal conductivity by 1.8% and 12.1%, respectively.

Gao et al. [127] performed long-term aging experiments on the porous geopolymer at a temperature of 50°C and a relative humidity of 98% to examine the durability of geopolymers. Compressive strength and thermal conductivity tests are performed on the specimens. The raw materials utilized were perlite and rock wool, while the alkali activator was Na_2SiO_3 solution. In addition, foaming agents H_2O_2 and foam stabilizers cetyltrimethylammonium bromide were both used. In the investigation, three distinct mixtures were produced. The ratio of perlite to sodium silicate in two of the mixtures is 0.8 and 1.2, respectively. The third mixture has 4% rock wool and a perlite/sodium silicate ratio of 1.2. The test findings show that Na cations have an impact on the porous

geopolymer's stability and that particular cations can even dissolve the gel binding. When the samples were preserved in HCl or $CaCl_2$ solution, geopolymerization is improved. Additionally, it was discovered in the investigation that the Cl anion and the Na cations in the matrix interact, preventing the Na cations from dissolving the geopolymer gel's bonds and enhancing the stability of the samples. It was determined that as the samples age over time, the porous perlite geopolymer continues to polymerize, enhancing the samples' compressive strength, lowering their porosity, and increasing their density. Fresh density of the mixtures varied from 0.146 to 0.178 g/cm^3, thermal conductivity of the mixtures differed from 0.046 to 0.064 W/m·K while compressive strength of the samples was ranged between 0.17 to 0.35 MPa.

Łach et al. [128] studied fly ash-based foam geopolymers. The investigation establishes the connection between the density of foam geopolymers and thermal conductivity. Geopolymer samples analyzed by strength tests and thermal conductivity tests. The alkaline solution mixture used in the experiment is composed of 14M NaOH with Na_2SiO_3 solution and liquid glass in a 1:2.5 ratio. As a foaming agent, H_2O_2 is utilized. Microspheres and H_2O_2 were combined with fly ash to create a geopolimer foam. The mix was placed in plastic molds and dried in a lab drier for 24 hours at 75°C. 7 different combinations were formulated in the study. According to the results, the compressive strength and the thermal conductivity coefficient were both influenced by the density of the geopolymer foams. The density and compressive strength of the material decreased as H_2O_2 concentrations increased. Thermal conductivity values range from 0.0826 to 0.1273 W/m·K, whereas the compressive strengths of the specimens range from 1.9 MPa to 3.4 MPa. The investigation also revealed that materials equivalent to fly ash may be used to produce geopolymer foams with a density of 400 kg/m^3 and a thermal conductivity of less than 1 W/m·K.

Kabay et al. [129] investigated the properties of geopolymer materials. Pumice powder and GGBFS are used to create the geopolymers in this work, which are then activated using solutions of NaOH, KOH, and Na_2SiO_3. In the study, siliceous sand and pumice are both employed as fine aggregate. The geopolymer specimens had a water/binder ratio of 0.34 and included 80% pumice powder by mass of binder. Separate studies were done on

NaOH and KOH as well as their combination with Na_2SiO_3. NaOH was utilized as 4M, 6M and 8M while KOH was employed as 6M in all specimens. KOH/Na_2SiO_3 ratio was 1.0 by mass. The results of the study revealed that adding more NaOH to the combination decreased its workability but employing KOH as an activator had the reverse effect. The paste specimens with mixtures of 4M NaOH and KOH had the greatest compressive strength, whereas those with 6M NaOH exhibited the least compressive strength. The maximum strength was measured at 6M KOH with SS and a KOH/Na_2SiO_3 ratio of 1. The strength of geopolymer mortars was found to decrease as pumice powder concentration increased. The strength of the geopolymer mortar was 10.6 MPa for 80% pumice powder and 20% GGBFS and 24.5 MPa for 50% pumice powder and 50% GGBFS. Higher pumice powder content was observed to have the lowest oven-dry density, which ranges from 1927 to 1873 kg/m^3. The thermal conductivity of the mortar was dropped by adding extra pumice, and the best thermal conductivity results were obtained by using 70% pumice powder (0.558 W/m·K).

Kakali et al. [130] investigated the development of FA-based geopolymers using expanded polystyrene (EPS). In this work, the geopolymer specimens were mainly evaluated for mechanical strength, thermal conductivity and fire resistance. F class fly ash activated with Na_2SiO_3 and NaOH are used to create geopolymer paste. Si/Al=2.4, Na/Al=0.85, and solid to liquid ratio of 2.8 were chosen for mixtures. In the range of 0.5-3% weight by weight, six varieties of EPS were put to the test. The mixes were cast in 50x50x50mm cubic molds. The compressive strength of geopolymers containing EPS differed based on the variety of EPS, ranging from 7.7 MPa to 29.57 MPa with a density range of 0.97-1.57g/cm^3, according to the test. The control geopolymer, on the other hand, showed 56 MPa compressive strength while having a density of 1.77g/cm^3. Due to its combination of compressive strength and density, which are 11 MPa and 1.05g/cm^3, respectively, geopolymer with 3% EPS addition is selected for further examination in the study. Flexural strength measurements for the reference mixture and the selected mixture were 6.03 MPa and 2.15 MPa, respectively. Geopolymer samples' thermal conductivity was evaluated using the Heat Flow method. While testing the specimens, the mean temperature was fixed at 10°C, and the temperature difference was 10°C. Thermal conductivity coefficients for the reference material with 0% EPS addition and the selected combination with 3% EPS addition were 0.30 and 0.16 W/m·K, respectively.

Wan Mastura et al. [131] investigated the correlation between the compressive strength and density of a lightweight geopolymer. Fly ash with a combination of NaOH and Na_2SiO_3 as an alkaline activator are used to produce geopolymers. The samples of geopolymer are also evaluated for their thermal insulating properties. Polyoxyethylene alkyether sulfate, a synthetic foaming agent, was employed as the foaming agent in this study. The ratio of Na_2SiO_3/NaOH used in the investigation was 2.5 by mass with a 12M NaOH solution. Na_2SiO_3 and NaOH solution were combined to create alkali solution. Foaming agent included to the paste made of adding alkaline solution and fly ash. The paste was then placed into molds and allowed to dry for 24 hours at 80°C before being tested. The test findings revealed that when the samples' densities decreased, there was an increase in the overall amount of air spaces, which decreased thermal conductivity and compressive strength of the samples. The lowest thermal diffusivity and thermal conductivity measured in the study were 0.26 mm^2/s and 0.63 W/m·K, respectively.

Posi et al. [132] examined the characteristics of lightweight geopolymer concrete that incorporated recycled lightweight aggregate. In this study, recycled lightweight aggregate is created using lignite fly ash, Na_2SiO_3, NaOH in concentrations of 5M, 10M, and 15M, and recycle lightweight block (RLB). In the experiment, three distinct mixes are created. The effects of alkaline to ash ratios, Na_2SiO_3/NaOH ratios, concentration of NaOH, curing temperature, and aggregate/ash ratios on compressive strength and density were the major subjects of the research. In the investigation, liquid alkaline/ash ratios were examined between 2 and 2.8, and the best compressive strength was found at 2.4 liquid alkaline/ash ratio with 10 M NaOH concentration. Additionally, the compressive strength increased from 2 to 11 MPa as the fine aggregate ratio increased. The density slightly increased as the liquid alkaline/ash ratios increased. Additionally, the compressive strength likewise shown an upward trend as the Na_2SiO_3/NaOH ratio, NaOH molarity, and curing temperature were raised. The mixtures' porosity increased with the incorporation of light aggregate, thereby reducing the density.

Ming et al. [133] investigated the effect of integration of lightweight aggregate and foam in the lightweight aggregate geopolymer concrete. Class F fly ash was employed as a precursor in the investigation, and a ratio of 2.5 of Na_2SiO_3 to NaOH was used as an alkali

activator. In the mixtures, expanded clay and river sand employed as coarse and fine aggregates, respectively. Hydrogen peroxide (H_2O_2) was used in the experiment as a foaming agent. According to the study's findings, the LWAGC had a density range of 1689–1815 kg/m^3, which is 8% less dense than geopolymers without lightweight aggregate. The density of the mixture was reduced to 1426–1593 kg/m^3 by the inclusion of the foaming agent. Since the samples had a lower density than the required 1850 kg/m^3, they were categorized as lightweight concrete. According to the study's findings, the LWAGC had a density range of 1689–1815 kg/m^3, which is 8% less dense than geopolymers without lightweight aggregate. Since the samples had a lower density than the required 1850 kg/m^3, they were categorized as lightweight concrete. The density of the mixture was reduced to 1426–1593 kg/m^3 by the addition of the foaming agent. The geopolymer paste utilized in the research had a thermal conductivity of 0.683 W/m·K, according to the measurements. When expanded clay aggregate was added, the thermal conductivity was lowered by 83% to 0.09–0.12 W/m·K, while samples that included foaming agent had thermal conductivity decreases of up to 46% to 0.07–0.09 W/m·K.

Shahedan et al. [134] investigated the effects of glass bubble in geopolymer concrete to improve its thermal insulation properties. River sand was employed as the fine aggregate in the study in 40% of the total mass of aggregate, while gravel was used as the coarse aggregate in 60% of the total mass. Additionally, F class FA, glass bubbles with a spherical form as a thermal insulation material, and Na_2SiO_3, NaOH as an alkali activator were employed. Glass bubbles were added to geopolymer concrete samples at rates of 2.5%, 5.0%, 7.5%, 10.0%, 20.0%, and 30.0% during the experiments. The density of geopolymer concrete was reduced by the addition of glass bubbles. The density of geopolymer exceeded the upper limit (2000 kg/m^3) for lightweight concrete, according to experimental findings. While the sample without glass bubble had a 28-day compressive strength of 71.4 MPa, the sample with 30% glass bubble had a compressive strength of 16.4 MPa. The samples' water absorption rates were between 3-6.5% of those of conventional concretes. Additionally, experiments have shown an inverse relationship between the thermal conductivity and the ratio of glass bubbles. The thermal conductivity value for the control sample without a glass bubble was 1.65 W/m·K, and the density was 2247 kg/m^3. Consequently, there was a general reduction in thermal conductivity of 20.44%.

3. MATERIALS AND METHODOLOGY

3.1 Materials

Materials utilized in the study are categorized into three subtopics: precursor CDW materials, alkali activators, and aggregates.

3.1.1 Precursor CDW Materials

CDW-based precursors, including RCB, HB, RT, C, and G were used for the production of geopolymer binders. These CDWs were sourced from chosen demolition sites in diverse urban renewal zones in Ankara, Turkey. Images of the precursors are shown in Figure 3.1. RCB, HB, and RT were obtained from multiple types of bricks that were gathered from the demolished walls, and roofs of the buildings. C was obtained from the demolished structural members of buildings such as columns and beams. The concrete pieces containing reinforcement and aggregates were only separated from the reinforcement and collected without separating the aggregates inside it. The windows of the structures as well as broken and glasses which cannot be recycled allowed for the collection of G, which is another kind of precursor.

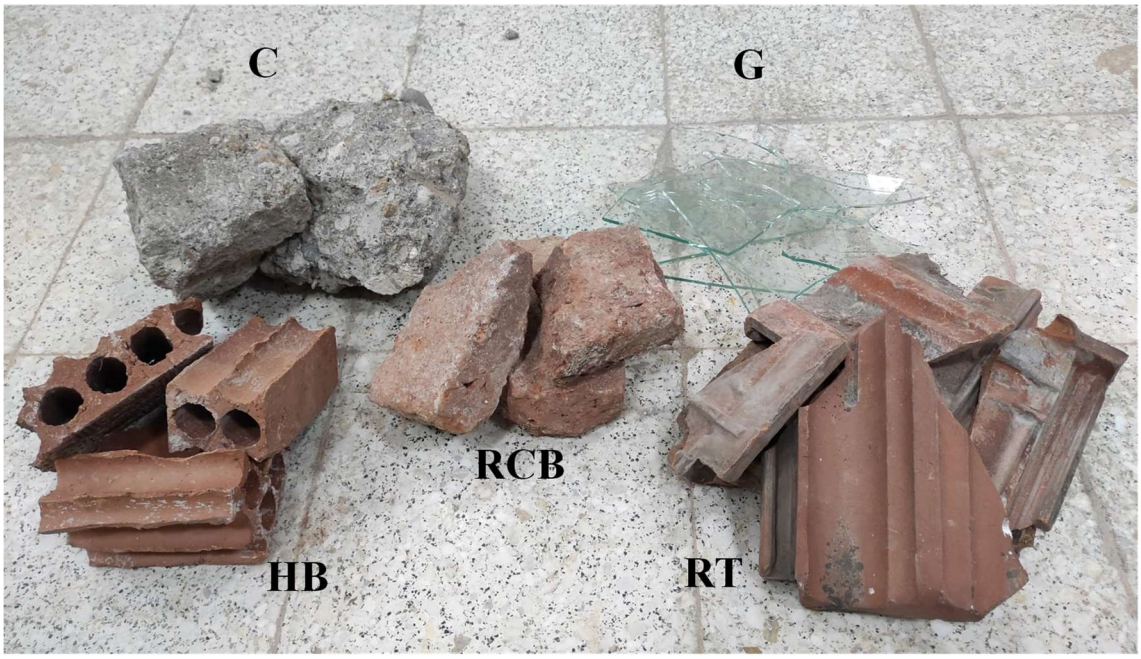

Figure 3.1 Representative images of CDW precursors in raw form

All these CDWs collected separately from the demolition sites were transported to the laboratory and each type of waste was crushed separately in the jaw crusher in order to

reduce their size for milling. Maximum discharge aperture of the jaw crusher is set to approximately 1 mm. The jaw crusher used is given in Figure 3.2.

Figure 3.2 Lab-type jaw crusher

After all type of CDWs were crushed and the particle size was reduced, materials were laid on a metal tray and dried in an oven at 105 °C for 24 hours to prepare them for milling process. Oven dried CDW materials were then ground into powder form individually in a ball mill for 60 minutes. The ball mill used for the milling process is given in Figure 3.3.

Figure 3.3 Lab-type ball mill

Preparation and representative images CDW-based precursors are given in Figure 3.4.

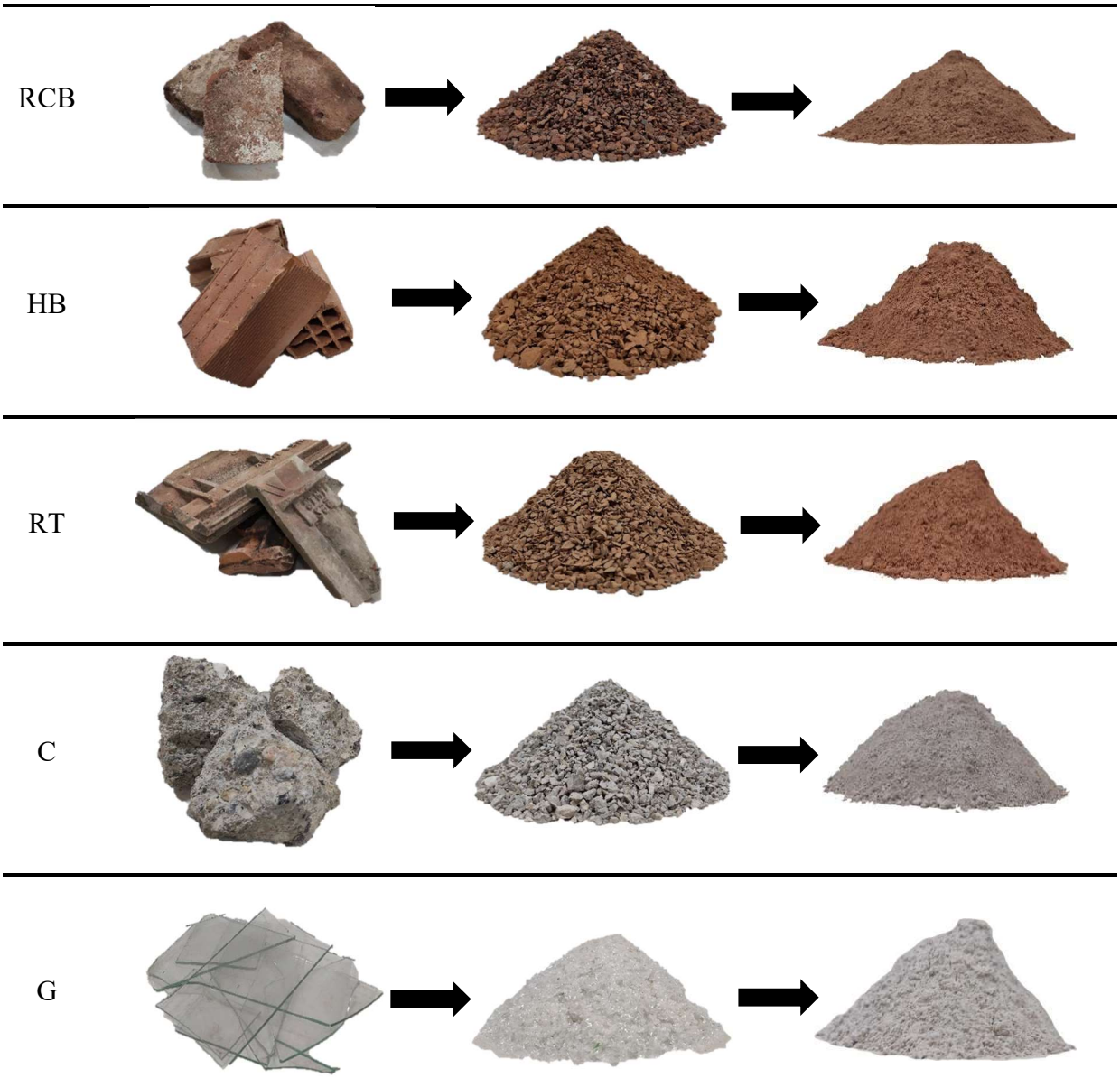

Figure 3.4 CDW precursors (from left to right; raw, crushed and milled)

In order to determine oxide composition (Table 3.1) and particle size and range distribution (Figure 3.5), X-ray fluorescence (XRF) and particle size distribution (PSD) analysis are applied on CDW-based powder formed precursors. Particle size and distribution analysis was carried out using the Mastersizer 2000, which has a measurement size boundary of 0.02-2000 μm and uses laser diffraction technique. XRF analysis was performed using the energy dispersive spectrometer device. Analyzed

samples were taken from different sections of each milled batch. Specific gravity of CDWs are also shown in Table 3.1.

As can be viewed from Table 3.1, SiO_2, Al_2O_3, and Fe_2O_3 were found to be predominant oxides in brick-based materials RCB, HB, and RT. The fourth major oxides in these brick-based CDW materials were CaO. In general, brick-based materials have a similar oxide composition. Additionally, C contains large quantity of SiO_2 and CaO, while minor amounts of MgO and Al_2O_3 are present in it. On the other hand, SiO_2 percentage in G is very high as expected since it is obtained from soda-lime based window glasses from demolished buildings. Chemical compositions of precursors indicate that CDW-based materials contain SiO_2, Al_2O_3, and Fe_2O_3 which are essential for geopolymer formation reactions [135–137]. Lastly, CDW-based materials with the highest and lowest specific gravities are HB and G, respectively.

Table 3.1 Oxide composition of CDW precursors

Oxides	Concentration (%)				
	RCB	**HB**	**RT**	**C**	**G**
SiO_2	41.7	39.7	42.6	31.6	66.5
Al_2O_3	17.3	13.8	15	4.8	0.9
Fe_2O_3	11.3	11.8	11.6	3.5	0.3
CaO	7.7	11.6	10.7	31.3	10
Na_2O	1.2	1.5	1.6	0.5	13.6
MgO	6.5	6.5	6.3	5.1	3.9
SO_3	1.4	3.4	0.7	0.9	0.2
K_2O	2.7	1.6	1.6	0.7	0.2
TiO_2	1.6	1.7	1.8	0.2	0.1
P_2O_5	0.3	0.3	0.3	0.1	0
Cr_2O_3	0.1	0.1	0.1	0.1	0
Mn_2O_3	0.2	0.2	0.2	0.1	0
Loss of Ignition (%)	8	7.8	7.5	21.1	4.3
Specific Gravity	2.81	2.89	2.88	2.68	2.51

Figure 3.5 represents the grain size distribution of CDW-based geopolymer precursors milled in a ball mill for 60 minutes. Despite clay based materials RCB, HB, and RT having almost the same size distribution, C and G materials are coarser. While approximately 95% of the grain size of the clay based materials were below 45 μm, ~82% of the C and ~69% of the G material were below 45 μm. G was the coarsest material

among CDW-based powder form precursors. Varying grindability characteristics and hardness values of materials might explain observing different particle sizes despite applying milling for the same amount of time. Since grinding all CDWs to have a similar particle distribution would cause ineffectiveness in terms of cost and energy, no additional application was made on the materials in terms of particle size.

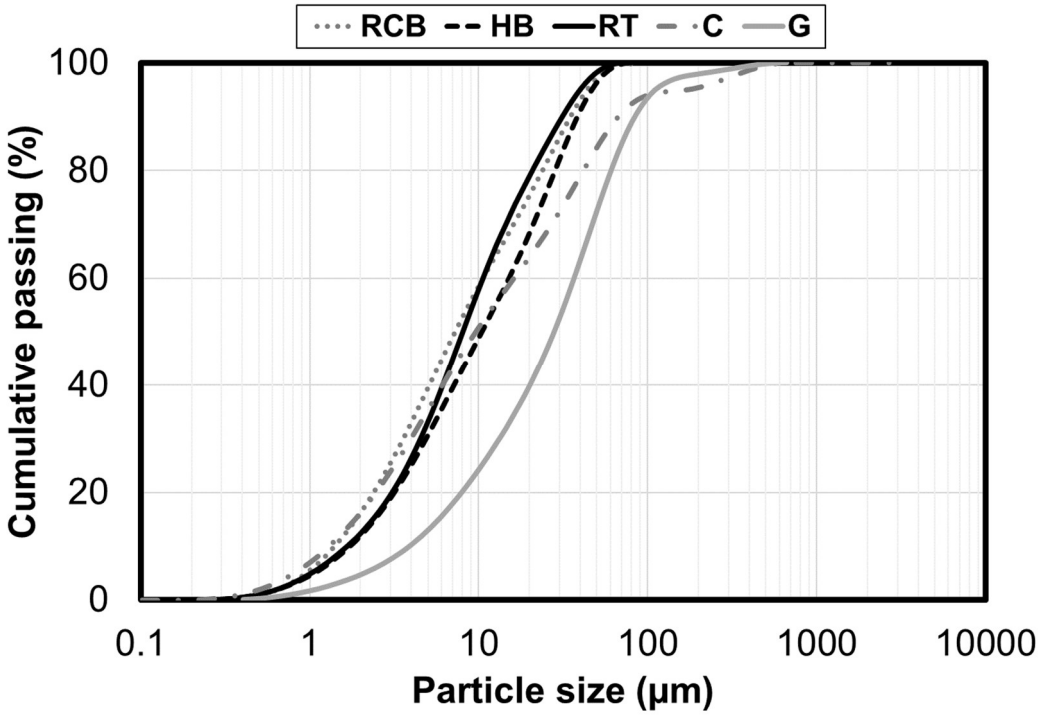

Figure 3.5 Particle size distribution of CDW precursors

Figure 3.6 presents the results of a SEM study performed from a distance of 10 mm in a vacuum of 30 kV. All of the CDW-based precursor materials were in angular shape following the crushing and milling procedures.

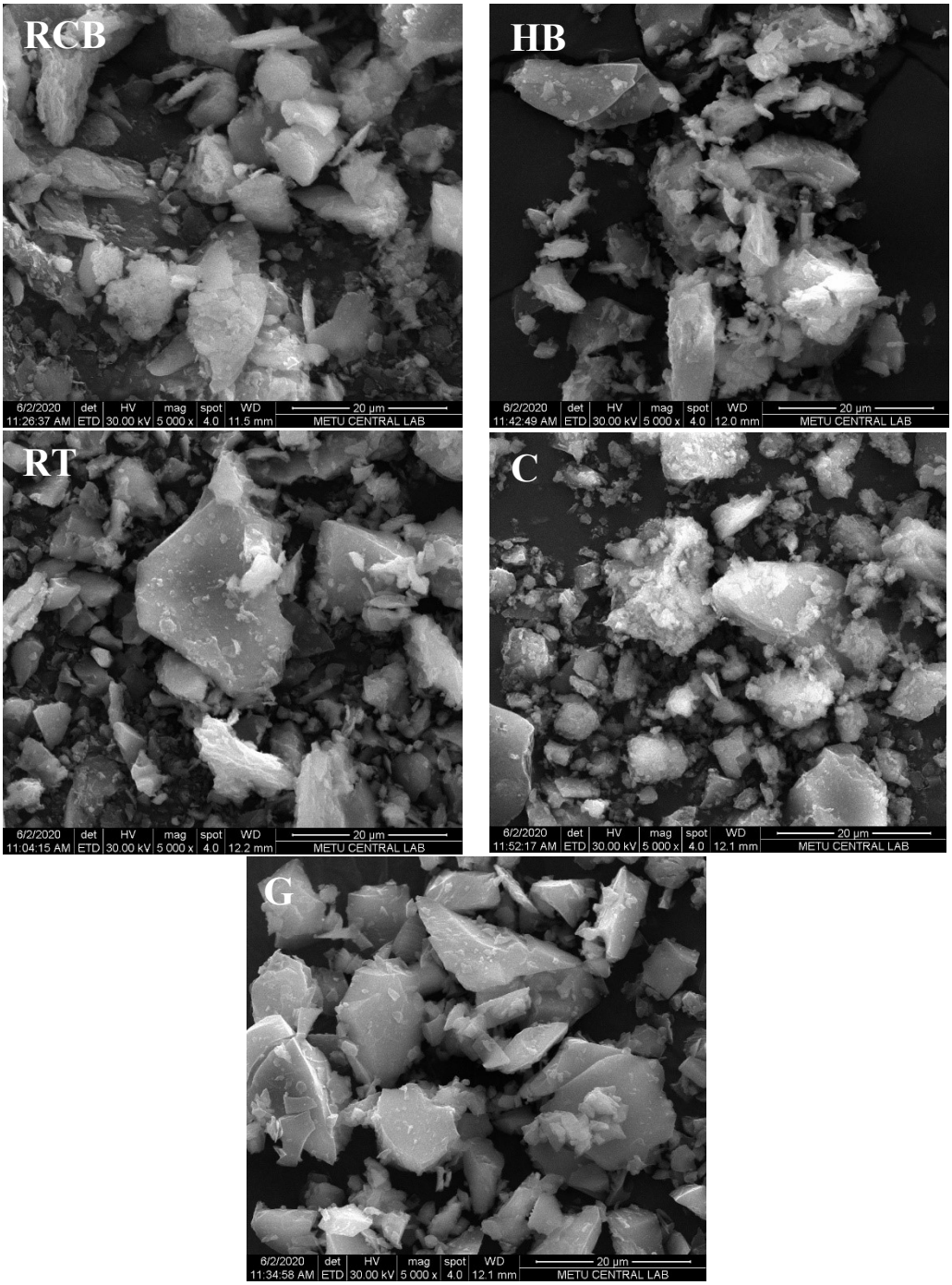

Figure 3.6 SEM analysis of CDW-based materials

Crystallographic structures of all CDW-based materials were investigated using X-ray diffraction (XRD) analysis, as seen in Figure 3.7. Materials were scanned between 5 and 55° using a portable benchtop XRD device, the Olympus BTX. The XRD analysis of the CDW-based materials revealed that clay-based RCB, HB, and RT show similar patterns with main peaks of Quartz and Diopside around 26-27 and 27-28°, respectively, with moderate Mullite peaks in varying angles. Crystobalite crystals were also observed in

clay-based RCB and HB. The Akermanite is only observed in RCB as a minor phase around 24°. The scanned main peaks for C were Quartz, Diopside, and Calcite alongside minor peaks of Mullite and Foshagite. Lastly, G was in the amorphous phase, as expected. The chemical formula of the crystalline structures identified from XRD analysis of CDW-based precursors as well as the powder diffraction file (PDF) numbers are given below.

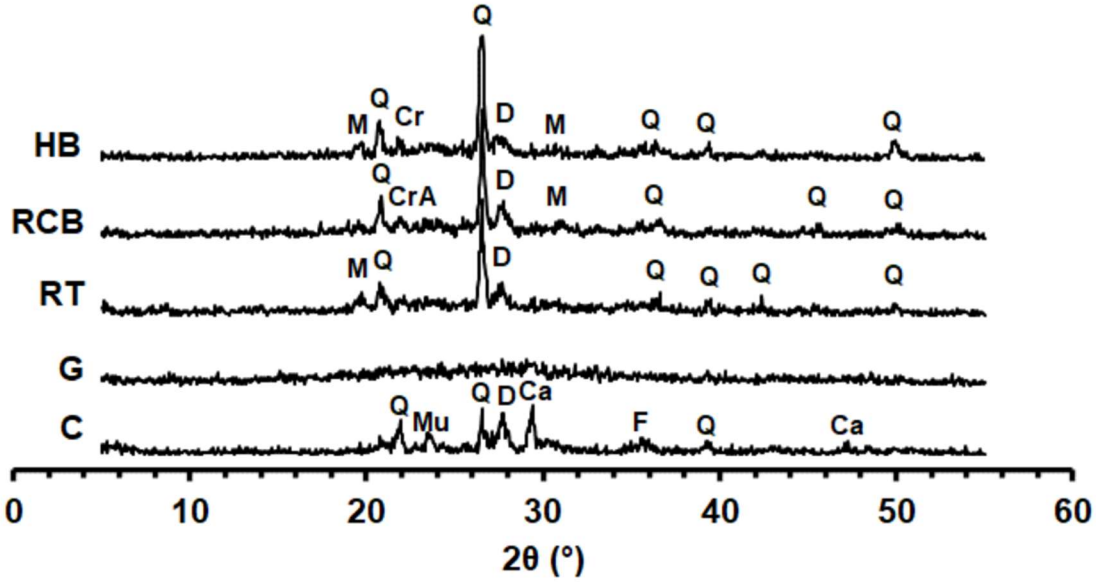

Crystalline Phase	Symbol	PDF Number	Chemical Formula
Quartz	Q	96-101-1160	SiO_2
Crystobalite	Cr	96-900-8230	SiO_2
Diopside	D	96-900-5280	$Al_{0.6}CaMg_{0.7}O_6Si_{1.7}$
Mullite	M	96-900-5502	Al_2O_5Si
Akermanite	A	96-900-6115	$AlCa_2Mg_{0.4}O_7Si_{1.5}$
Calcite	Ca	96-900-9668	$CaCO_3$
Muscovite	Mu	96-101-1050	$Al_3H_2KO_{12}Si_3$
Foshagite	F	96-901-1044	$Ca_4H_2O_{11}Si_3$

Figure 3.7 XRD pattern and corresponding crystals of CDW-based precursors.

3.1.2 Alkaline Activators

In this study, CDW-based precursors were activated using the alkaline activators NaOH and $Ca(OH)_2$. In the subtopics, specific information regarding alkali activators is provided.

3.1.2.1 Sodium Hydroxide (NaOH)

Sodium, oxygen, and hydrogen make up the chemical compound known as NaOH, also known as sodium hydroxide. It typically exists as a solid white substance and easily

dissolves in water [138]. NaOH is also known as caustic soda and can be in solid flakes or beads form. It has no smell. Since NaOH has strong basic characteristics, can be used to create alkaline solutions and control pH. The use of NaOH cover a variety of sectors, including the production of paper, soap and detergent, textiles, cleaning supplies, and water treatment.

Sodium hydroxide functions as an activator as part of the geopolymerization reaction [139]. The key elements of the geopolymer binders, aluminosilicates, interact with the alkali activators throughout the activation process. NaOH releases Na^+ and $(OH)^-$ ions that increase the environment's alkalinity and catalyze the synthesis of the geopolymer binder by the hydrolysis of silicate and aluminate groups. High alkalinity is essential for initiating geopolymer reactions. NaOH concentration significantly affects the mechanical characteristics as well as the chemically formed structure of geopolymers [118,140].

In this study, NaOH utilized in the geopolymerization process is KOSFLAKE® product of Koruma Klor Alkali Sanayi ve Ticaret Anonim Şirketi. The provided NaOH is in a flake form (Figure 3.8) and contains a minimum 98 percentage sodium hydroxide along with a maximum of 0.10% sodium chloride.

Figure 3.8 NaOH (in flake form)

3.1.2.2 Calcium Hydroxide ($Ca(OH)_2$)

The process of hydrating calcium oxide, which naturally exists as limestone, produces the chemical $Ca(OH)_2$, which is composed of the elements of calcium, oxygen, and hydrogen. It commonly exists in the form of a white solid and dissolves easily in water. Another

name for $Ca(OH)_2$ is slaked lime. As hydroxyl ions (OH^-) are released when calcium hydroxide is dissolved in water, it exhibits alkaline characteristics and is categorized as a strong base. It is used in numerous commercial, industrial and domestic applications such as chemical processes, water treatment, pH adjustment, leather processing and more.

$Ca(OH)_2$ can also be used in geopolymerization reactions due to being a strong base. $Ca(OH)_2$ releases the ions of Ca^{+2} and OH^- when dissolved in water, thus increasing the level of the alkalinity similar to the NaOH and catalyzing the synthesis of the geopolymer binder [141]. Additionally, it speeds up the hardening process and increases the viscosity of the mixture [142]. Moreover, $Ca(OH)_2$ contributes to enhance the strength gain of geopolymer by promoting the production of more gel products [118,142]. $Ca(OH)_2$ takes on a crucial function as an alkali activator and calcium source in the geopolymerization process as a result of these advantages. In this thesis, $Ca(OH)_2$ supplied by Tekkim Kimya Sanayi Ticaret Ltd. Şti. was used. Provided $Ca(OH)_2$ (Figure 3.9) has a minimum purity of 87% and contains a maximum of 1% magnesium oxide.

Figure 3.9 $Ca(OH)_2$ (in powder form)

3.1.3 Recycled Concrete Aggregate (RCA)

As mentioned before, concrete waste was utilized as a precursor for geopolymer binder production. In addition to this, RCA, obtained from the end-of-life concrete which constitutes the majority of CDW materials [143], was used as the aggregate in the geopolymer binders to maximize the upcycling of concrete waste. Concrete wastes collected from demolition sites were crushed in a jaw crusher individually to minimize particle size to produce RCA. The specific gravity of RCA is 2.5. The crushed RCA was sieved to obtain the desired particle size RCA (Figure 3.10).

Figure 3.10 Representative image of the RCA

The maximum grain size of RCA was chosen to be 4.75 mm to show the viability of 3D printing utilizing mixtures comprising aggregates with even larger size. Particle size distribution of the RCA is given in Figure 3.11. The goal was to create low-cost geopolymer mortars with the least amount of processing possible and allow for the efficient use of larger-sized aggregates.

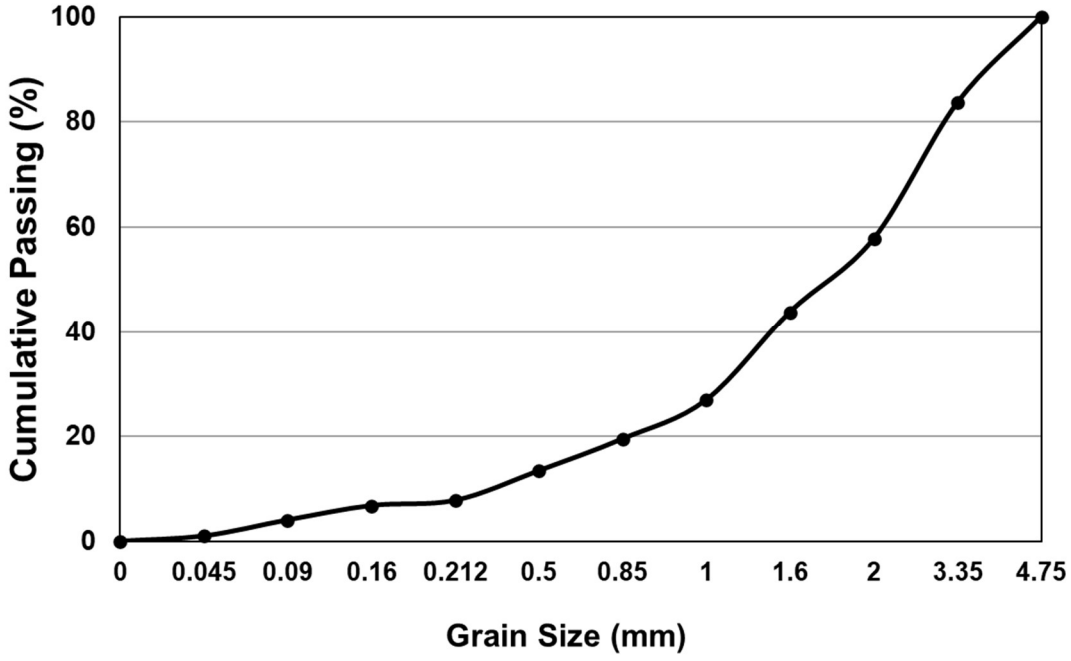

Figure 3.11 Particle size distribution of the RCA

3.1.4 Expanded Perlite Aggregate (EPA)

Perlite, a naturally formed volcanic rock, undergoes expansion when subjected to high temperatures. Perlite is formed during expansion process of the vaporization of trapped water within the volcanic rock obsidian at high temperatures. When heated to temperatures between 1400 and 2000°C, perlite expands up to 20 times its original size, which results in a large increase in volume. This process of expansion results in a porous, lightweight expanded perlite with tons of internal bubbles. The expanded perlite has a lower density and more porosity as a consequence of these bubbles. Furthermore, expanded perlite's distinct porous structure provides beneficial properties like thermal and acoustic insulation. The high melting point of expanded perlite also results in great resistance to fire, acting as a natural fire barrier and preventing the spread of flames. Expanded perlite is white, although raw perlite can range from gray to black in appearance. The oxide compositions and specific gravity of expanded perlite are shown in Table 3.3.

Table 3.2 Oxide compositions of EPA

Oxides	Concentration (%)
	EPA
SiO_2	75.49
Al_2O_3	14.31
Fe_2O_3	1.29
CaO	0.98
MgO	0.23
SO_3	0.001
Na_2O	0.52
K2O	5.49
TiO_2	0.12
Cr_2O_3	0.03
Mn_2O_3	0.09
P_2O_5	0.04
SrO	0.01
Ba	0.09
Loss of Ignition (%)	1.31
Specific Gravity	0.16

Expanded perlite is provided with 100-liter bags. EPA with a maximum grain size of 4.75 mm was sieved to be utilized in the geopolymer mortar mixes. Particle size distribution of EPA is given in Figure 3.12. A typical picture of the EPA is also shown in Figure 3.13.

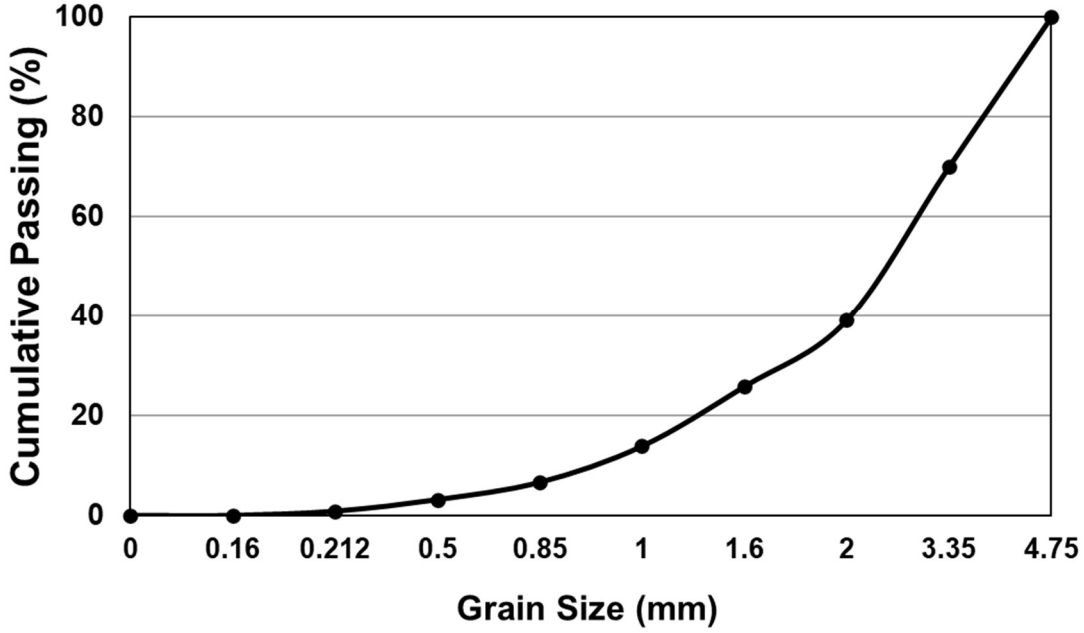

Figure 3.12 Particle size distribution of the EPA

Figure 3.13 Representative image of EPA

3.2 Methodology

3.2.1 Mixture Proportions

The mixture proportions of geopolymer binder were determined by the preliminary studies carried out by the author [119]. In this context, 80% of the dry mixtures of the geopolymer mortars by weight were composed of clay based RCB, HB, and RT materials. Equal proportions of clay based RCB, HB, and RT materials were used as 26.67% by weight in the mixture due to the similarity of physical and chemical properties. The individual usage ratio of C and G was set to 10%.

After each type of geopolymer mortar was prepared at 0.35 water/binder (w/b) at the mixing stage, different amount of extra water was added to the mixtures to have similar flowability properties and thus to be successfully pumped and extruded. It was not possible to prepare comparable and printable mixtures for the same w/b ratio for all types of mixtures. Developed geopolymer mortars were alkali activated by employing 10M NaOH and 4% $Ca(OH)_2$ by weight of the total amount precursors. Detailed mixtures proportions are presented in Table 3.4.

Table 3.3 Proportions of the geopolymer mixtures

Mix ID	Ag. (% vol. of total Ag.)		Ag./Pr. Ratio (by vol.)	W/B	Dry Mixture (g)							Alkali Activators (g)	
					Precursors					Aggregates			
	RCA	EPA			RCB	HB	RT	C	G	RCA	EPA	$Ca(OH)_2$	NaOH
PE0	100	0	1.68	0.45	266.7	266.7	266.7	100	100	1500	-	40	140
PE25	75	25		0.43						1125	24		
PE50	50	50		0.42						750	48		
PE75	25	75		0.41						375	72		
PE100	0	100		0.41						-	96		
PE100-M	0	100	2.28	0.46						-	130		

Note: Ag.: Aggregate, Pr.: Precursor, Vol.: Volume, W/B: Water/Binder

The aggregate/precursor ratio for reference (PE0) mixture which is incorporated solely RCA was chosen to be 1.68 by the total weight of the precursors. Due to EPA having a very low density, it was substituted to RCA in the mixtures by volume of total aggregate while keeping the total volume of the aggregate in all mixtures constant except for PE100-M. The PE100-M mixture was developed to constitute the maximum limit for the EPA content in the 3D printable geopolymer mortars. This maximum limit was determined in

the preliminary studies. More specifically, the mixture coded as PE25 contains 25% EPA and 75% RCA by volume of the total aggregate in that mixture. The PE100 mixture contains the same volume of EPA aggregate as the total volume of RCA aggregate incorporated in the PE0 mixture.

3.3 Mixture Preparation

The preparation stage of the mixtures commenced with the preparation of the NaOH solution. The required amount of the flake form NaOH was weighed and added to tap water in a glass container to prepare 10M NaOH solution. After adding tap water to NaOH and mixing, the caps of solution containers are tightened immediately to prevent water evaporation. Containers were then reserved in the laboratory to naturally cool down until reached ambient temperature. This is due to prevent the effects of high temperature of the alkali solution on the geopolymerization reaction and fresh state characteristics of the geopolymer mixtures since the reaction between NaOH and water is exothermic. Then, required amount of the powder materials, also named as dry mixture which is composed of precursors and $Ca(OH)_2$ activator were mixed with a laboratory type mortar mixer at slow speed for 60 seconds. Prepared NaOH solutions were slowly added to the dry mixture and mixed at a slow speed for 60 more seconds. After that, the required type and amount of aggregates and essential amount of extra water is gently added in the mixtures to have similar flowabilities (for a given mixture proportion) was slowly added to the homogenously mixed geopolymer paste one-by-one and mixed at a slow speed for 90 seconds at medium speed, completing the mixture preparation process. The laboratory type mixer is shown in Figure 3.14.

Figure 3.14 Lab-type mortar mixer

Upon analyzing the 6 designed mixtures in terms of their density, mechanical and thermal characteristics, three different mixtures were selected for 3D printing studies. These mixtures include the one with the highest compressive strength and lowest insulation property control mix (PE0), the one with average strength and insulation property (PE75), and the one with the lowest thermal conductivity and mechanical properties (PE100-M). The selected geopolymer mortar mixtures for 3D printing were prepared using a pan-type laboratory mixer shown in Figure 3.15. First, the dry mixture was added to the pan mixer and homogenized for 2 minutes. After that, the NaOH was slowly incorporated into the prepared dry batch while the mixer is operating. The NaOH solution was previously cooled down to room temperature. Once all the alkali solution was poured to the dry mixture, the mixture was allowed to blend for an additional 3 minutes until a homogeneous geopolymer paste was achieved. Geopolymer mortars were finally obtained by adding the required type of aggregates based on the mixture proportion and mixing for further 5 minutes.

Figure 3.15 Lab-type type mixer

3.4 Specimen Preparation and Curing

The prepared geopolymer mixtures were carefully poured into prismatic molds with dimensions of 40×40×160 mm for conducting flexural strength tests. Geopolymer mortars were likewise filled in 50 mm cubic molds to determine the ambient cured compressive strength and high temperature resistance of the mixtures. Another set of prismatic molds with dimensions of 300×300×30 mm were filled with mortars for thermal conductivity experiments. A two-step procedure was followed to make sure the geopolymer mortars in the molds were properly compacted and air voids are removed. The molds were first half-filled before being vibrated for 15 seconds on a vibrating table. The molds were then completely filled up and exposed to vibration once again for a total of 15 seconds. All the prepared samples were stored in ambient for 24 hours, then they were removed from the molds and cured in ambient conditions (23±2 ℃ and 50±5% relative humidity) until testing ages of 7, 14 and, 28 days. In order to measure the fresh densities of geopolymer mortars, they were poured in a tared container with a known volume in two layers. Between and at the end of pouring layers, the container was tilted

10 times on its opposite sides, and then weighed. Fresh densities of the mixtures were calculated by dividing the material weight in the container by the container volume. On the 28th day, geopolymer samples were weighed for measurement of the dry density. By dividing the weights of the 3 weighted samples from each mixture by their volumes individually, the dry densities of the mixes are determined. Figure 3.16 shows the mold used for the preparation of samples and the geopolymer samples removed from the molds after 24 hours.

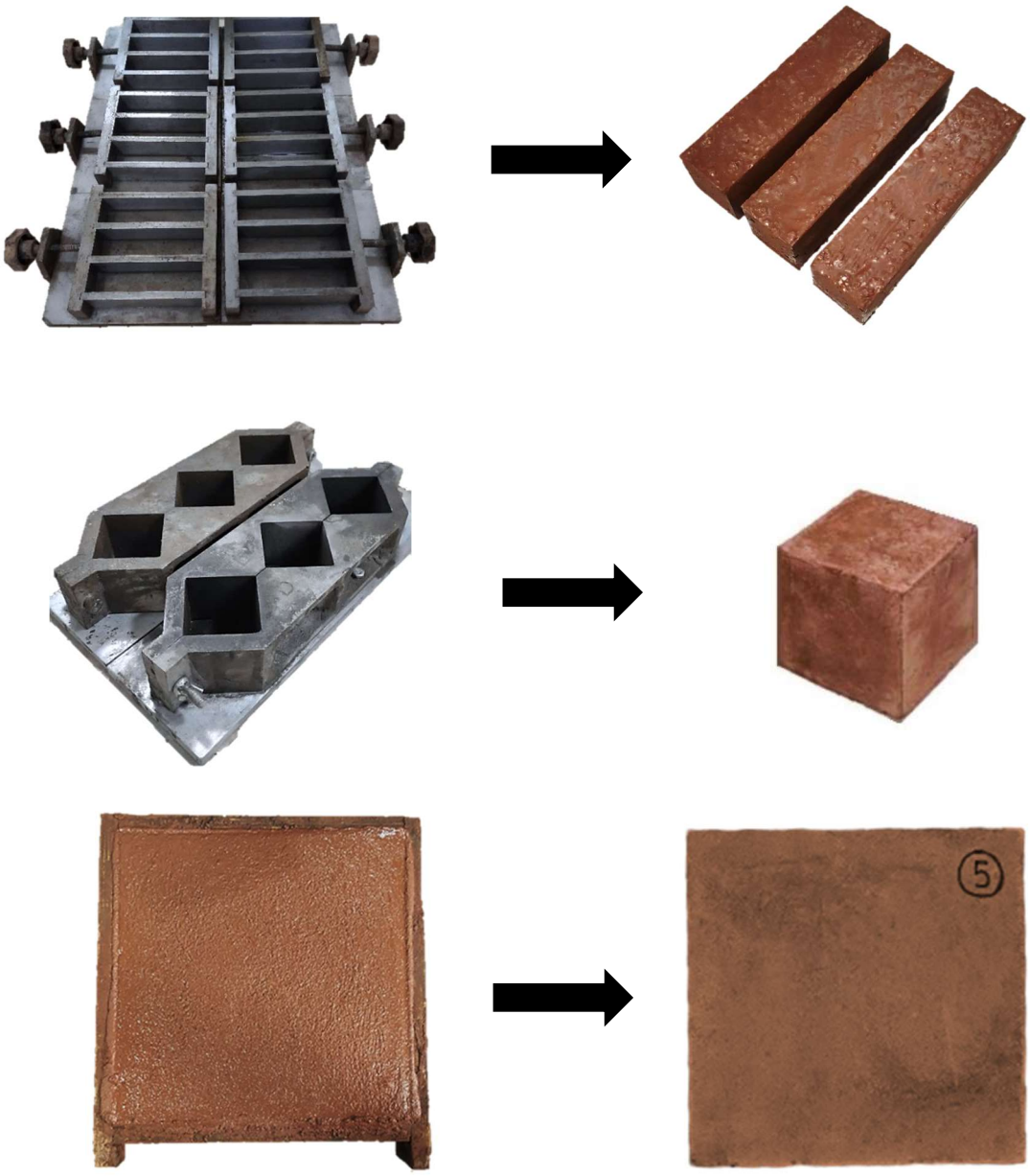

Figure 3.16 Specimen molds and geopolymer samples

In 3D printing applications of the study, a laboratory-scale 3D-printer is utilized, serving as a prototype for the industrial gantry-type 3D-printers. A CNC router, a computer-controlled machine designed specifically for 3D printing, is main component of the 3D printing system. The system also includes a mortar pump that feeds the geopolymer mortar along with a mortar transmission line that is attached to the pump. Other units of the system are a printing platform, a nozzle for material deposition, and a computer control unit that manages the entire printing operation. The printing path is defined by converting the designed shapes for 3D printing into texts in G-code (geometric code) format and loading the code to the CNC router. In other words, G-code guides the machine and determines the path that the machine will follow.

The printer and schematic diagram of the 3D printing system is illustrated in Figure 3.17.

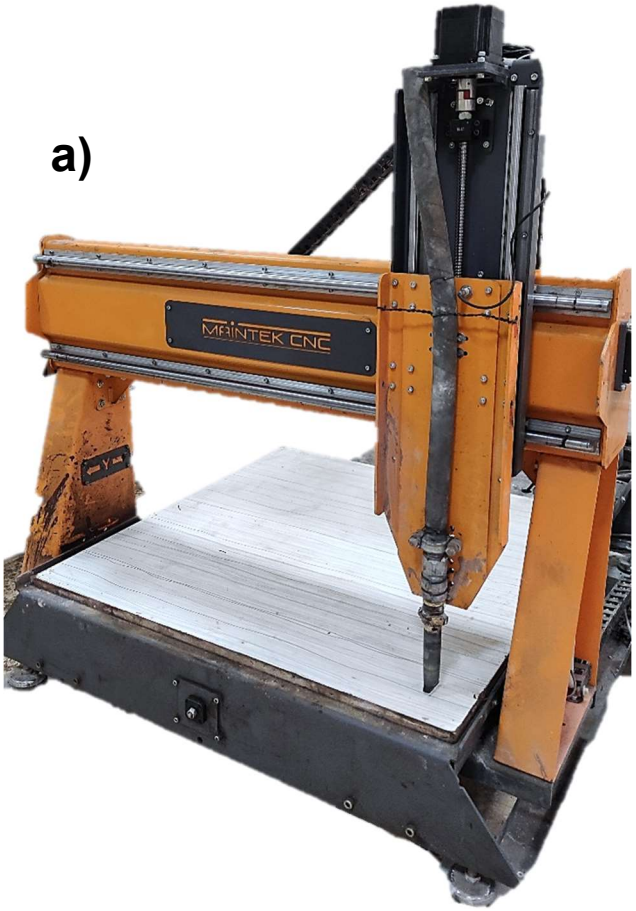

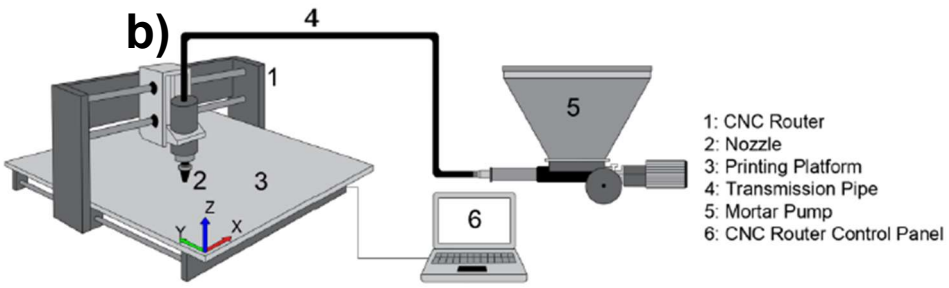

Figure 3.17 General view of 3D printing system a) Lab-scale 3D-printer, b) Schematic diagram

The prepared geopolymer mortars were transferred to the mortar pump and 3D printed through a 20x40 mm rectangular nozzle which is connected to the CNC router. Travel speed of the nozzle was set to 60 mm/s. 800 mm length, 40 mm thickness double layer lines with 40 mm height were created by extruding PE0, PE75 and PE100-M mixtures to assess the effect of EPA substitution on overall quality of the printed units. Printed lines are demonstrated in Figure 3.18.

Figure 3.18 3D printed filaments

In addition, a 10-layer wall with a height of 20 cm and a length of 32 cm, representing a scaled-down version of a masonry wall, was 3D printed with the PE100-M mixture. Moreover, the mixture was visually examined in terms of cracking and rupturing while 3D printing in a low-angle zigzag path. Lastly, a multi-layered geopolymer specimen with thickness of 30 mm is printed by adding successive layers to each other in a parallel direction to the printing platform. A 300x300x30 mm thermal plate was then extracted

from the printed sample using a spatula before the material get hardened to analyze the thermal insulation capacity of the 3D printed insulation plate of the PE100-M mixture. The 3D printed plate sample was cured under ambient conditions until testing age. Extraction steps of 3D printed plate is presented in Figure 3.19.

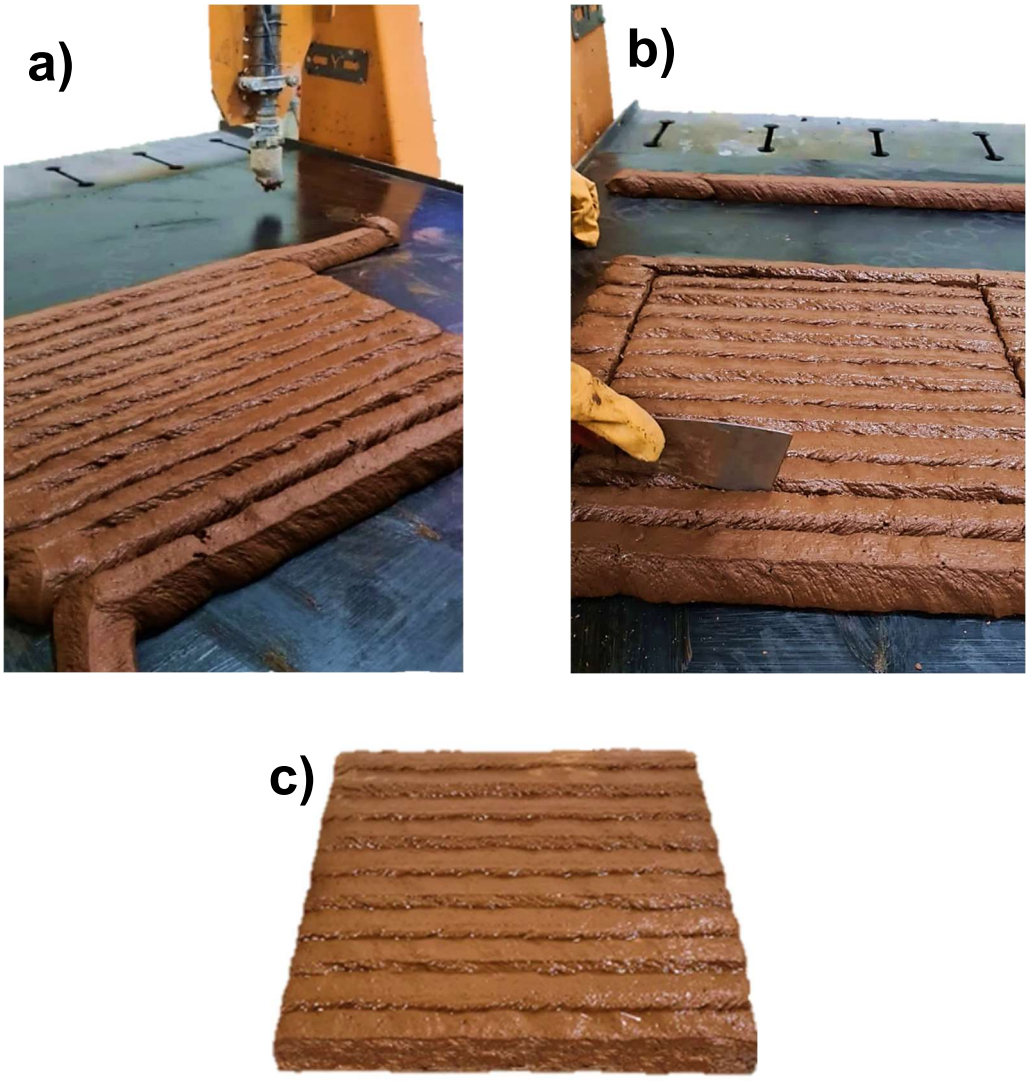

Figure 3.19 Production of 3D printed thermal plate, a) multi-layered 3D-printed shape, b) extraction of plate sample, c) the thermal plate after extraction

3.5 Testing

The test methods used in this study are based on the determination of the fresh rheological characteristics, measurement of the fresh density of mixtures to correlate it with thermal insulation property, assessment of mechanical properties, and fire resistance of the 3D printable lightweight geopolymer mortars. Open time flow table and buildability tests are performed to pre-assess the rheology of the mixtures at fresh state for 3D printability properties while a thermal conductivity test is applied on the 28th day to assess the thermal insulation capability of geopolymer mortars containing different types and amounts of aggregates. In addition to that, compressive and flexural tests on ambient-cured geopolymer lightweight samples were performed on the 7, 14, and 28th days. Moreover, compressive strength of the specimens upon elevated heat exposure was examined in order to determine the fire resistance of 28-day ambient-cured geopolymer mortars.

3.5.1 Flow Table Test

Flow table tests have been conducted in accordance with ASTM 1437 [144] to assess the flowability of geopolymer mixes at fresh state, immediately after their preparation. In this test, the geopolymer mortars was poured halfway into the conical mold, which was placed on the flow table. Then, mold was tamped 20 times to ensure the mixture is uniformly filled. After that step, a second layer of geopolymer mixture was added until the mold is full, then tamped again. Overspilling material on the mold was removed by sweeping a trowel across the top of the mold. One minute after the filling was done, the mold was removed. The table was then dropped 25 times continuously in the following 15 seconds. Finally, the maximum diameter of spread and the spread diameter perpendicular to the first measurement axis was measured and noted. After initial measurement at the 0th minute, each specimen was tested at the 30th, 60th, and 90th minute to measure the open time flow characteristics of the mixtures. According to Sahin et al. [117], this empirical method could be used to assess applicability of mortars for 3D printing. The schematic view of flow table test is given in Figure 3.20.

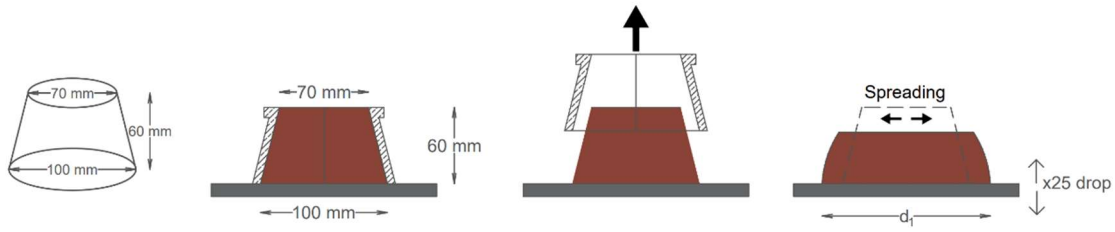

Figure 3.20 Schematic view of the flow table test

The flowability index was calculated from the recorded spread diameters of the geopolymer mortars using the equation shown below, where d_1 denotes the highest spreading diameter and d_2 denotes the spreading diameter perpendicular to d1 and d_0 is the inner diameter of the mold.

$$\Gamma = \frac{d_1 d_2 - d_0^2}{d_0^2}$$

The determined flowability index and the visually inspected 3D printing quality of the mixtures were correlated. The results obtained from this correlation as well as the mechanical and thermal properties of mortars allowed the selection of the most effective mixture for 3D printing.

3.5.2 Buildability Test

Buildability, another important property for 3D printing, is the capacity of the newly printed material to maintain its original shape under the influence of the weight of successive layers that are constantly overlapping, without exhibiting large deformations and collapsing until it reaches a sufficient height [145]. There are several non-standardized test techniques for evaluating the buildability of mixes in the literature. The first buildability assessment method which is performed in this study is suggested by Nematollahi et al. [146] and inspired by the ASTM C1437 flow test adapted to be compatible with material behavior analysis. First, a mini-slump cone was filled with geopolymer mixtures according to this method. 1 minute after filling, the cone was gently lifted and separated from the geopolymer mixture. A load of 600 grams was applied to the upper surface of the material for 1 minute by ensuring that the load was homogeneously distributed with the help of a round plate placed between the load and the

material. The slump is measured right after removing the load and recorded on the Z axis from 2 non-opposite sides. The mixture with the lowest average slump value was defined as the mixture with the most buildable and shape retention ability. In order to determine the open time buildability characteristics of the mortars, the modified mini-slump test is performed at the 0^{th},30^{th}, 60^{th}, and 90^{th} minute after mixture preparation. Schematic view of the buildability test is shown is Figure 3.21.

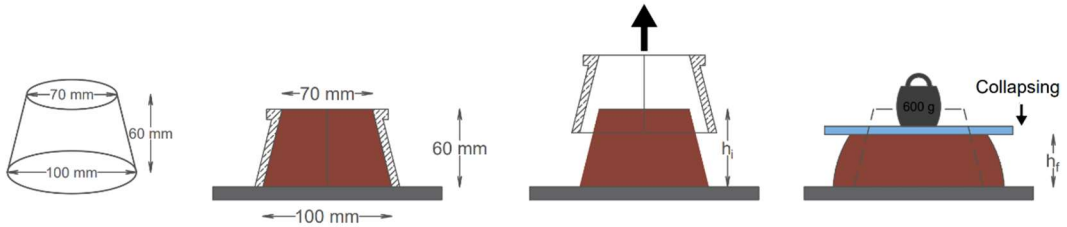

Figure 3.21 Schematic view of the buildability test

In the second method used in this study to assess the ability of buildability of the selected geopolymer mixture, the material was printed at a height of at least ten layers without interruption. If it was observed that there was no visual deformations and noticeable changes in the geometry of these printed elements the mixture was defined as buildable.

3.5.3 Flexural Strength Test

The 40×40×160 mm prismatic geopolymer specimens cast for the flexural strength testing using a 200 kN load capacity universal testing machine at 100 N/s testing speed under three-point loading at the 7, 14, and 28^{th} days. The flexural strength of each type of mortars was determined by testing three identical samples and averaging the strength results. The flexural strength of each tested specimen is calculated by using the formula below where F_f is the load exerted to the sample's midpoint at the moment when it breaks. Distance between supports (100 mm) denoted as l and the specimen's square cross-section's side length is indicated by the letter b (40 mm).

$$\sigma_f = \frac{1.5F_f l}{b^3}$$

Representative image of flexural testing is represented in Figure 3.22

Figure 3.22 Representative image of flexural testing of the specimens

3.5.4 Compressive Strength Test

Compressive strength test is carried out according to ASTM C109 standard on the cubic samples. Geopolymer samples are loaded at a rate of 900 N/s using a hydraulic test equipment. For each geopolymer mixture, a total of 3 specimens were tested at 7, 14 and 28th days. The average compressive strength of the mortar mixture was then determined. The compressive strength test is demonstrated in Figure 3.23.

Figure 3.23 Representative image of compressive testing of the specimens

3.5.5 High Temperature Resistance Test

The geopolymer mixtures that were poured into pre-lubricated 50 mm cubic molds were extracted after 24 hours and subsequently cured at ambient conditions for a period of 28 days until the day of testing. All samples were placed in an oven set at 80℃ for 24 hours to dry prior to exposing high temperatures as shown in Figure 3.24.

Figure 3.24 The geopolymer samples placed in an oven to dry

Oven dry samples were then placed in a high-heat capacity oven at room temperature and subjected to a heating rate of 5℃ per minute until the oven reached target temperatures. After exposing specimens to the 300, 600, and 900℃ for 60 minutes, the samples were allowed to reach room temperature inside the oven. The same procedure was followed 3 times individually for target temperatures of 300, 600, and 900℃. Finally, a compressive strength test is applied following the same procedure with ambient cured specimens to investigate how the mechanical characteristics of the mortars changed and estimate the residual strength of the geopolymers under high heat exposure. Three cubic samples were prepared for three different temperature values from each type of mixture, therefore a total of 9 cubic specimens were tested for each individual mixture type. The images from heating process are given in Figure 3.25.

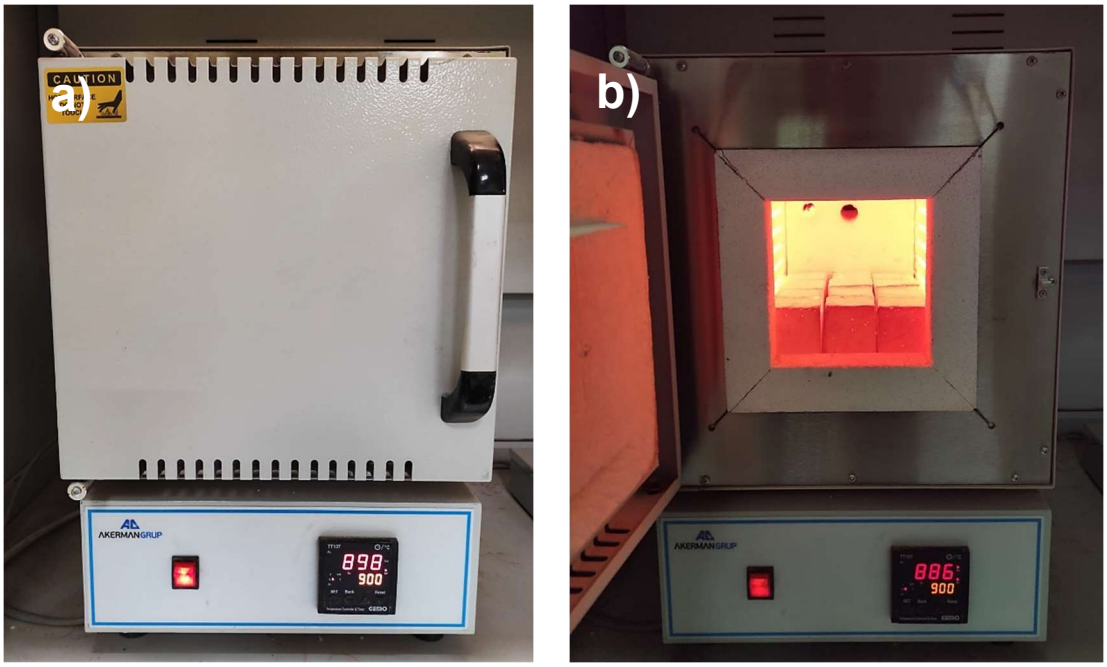

Figure 3.25 High temperature exposure of the samples, a) the oven set to 900 ℃, b) geopolymer samples after exposing of 900℃

3.5.6 Thermal Conductivity Test

The thermal conductivity of the geopolymer plate samples tested based on the ASTM C518 [147] standard. Flat surface plate-shaped prismatic specimens were inserted between hot and cold plates of the testing device. Over the whole thickness of the material, a temperature gradient is established. The thermal conductivity coefficient (TCC) of the sample between plates of the device is determined in W/m·K by the interaction of the sensors with the material in contact with the material surface. The thermal conductivity of all cast and one 3D-printed geopolymer plate samples are tested to compare their insulation properties. All plate samples at 28 days were dried at 105 °C for 24 hours in a dryer to remove any moisture content prior to the test.

4. RESULTS AND DISCUSSION

4.1 Open Time Rheological Behavior Change of the Geopolymer Mortars

Open-time rheological performance of the material is significant in terms of applicability in 3D printing applications. In the study, open-time flow table and buildability tests were performed on 3D printable lightweight geopolymer mortars to determine open-time rheological properties of the mixtures and the effect of EPA substitution on the flowability and buildability properties were presented in Figure 4.1 and Figure 4.2, respectively. Open time tests were conducted at the 0^{th}, 30^{th}, 60^{th}, and 90^{th} minute after the geopolymer mortars were prepared. In the experiments, the change in the flowability index and buildability over time is crucial to estimate how mixtures perform in 3D printability in the fresh state and how 3D printability characteristics changed over time.

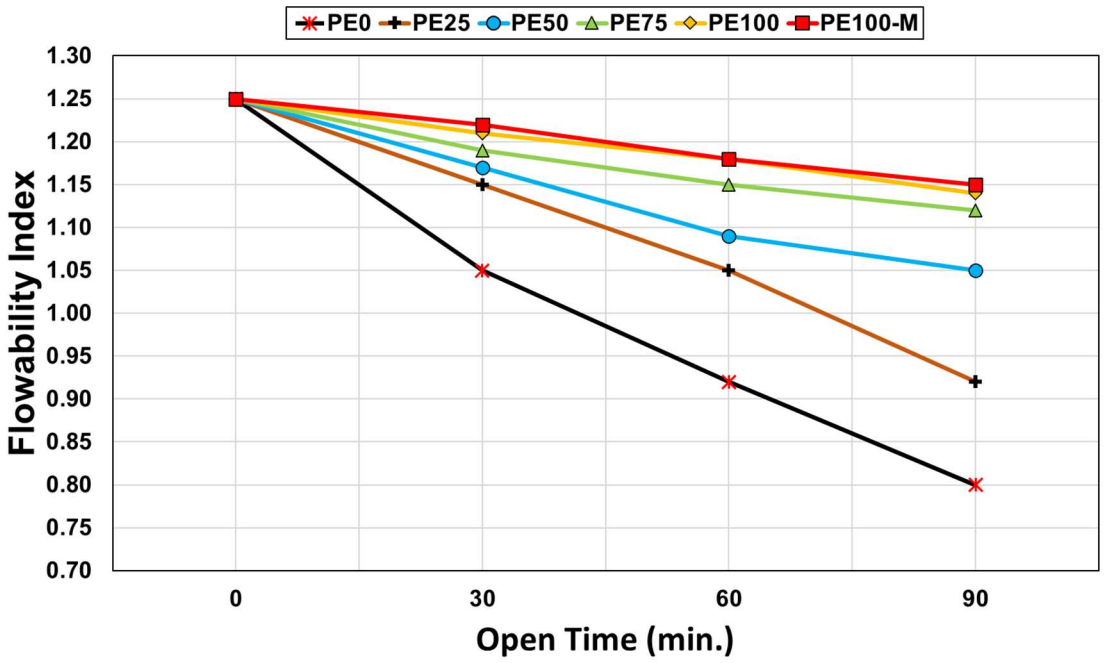

Figure 4.1 Open time flowability indexes of geopolymer samples

The overall flowability indexes decreased as expected at 30, 60, and 90 minutes after the mixtures' preparation as shown in Figure 4.1. This was due to the ongoing geopolymerization reactions over time [118]. There was no significant change in flowability index values for the mixtures containing EPA higher than 75% (PE75, PE 100, PE100-M) from 0 to 90th minutes. In contrast, PE0, PE25, and PE50 experienced a relatively higher reduction in flowability during the testing period. This can be explained

by different aspects related to aggregate type, content, and size. In the case where RCA was used entirely, the ongoing geopolymerization reactions of RCA as well as the additional hydration due to the un-hydrated cement content can cause the matrix to exhibit a rapid stiffening behavior [148]. Besides, if EPA is present in the matrix, it is expected that flowability will decrease after a certain substitution rate due to increased water demand of EPA [149]. However, the output observed in the present study was that increasing the amount of EPA increased the workability and flowability, in line with the literature [150–152]. This was attributed to the increase in the air content of the mixture due to the porous structure of EPA [150,151]. This positive effect of EPA on fresh properties was decisive in achieving the same base flowability indexes (1.25) for lower w/b ratios. Another noteworthy output is that for 75% and above EPA content (PE75, PE100, PE100-M), the flowability index could be significantly maintained for a prolonged open time. Considering that the ability of mixtures to maintain their flowability properties for a long time is critical in 3D printing technique, it is evident that mixtures with high EPA content have very suitable characteristics for 3D printing.

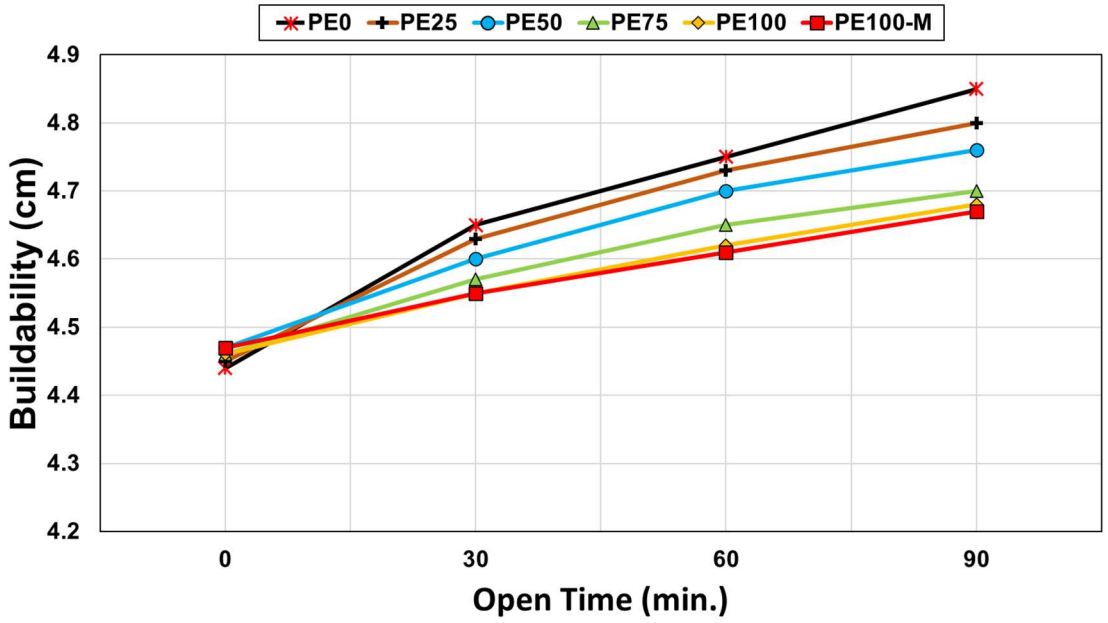

Figure 4.2 Open time buildability indexes of geopolymer samples

Figure 4.2 illustrates the buildability results of the geopolymer mixtures, which have the same flowability. At the initial stage, immediately after the mixing, the buildability values were found to be quite similar, in a range of 4.4-4.5 cm. This was not only a sign of a successful reflection of the flowability-based design but also a validation of the high

buildability performance of RCA and EPA-based geopolymer mixtures. On the other hand, the buildability values of the EPA-based geopolymers were slightly higher than the RCA-based geopolymers. This can be attributed to the decreased density of the mixtures as the included EPA amount increased, hence the lessened influence of the gravitational force. Besides, this positive influence of the EPA can be supported by the hydrophilic nature of EPA, which causes it to absorb water in a medium [153,154] and increase the consistency of the mixture. For all testing durations after the initial stage, the EPA-based mixtures' buildability values were lower than the RCA-based mixture. Moreover, the buildability values decreased as the EPA content increased. This can be explained by the increased workability of the EPA-based mixtures, even if produced with lower water content than RCA-based ones. Besides, the water retention ability of the EPA can decelerate the geopolymerization of the mixtures; thus, the mixtures' stiffening duration can prolong. This outcome is beneficial for 3D-AM since the process requires adequate open time to accomplish the production without any collapse.

Overall, in this section where open-time rheology was examined, a significant difference between 0 to 90th minutes was not observed among the mixtures except for the PE0, PE25 and PE50 mixtures. Considering that the 3D printability performance of mixtures with different aggregate contents and types will be examined in the later steps by 3D printing applications, the fact that the mixtures to be 3D printed showing similar fresh properties will be beneficial to directly examine the 3D printability characteristics and 3D printing quality of the mixtures without depending on the rheological parameters.

4.2 Effect of EPA Substitution on Density of the Geopolymer Mortars

The influence of EPA on the fresh and dry density of 3D printable geopolymer mortars is shown in Figure 4.3. Replacement of RCA with EPA in the mixtures decreased the fresh and dry density of mortars overall as observed from the measurement results. In other words, EPA substitution rate was inversely proportional to the density of geopolymer mortars. This can be explained by EPA having a lower specific gravity value than RCA. The use of aggregate with a lower specific gravity value reduced the fresh and dry density of geopolymer mortars. Also, considering the amount of extra water added to the mixtures to have similar fresh properties, excessive water in the matrix may have caused the

formation of internal air voids thus, a decrease in density for mixtures with a relatively high w/b ratio [155].

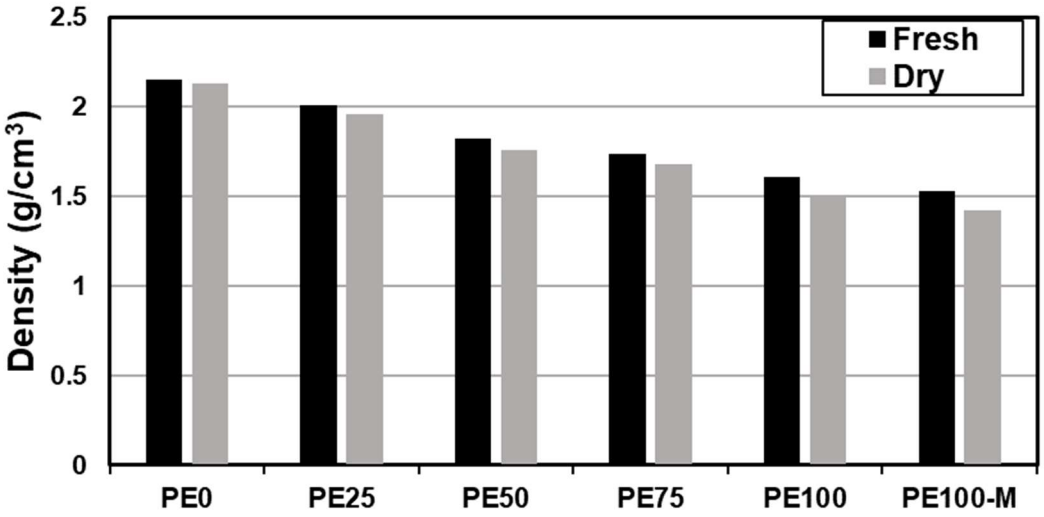

Figure 4.3 Fresh and dry density of geopolymer mortars

According to the measurements shown in Figure 4.3, the fresh (1.53 g/cm^3) and dry density (1.42 g/cm^3) of the PE100-M mixture containing the highest percentage of EPA was 29 % and 33% less than the fresh (2.15 g/cm^3) and dry density (2.13 g/cm^3) of the base mixture PE0, respectively. The fresh and dry density of the PE100 mixture was determined as 1.61 and 1.51g/cm^3, respectively. The fresh and dry density of the PE75 mixture was measured to be 1.74 and 1.68 g/cm^3, while the dry density of the PE50 mixture is 1.76 g/cm^3. According to the ACI Committee 213 [156], lightweight concrete has an equilibrium density of 1120 to 1920 g/cm^3. Accordingly, mixtures PE50, PE75, PE100, and PE100-M can be classified as lightweight mortars.

It should be noted that the high-volume coarser EPA grains might be damaged and crushed by pressure in the mixing and molding process, have lost their porosity, and occupied less volume in the mixture [157]. This resulted in an increase in variation in the calculated and apparent density of the mixtures as the incorporation of EPA increased. Therefore, a lesser volume of mortar might be obtained for high incorporation of EPA. Similar findings were remarked by the authors in the literature. Verma et al. [158] reported that the mixing technique is highly influential on the breakdown of perlite particles and the density of the produced material. Arifuzzaman et al. [159,160] also

reported that EPA particles are fragile and prone to damage while mixing with binder resulting in a high density to strength ratio.

4.3 Effect of EPA Substitution on Mechanical Properties of the Geopolymer Mortars

The mechanical properties of lightweight geopolymer mortars are as significant as their low densities and low thermal conductivities. The mechanical strength of the printable lightweight geopolymer mortars differed with the replacement of RCA in the mixtures. The average compressive and flexural strength values of 7, 14, and 28-day-old 3D printable geopolymer mortars including the different percentages of RCA and EPA are presented in Figure 4.4 and 4.5. According to Figure 4.4 and 4.5, compressive strengths of geopolymer mortars were found to be between 5.2 to 13.2 MPa after 28-day ambient curing, and flexural strength after 28-day ambient curing varied from 1.4 to 3.9 MPa. The test results indicate that when the substitution rate of EPA increases, the compressive and flexural strength decreases. The compressive and flexural strength of the 28-day-old PE100-M mortar decreased by 60.7% and 63.6% compared to the PE0 specimen on the same curing day, respectively. The main reason of that strength of the mixture tends to decrease with the addition of EPA in all curing days is that the lower density and higher void ratio of the EPA compared to RCA [161]. Since density has a major influence on mechanical properties, the low density of EPA reduced the mechanical strength of mortar [162]. Loss of strength with increasing rate of EPA was reported in other studies in the literature [121,163,164]. The influence of reducing the molarity of the NaOH by up to 2.5M by adding extra water to the mixtures on compressive strength was neglected as compressive strength change by the reduction of NaOH from 10 to 7.5M was minor reported by Ilcan et al [118]. All 3D printable lightweight geopolymer mixtures developed in this study intended be used more intensively in masonry construction due to the nature of the 3D-AM production method. For this reason, it is crucial that the developed novel materials fulfill the mechanical requirements of relevant standards in order to demonstrate viability. The acceptable range of the compressive strength of mortars to construct masonry walls should be between 1.4 and 14.6 MPa, according to TBEC 2018 [165]. IBC 2015 [166] specifies that masonry must have an average compressive strength of 2.07 MPa. The compressive strength of the PE100-M mixture (5.2 MPa) which has the maximum amount of EPA has minimum compressive strength

among all specimens. All mixtures met the minimum strengths in the specified standards for masonry at the end of the 28 days curing period. Moreover, PE0 mixture achieved 13.2 MPa compressive strength at day 28 and complied with the MSJC-determined standards for compressive strength for masonry constructions (10.34-27.58 MPa) [167].

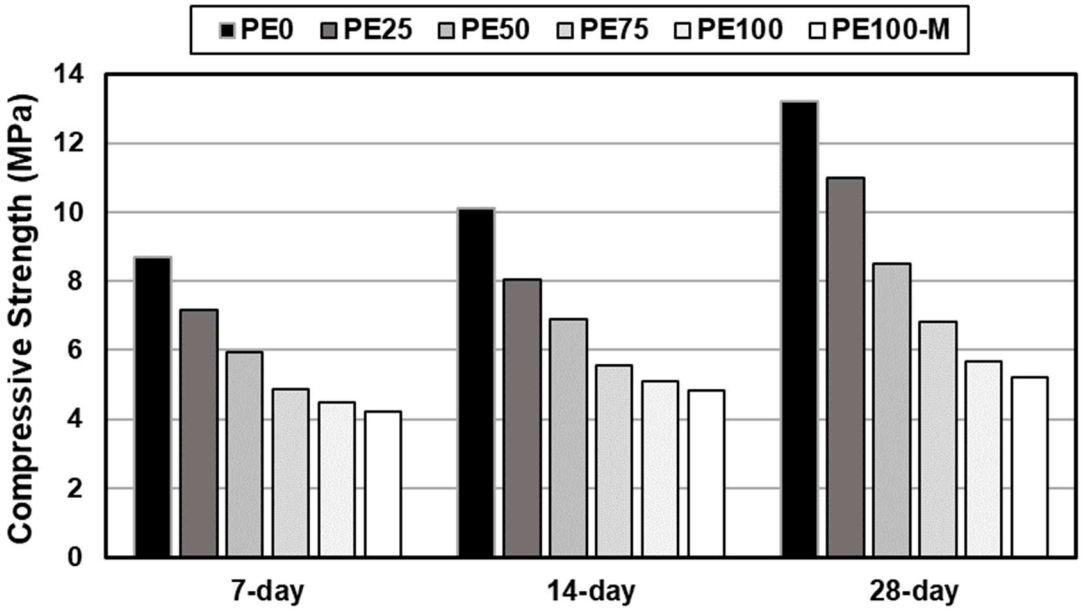

Figure 4.4 Compressive strength of the geopolymer mortars at different curing ages

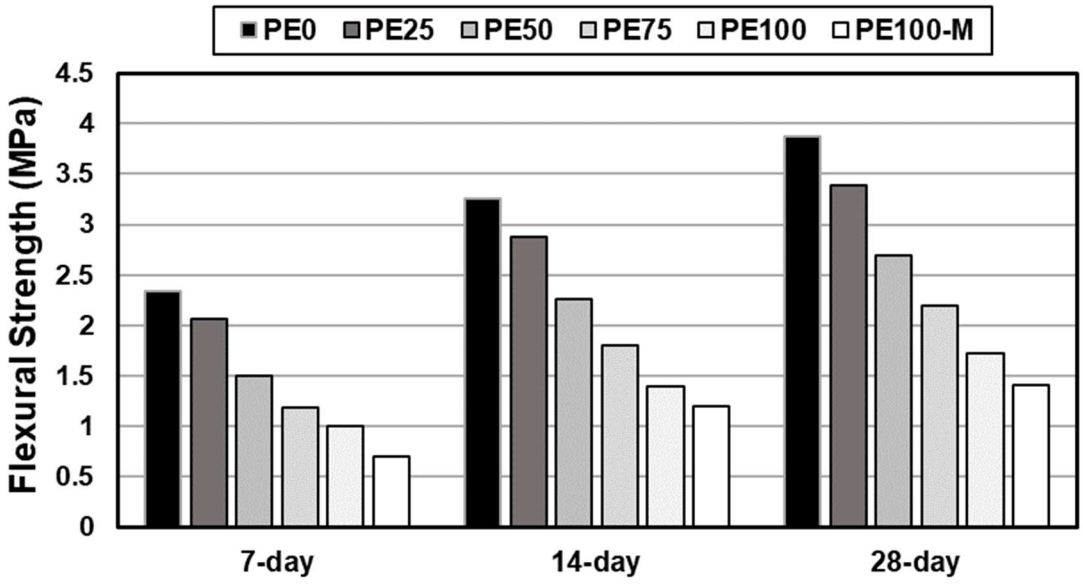

Figure 4.5 Flexural strength of the geopolymer mortars at different curing ages

4.4 Effect of EPA Substitution on Thermal Conductivity of the Geopolymer Mortars

The thermal conductivity coefficients (TCC) of geopolymer mortar samples produced with RCA and EPA are shown in Figure 4.6. According to the test results, the TCC of the samples incorporating EPA and RCA (PE0, PE25, PE50, PE75, PE100, and PE100-M) were 0.3482, 0.3352, 0.3189, 0.2803, 0.2568, and 0.2336 W/m·K, respectively. The highest TCC (0.3482 W/m·K) belongs to the sample that incorporates only RCA as aggregate which also has the highest density and mechanical strength among all tested samples. Besides, the specimen of the mixture that contains the most EPA and the lowest density (1.42 g/cm^3) had the lowest TCC (0.2336 W/m·K). It is also seen from the figure that there is an overall decrease in the TCC with the increasing EPA in geopolymer mixtures. A total of 33% drop in the TCC is achieved by utilizing EPA in the CDW-based lightweight geopolymer mixtures. This decline in TCC can be attributed to the very low density and unconnected porous structure of the EPA [168]. The disconnected pores in EPA interrupts the mortar matrix and disrupts the thermal bridges between the hotter and colder surfaces [149,169]. It is also well-known that the TCC typically decreases as the density of the material decreases [170,171]. The addition of the lightweight EPA, provided samples to have lower densities, hence reduced the TCC of the mixtures. Geopolymer mortars exhibited great thermal insulation properties with TCCs ranging between 0.2336 to 0.3482 W/m·K.

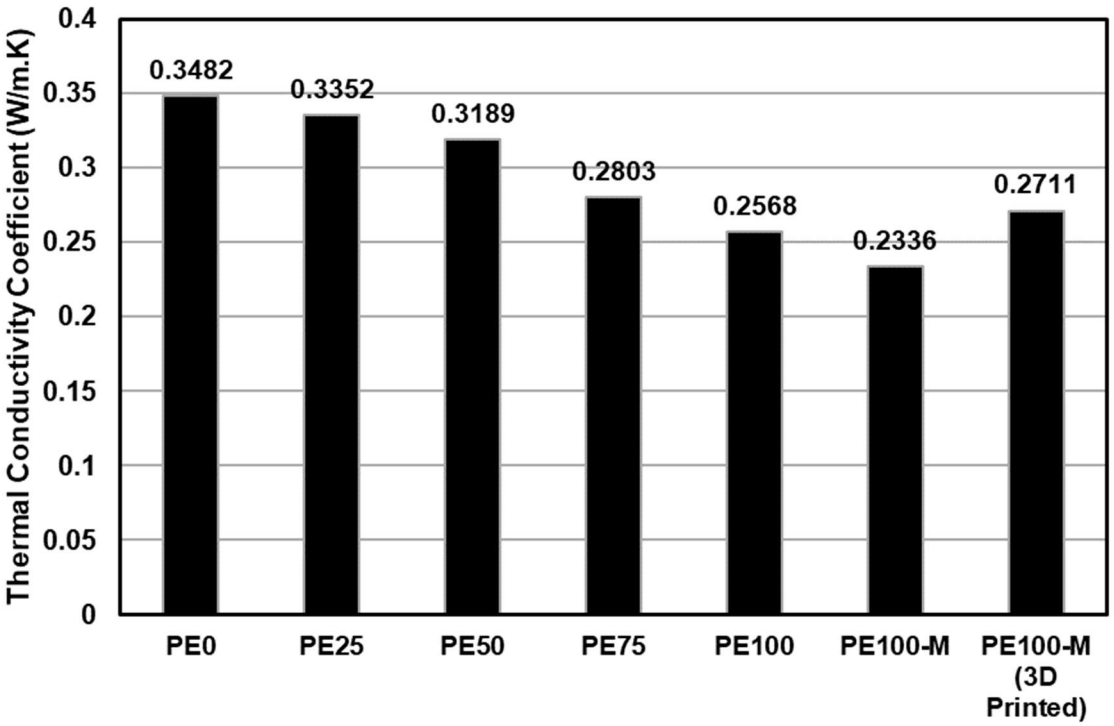

Figure 4.6 Thermal conductivity coefficient of the geopolymer mixtures

The comparison of TCC of casted and 3D printed plate samples of the PE100-M mixture is also given in Figure 4.6. According to the test results, the 3D printed specimen exhibited higher thermal conductivity than the casted specimen. An increase in the TCC of 16% is observed when the same plate sample produced with 3D printing technique. As a characteristic feature of the 3D plate, which is produced layer by layer by 3D printing, the sample thickness decreases on the layer interface regions. The increase in the TCC of the 3D printed plate sample can be attained to increase in the heat transfer between interlayer regions of the printed sample [169,172]. Additionally, EPA particles in the mixture might be compressed and deformed between the rotor and stator of the mortar pump while being transmitted to the nozzle, resulting in the densification of mortar and destruction of the unconnected porous structure. This might be another reason of TCC increase in 3D printed plate. The disruptive effect of extrusion processes on EPA was also reported in study by de Oliviera et al. [173].

4.5 Effect of EPA Substitution on High Temperature Exposure Resistance of the Geopolymer Mortars

Geopolymer mortars were exposed to temperatures of 300, 600, and 900 ℃, and the residual compressive strength of samples were investigated in order to ensure high heat

exposure resistance of the material in case of a fire breakout. The building must be able to withstand an unforeseen fire in order to comply with building codes [174]. Determination of the fire resistance of the material is crucial to develop a safe and promising building material. Residual compressive strength of 28-day cured geopolymer mortars exposed to high temperatures is demonstrated in Figure 4.7.

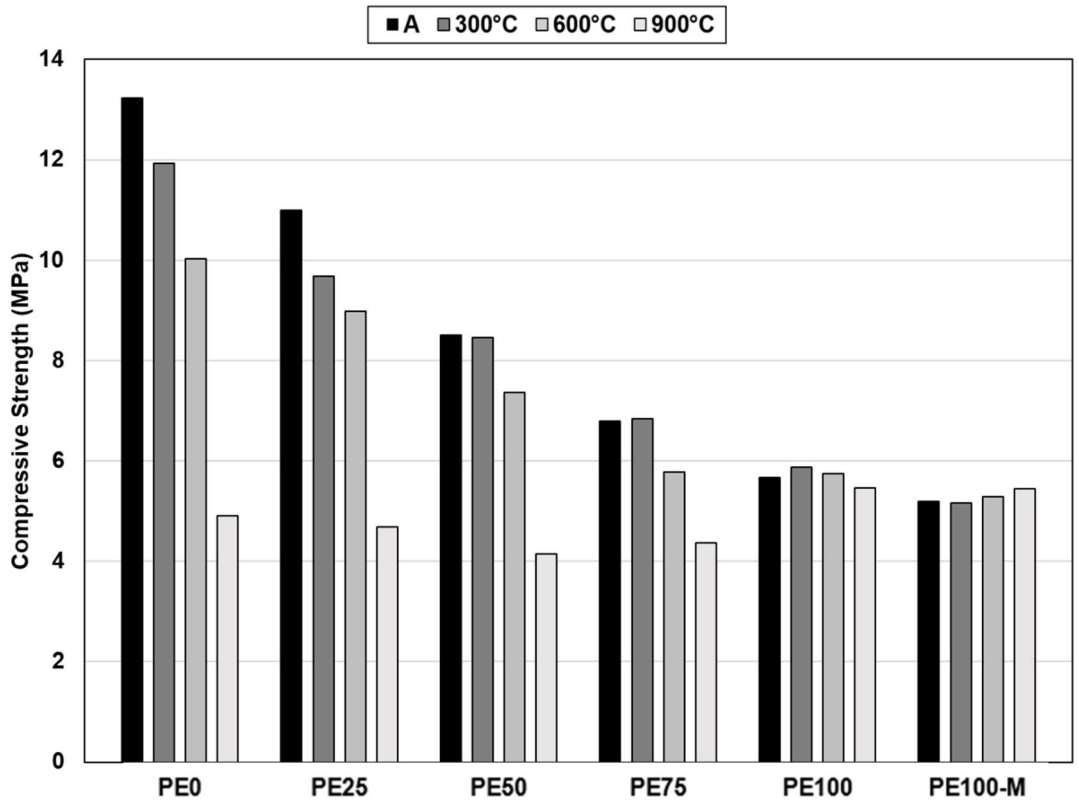

Figure 4.7 Compressive strength of the geopolymer samples after fire exposure at 300, 600 and 900℃, A: 28-day ambient cured samples

After exposing to 300, 600, and 900 ℃, the compressive strength of the PE0 samples decreased by 10, 24, and 63%, respectively, compared to the samples cured at ambient. The compressive strength of the 28-day ambient cured PE25 mixture was decreased by 12, 18, and 57%, respectively, at 300, 600 and 900℃. Similarly, the compressive strength of PE50 mixture decreased by 13 and 51% at 600 and 900℃ temperatures, respectively. A decrease of 15 and 36% was observed in compressive strength of the 28-day cured PE75 specimens exposed to 600 and 900℃ while there was a negligible change detected at 300℃ similar to the PE50. There was no strength loss observed at 300℃ in the PE50 and PE75 mixtures.

In particular, it can be observed in Figure 4.8 that the cracks formed on samples of the mixtures containing RCA type aggregates. As the temperature rises, the excess water in the matrix may have evaporated and formed voids [120,175]. These voids then led to the formation of surface cracks. The reason for the decrease in the fire resistance of geopolymer samples can be explained by the fact that these cracks, which are seen on almost every surface of the cubic samples, cause structural imperfections. A similar study done by Kong et al. reported that the aggregates used in the geopolymer mixtures expanded and the geopolymer matrix shrank at high temperatures [176].

Figure 4.8 Illustration of the surface cracks

Another explanation of the decrease in the strength might be the different expansion coefficients of the RCA and EPA used in the mixture within the geopolymer matrix [120]. When the aggregates were exposed to high temperatures, they showed a more rigid feature than the geopolymer matrix, so stresses occurred between the shrinking matrix and led to the formation of cracks from the inner side to the surface of the sample.

The differences in compressive strength of the P100 and PE100-M samples were considered negligible after the high temperature exposure except for a slight increase at 900°C for the PE100-M. Karakas et al. [163] reported a mechanical strength improvement of high EPA content geopolymers when exposed to 900°C, supports this view. Moreover, a study by Lahoti et al. [120] reported that geopolymers exhibit fire resistance up to 1200°C when used with proper aggregates. PE75, PE100, and PE100-M mixtures have a more porous structure thanks to the high EPA content that reduces heat transfer between

elevated temperature ambient and matrix. Consequently, less heat could reach the inner parts of the geopolymer matrix, and less evaporation of water could be occurred [177]. Due to this reason, geopolymer samples were subjected to less volumetric change resulting in less compressive strength loss in samples containing high amounts of EPA [120]. It has also been reported that the use of EPA in mortar mixtures enhances the thermal resistance in the studies conducted by Rashad et al. [150] and Zongjin et al.[178].

4.6 Effect of EPA Substitution on 3D Printing Qualities of the Geopolymer Mortars

The purpose of the visual inspection performed on the 3D-printed mixtures is to examine the defects in the printed shapes such as cracking, breaking, and surface roughness to determine the mixture with the best 3D printing quality and performance. Despite the fact that all mixtures are developed to have similar fresh properties to be 3D printable, differences in 3D printing qualities and even printing failures might be observed due to the differences in mixture proportions and aggregate types. For this purpose, mixtures with the highest compressive strength and lowest insulation property control mix (PE0), the mixture with average strength and insulation property (PE75), and the mixture with the lowest thermal conductivity and mechanical properties (PE100-M) were used in 3D printing trials and all three mixtures were successfully 3D printed. Detailed examinations on 3D printed mixtures were then carried out.

When the printed units of the PE0 mixture are examined in Figure 4.9a, it is observed that there are many pores on the surface and edges of all 3D printed lines. These pores on every printed element of PE0 were observed repeatedly as the printing process continued (Figure 4.9a). Considering that the entire aggregate content of the mixture is RCA and this type of aggregate, which is obtained from crushed concrete waste in jaw crushers, has flatter and sharp-edged particles. The pores on the printed elements of PE0 may be attributed to sharp-edged aggregates separating from the geopolymer matrix as the nozzle deposits the material onto the printing surface during the extrusion process. Another reason might be that flat aggregates tear the surface of the printed shape by getting stuck on the nozzle exit due to friction on the edges of the nozzle exit. Despite being printed from a rectangular nozzle, the side surfaces of the printed units of the PE0 mixture had rough and wavy edges (Figure 4.9b).

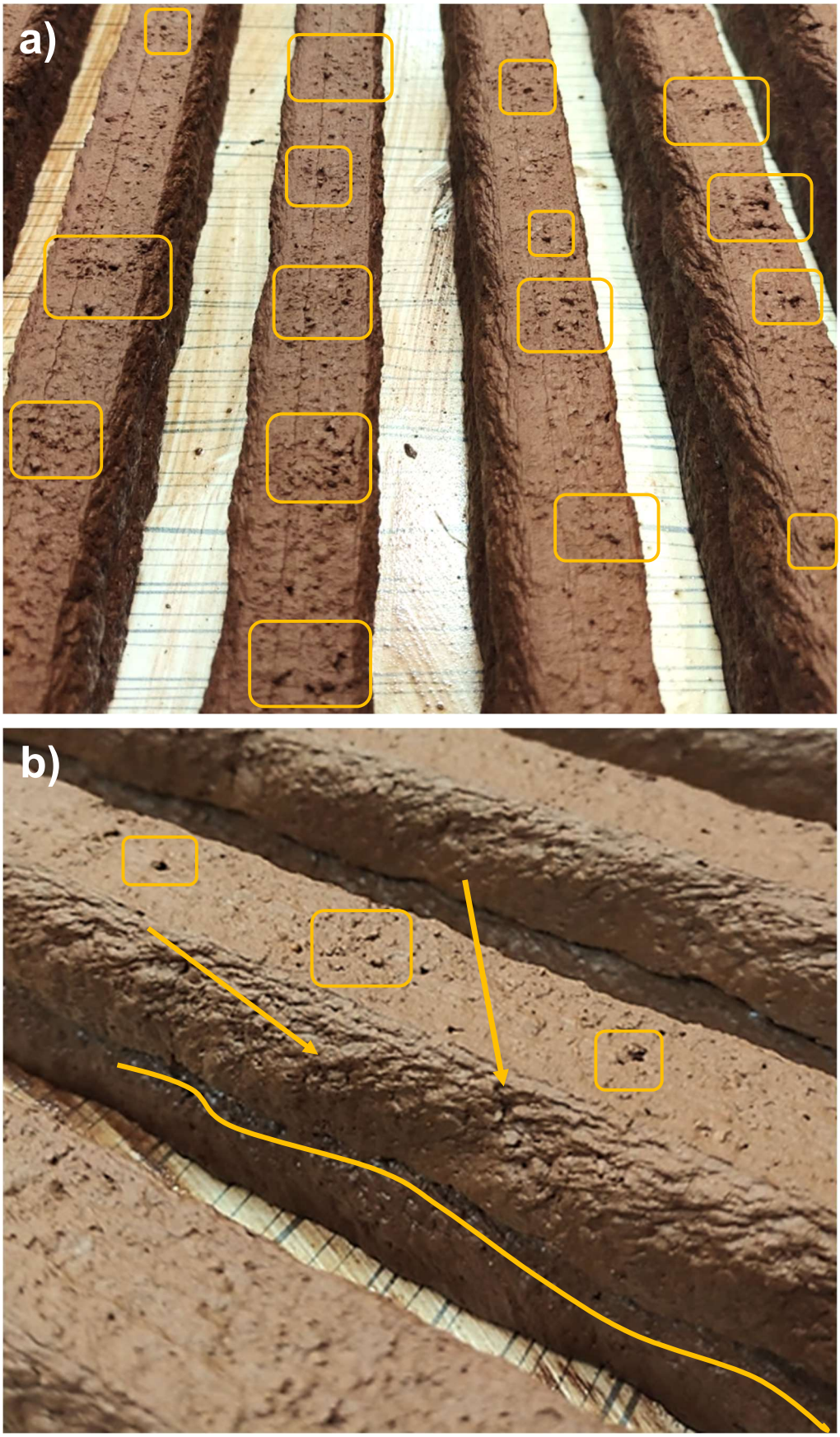

Figure 4.9 Printed units of PE0 mixture, a) Defects and pores, b) Close-up view of wavy edges

The effect of replacing 75% of the RCA with EPA by volume on the 3D printing performance can be clearly observed visually, compared to the PE0 mixture when examining the 3D printing performance of the PE75 mixture. When the upper surface of the printed samples is examined, the repeated pore defects were seen on the surface of the PE0 samples were largely decreased in the PE75 samples (Figure 4.10a). The cause of the defects observed on the surface of the PE75 samples can be attributed to the large EPA and RCA particles encountering the mortar surface during printing and separating from the geopolymer matrix similar to the PE0 samples. The EPA, which is almost entirely round shaped compared to the RCA, helped to create a smoother appearance on the surfaces of the printed samples. Although the edges of the samples printed with the PE75 mixture have a more prismatic appearance and an even texture, there were pores on both the upper and sides of the printed units observed. (Figure 4.10b).

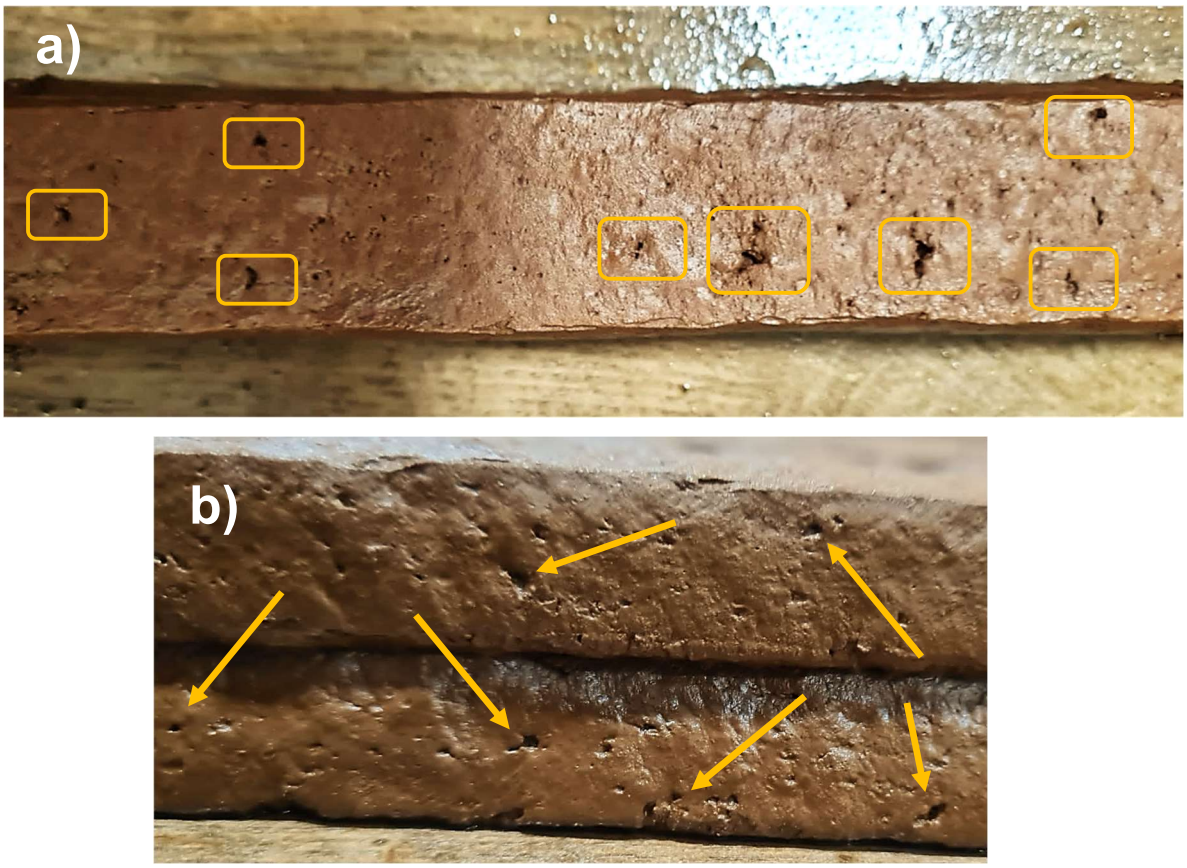

Figure 4.10 Representative image of 3D printed unit using PE75

There was a noticeable change in the 3D printing quality of the units with utilizing PE100-M in the process as shown in Figure 4.11a. In the scenario where the 3D printing geopolymer mortar contains a high volume of EPA (PE100-M), all surface texture problems observed in the PE0 and PE75 mixtures are effectively solved, resulting in a flawless top and side surfaces with only minimal defects in printed elements (Figure 4.11b). Furthermore, a complete prismatic appearance is obtained on the side surfaces, eliminating the wavy and porous texture observed in the PE0 and PE75. This effect can be explained by the fact that the PE100-M mixture contains solely sphere-like and porous EPA, which provides better adhesion between the geopolymer paste and EPA, making it more difficult for the EPA particles to separate from the geopolymer paste when exiting the nozzle. An improvement in paste-aggregate bonding by introducing EPA is also reported by Sengul et al. [149].

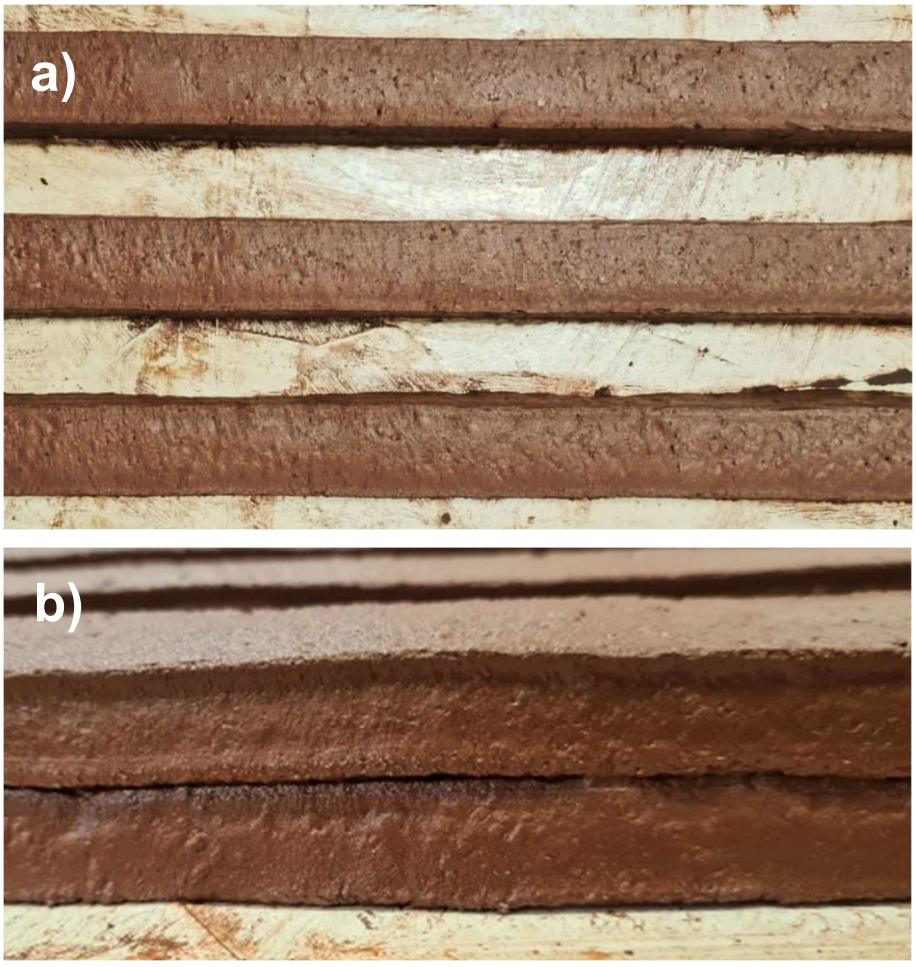

Figure 4.11 3D printed filaments of PE100-M mixture

The printing quality of 3D printable materials is important for creating unique designs, which is one of the main advantages of 3D printing technology. In this context, different

designs with various geometries and shapes were tested for 3D printing with the PE100-M mixture presented in Figure 4.12. There were no ruptures and cracks observed ensuring excellent printing quality for the PE100-M mixture.

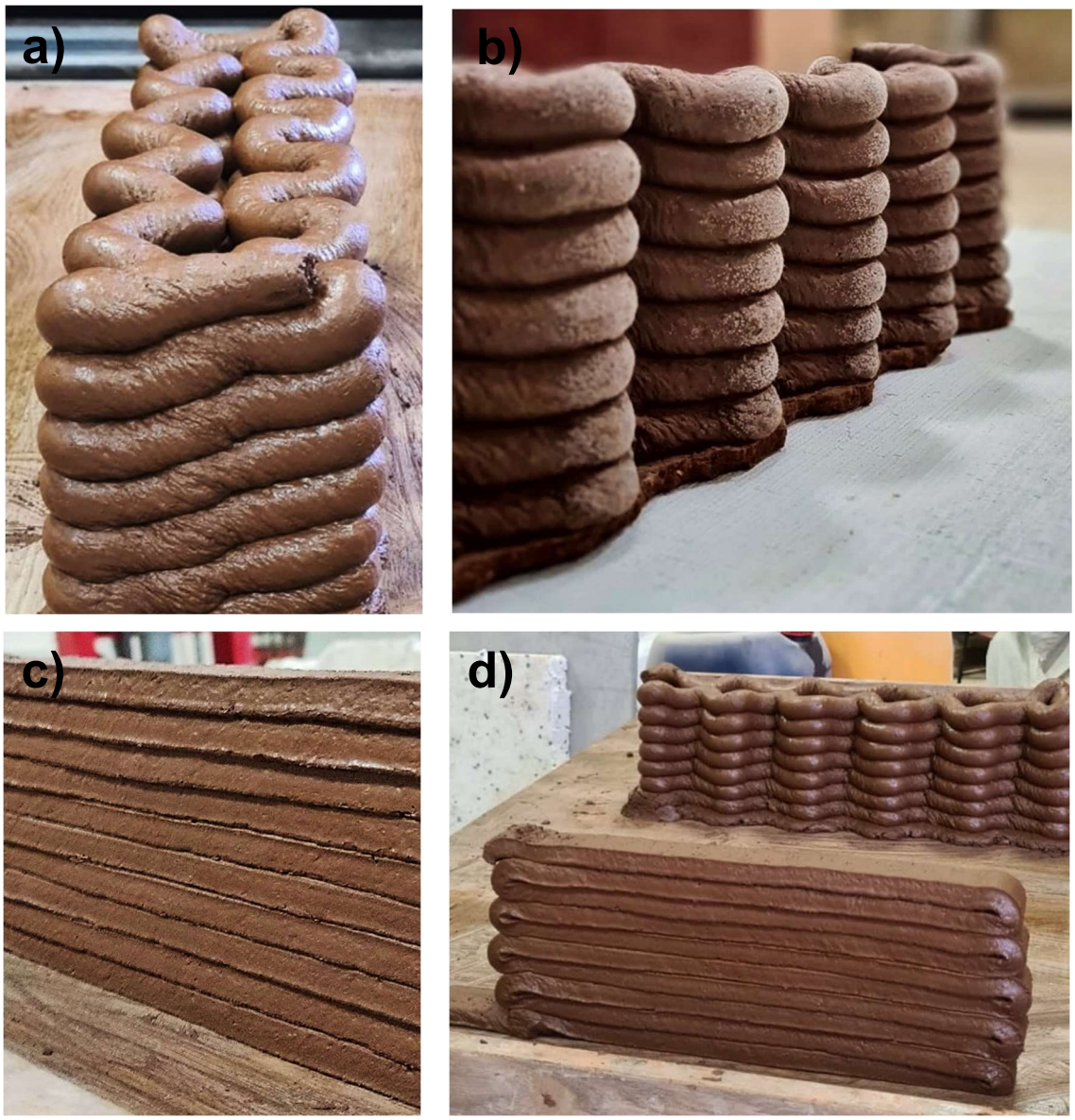

Figure 4.12 Various 3D printed shapes, a) Curved-shape design, b) hardened image of the curved-shape, c) Small-scale wall, d) curved-shape and wall

5. CONCLUSIONS

The major goal of this thesis is to develop end-of-life CDW-based lightweight, thermal insulative geopolymer mortars suitable for 3D printing applications. In this context, RCB, HB, RT, C, and G are activated to produce an entirely CDW-based green geopolymer binder. The developed geopolymer binder serves as a substitute for Portland cement with the goal of reducing greenhouse gas emissions associated with Portland cement manufacturing, while also eliminating the environmental effects of CDW and improving resource efficiency through the upcycling of CDWs. The developed alkali activated geopolymer binder comprising 100% end-of-life CDW was combined with RCA and lightweight, porous EPA to create geopolymer mortar mixtures. By substituting EPA with RCA in the mortar mixture, lightweight, low thermal conductivity 3D printable geopolymer mortars have been developed. A range of investigations were performed on the 3D printable lightweight geopolymer mortars to evaluate their mechanical characteristics, thermal insulation properties, fresh state open-time rheological properties, fresh and dry densities, and resistance to high temperatures. Three chosen mixtures among the developed geopolymer mortars were utilized in lab-scale 3D printing trials and the printing quality of the mixtures with varied characteristics was evaluated visually. To further examine the influence of the 3D printing technique on the thermal insulation capacity of thermal plates, the thermal conductivity coefficients of molded and 3D printed thermal plates produced using the geopolymer mortar with the lowest density were also compared.

The following conclusions were drawn as a result of all studies carried out in this thesis:

- The overall flowability indexes decreased as expected at 30, 60, and 90 minutes. This was due to the ongoing geopolymerization reactions over time. There was no significant change in flowability index values for the mixtures containing EPA higher than 75% from 0 to 90th minutes. In contrast, PE0, PE25, and PE50 experienced a relatively higher reduction in flowability during the testing period due to the un-hydrated cement content in RCA. In general, as the amount of RCA in the mixtures decreases, the decrease in the flowability index slows down in open time. Considering that the ability of mixtures to maintain their flowability

properties for a long time is critical in 3D printing technique, it is evident that mixtures with high EPA content have very suitable characteristics for 3D printing.

- The buildability values were found to be quite similar immediately after the mixing, proving that flowability-based approach is successfully applied. For all testing durations after the initial stage, the EPA-based mixtures' buildability values were lower than the RCA-based mixture. Moreover, the buildability values decreased as the EPA content increased. This can be explained by the increased workability of the EPA-based mixtures. Another reason for lower buildability in EPA-based mixtures might be slowed down geopolymerization rate and extended stiffening period due to EPA's water retention ability. Overall buildability values exhibit an increasing trend over time.

- Substitution of RCA with EPA in the mixtures decreased the fresh and dry density of mortars overall. This can be explained by the fact that EPA has a lower specific gravity value than RCA. The use of aggregate with a lower specific gravity value reduced the fresh and dry density of geopolymer mortars. Moreover, addition of extra water to the mixtures to have similar fresh-state properties may have caused the formation of internal air voids in the matrix thus, a decrease in density occurred. The PE0 mixture was measured to have the highest fresh and dry densities of 2.15 and 2.13 g/cm^3. Substitution of EPA led to a maximum decrease in the density of the PE100-M mixture by 33% at dry state. The PE100-M, PE100, PE75, and PE50 mixtures with dry densities of 1.42, 1.51, 1.68, and 1.76 g/cm^3 can be classified as lightweight mortars according to the lightweight concrete density ranges provided by the ACI Committee 213[156].

- The mechanical tests indicate that compressive strengths of geopolymer mortars were found to be between 5.2 to 13.2 MPa after 28-day ambient curing and flexural strength after 28-day ambient curing varied from 1.4 to 3.8 MPa. The findings indicate that the compressive and flexural strength decreases as the substitution rate of EPA increases. 28-day compressive and flexural strength of the PE100-M mortar decreased by 64% and 33% respectively, compared to the PE0 mixture. The mechanical properties of the mortars displayed a decreasing trend in all curing ages as the substitution rate of EPA increases. The main reason for that is the lower density and higher void ratio of the EPA compared to RCA.

- The thermal conductivity tests demonstrate that the thermal conductivity coefficients (TCC) of the geopolymer mortars PE0, PE25, PE50, PE75, PE100, and PE100-M were 0.3482, 0.3352, 0.3189, 0.2803, 0.2568, and 0.2336 W/m·K, respectively. A maximum of 33% reduction in the thermal conductivity coefficient were achieved by utilizing EPA in the CDW-based lightweight geopolymers. The mixture PE0 incorporating only RCA as aggregate was tested to be with the highest density and mechanical strength among all tested samples as well as with the highest TCC (0.3482 W/m·K). On the other hand, the PE100-M mixture containing the most EPA and with the lowest density (1.42 g/cm^3) were tested to have the lowest TCC (0.2336 W/m·K). There was an overall decrease in the TCC with the increasing EPA in geopolymer mixtures. This reduction can be attributed to the very low density and unconnected porous structure of the EPA disrupting thermal bridges. The 3D printed plate of PE100-M mixture exhibited 16% increased TCC compared to the casted plate sample might be due to the deformation of unconnected porous of EPA in printing process and thickness reduction of the printed sample at layer bonding areas increasing the heat flow.

- High temperature resistance tests revealed that after exposure to temperatures of 300, 600, and 900 ℃, the compressive strength of the PE0, PE25, and P50 samples exhibited a reducing trend. There was no strength loss observer in strength at 300℃ for the PE50 and PE75 mixtures. 50% and more substitution rate of EPA suppressed strength loss at elevated temperatures. Moreover, no loss observed in compressive strength for the PE100 and PE100-M after the high temperature exposure at 300, 600, and 900 ℃ with a slight increase at 900°C for the PE100-M, indicating that high EPA content mixtures have superior resistance to elevated temperatures.

- The visual inspections of the selected mortars revealed that there were many defects and pores as well as rough and wavy edges observed on 3D printed elements of the PE0 mixture. This might be attributed to RCA particles tearing the surface of the printed shape. The PE75 mixture, however, performed slightly better than PE0, having only small pores on the surface of the top and edges of the printed units. Edges of the printed units of PE75 were more prismatic than printed units of the PE0 mixture. The best 3D printing quality was reached with the utilization of the PE100-M mixture. All surface texture problems were

effectively solved with tiny negligible defects on the surfaces of the 3D printed units. This effect can be explained by the sphere-like and porous EPA grains, which provides better adhesion between the geopolymer paste and EPA, making it more difficult for the EPA particles to separate from the geopolymer paste when exiting the nozzle. The PE100-M mixture also exhibited excellent printing quality when printing a complex shape and a miniature wall.

- Finally, the mixtures developed from 100% end-of-life CDW-based materials PE50, PE75, PE100, and PE100-M were classified as lightweight mortars. These mixtures met the minimum strength requirements for masonry in various standards and exhibited great thermal insulation properties with TCCs ranging between 0.2336 to 0.3482 W/m·K. Additionally, PE0 mixture achieved 13.2 MPa compressive strength at day 28 and complied with the MSJC-determined standards for compressive strength for masonry constructions (10.34-27.58 MPa) [167]. Although all selected mixtures (PE0, PE75, and PE100-M) were 3D printed successfully, the PE100-M stands out with adequate strength for masonry (5.2 MPa at 28^{th} day), low density (1.42 g/cm^3), excellent 3D print quality, improved thermal insulation (0.2336 W/m·K for casted, 0.2711 W/m·K for 3D printed) and superior fire resistance among all developed mixtures.

6. REFERENCES

[1] L. Jeremy, The energy crisis, global warming and the role of renewables, Renewable Energy World. 8 **(2005)** 23–28.

[2] M.K. Najjar, K. Figueiredo, A.W.A. Hammad, V.W.Y. Tam, A.C.J. Evangelista, A. Haddad, A framework to estimate heat energy loss in building operation, J Clean Prod. 235 **(2019)** 789–800.

[3] M.A. Hossain, A. Nadeem, Towards digitizing the construction industry: State of the art of construction 4.0, in: Proceedings of the ISEC, **2019**: pp. 1–6.

[4] J.J. Biernacki, J.W. Bullard, G. Sant, K. Brown, F.P. Glasser, S. Jones, T. Ley, R. Livingston, L. Nicoleau, J. Olek, Cements in the 21st century: challenges, perspectives, and opportunities, Journal of the American Ceramic Society. 100 **(2017)** 2746–2773.

[5] M. Sakin, Y.C. Kiroglu, 3D Printing of Buildings: Construction of the Sustainable Houses of the Future by BIM, Energy Procedia. 134 **(2017)** 702–711.

[6] S.C. Paul, G.P.A.G. Van Zijl, M.J. Tan, I. Gibson, A review of 3D concrete printing systems and materials properties: Current status and future research prospects, Rapid Prototyp J. **(2018)**.

[7] J. Zhang, J. Wang, S. Dong, X. Yu, B. Han, A review of the current progress and application of 3D printed concrete, Compos Part A Appl Sci Manuf. 125 **(2019)** 105533.

[8] O.D. Repinskiy, N.B. Romaneskul, N.A. Studenkova, Using of additive manufacturing (AM) in construction economics–shortcomings, advantages, prospects, in: IOP Conf Ser Earth Environ Sci, IOP Publishing, **2021**: p. 012170.

[9] M.H. Ali, G. Issayev, E. Shehab, S. Sarfraz, A critical review of 3D printing and digital manufacturing in construction engineering, Rapid Prototyp J. **(2022).**

[10] P. Wu, J. Wang, X. Wang, A critical review of the use of 3-D printing in the construction industry, Autom Constr. 68 **(2016)** 21–31.

[11] I. Krimi, Z. Lafhaj, L. Ducoulombier, Prospective study on the integration of additive manufacturing to building industry—Case of a French construction company, Addit Manuf. 16 **(2017)** 107–114.

[12] Y.W.D. Tay, B. Panda, S.C. Paul, N.A. Noor Mohamed, M.J. Tan, K.F. Leong, 3D printing trends in building and construction industry: a review, Virtual Phys Prototyp. 12 **(2017)** 261–276.

[13] R.J.M. Wolfs, F.P. Bos, T.A.M. Salet, Early age mechanical behaviour of 3D printed concrete: Numerical modelling and experimental testing, Cem Concr Res. 106 **(2018)** 103–116.

[14] F. Bos, R. Wolfs, Z. Ahmed, T. Salet, Additive manufacturing of concrete in construction: potentials and challenges of 3D concrete printing, Virtual Phys Prototyp. 11 **(2016)** 209–225.

[15] J. Tan, J. Cai, J. Li, Recycling of unseparated construction and demolition waste (UCDW) through geopolymer technology, Constr Build Mater. 341 **(2022)** 127771.

[16] M. Frías, S. Martínez-Ramírez, R.V. de la Villa, L. Fernández-Carrasco, R. García, Reactivity in cement pastes bearing fine fraction concrete and glass from construction and demolition waste: Microstructural analysis of viability, Cem Concr Res. 148 **(2021)** 106531.

[17] P.V. Sáez, M. Osmani, A diagnosis of construction and demolition waste generation and recovery practice in the European Union, J Clean Prod. 241 **(2019)** 118400.

[18] D. Erten, Towards zero waste in construction: A case study using green building certification systems, Dicle Üniversitesi Mühendislik Fakültesi Mühendislik Dergisi. 11 **(2020)** 875–888.

[19] J.J. de Oliveira Andrade, E. Possan, J.Z. Squiavon, T.L.P. Ortolan, Evaluation of mechanical properties and carbonation of mortars produced with construction and demolition waste, Constr Build Mater. 161 **(2018)** 70–83.

[20] J. Xiao, Q. Deng, M. Hou, J. Shen, O. Gencel, Where are demolition wastes going: reflection and analysis of the February 6, 2023 earthquake disaster in Turkey, Low-Carbon Materials and Green Construction. 1 **(2023)** 17.

[21] I. Agenda, Shaping the future of construction a breakthrough in mindset and technology, in: World Economic Forum, **2016**.

[22] N. Mohamad, K. Muthusamy, R. Embong, A. Kusbiantoro, M.H. Hashim, Environmental impact of cement production and Solutions: A review, Mater Today Proc. 48 **(2022)** 741–746.

[23] O.E. Ige, O.A. Olanrewaju, K.J. Duffy, O.C. Collins, Environmental Impact Analysis of Portland Cement (CEM1) Using the Midpoint Method, Energies (Basel). 15 **(2022)** 2708.

[24] R. Bajpai, K. Choudhary, A. Srivastava, K.S. Sangwan, M. Singh, Environmental impact assessment of fly ash and silica fume based geopolymer concrete, J Clean Prod. 254 **(2020)** 120147.

[25] K. Neupane, D. Chalmers, P. Kidd, High-strength geopolymer concrete-properties, advantages and challenges, Advances in Materials. 7 **(2018)** 15–25.

[26] M. Amran, A. Al-Fakih, S.H. Chu, R. Fediuk, S. Haruna, A. Azevedo, N. Vatin, Long-term durability properties of geopolymer concrete: An in-depth review, Case Studies in Construction Materials. 15 **(2021)** e00661.

[27] M. Albitar, M.S.M. Ali, P. Visintin, M. Drechsler, Durability evaluation of geopolymer and conventional concretes, Constr Build Mater. 136 **(2017)** 374–385.

[28] S.A. Bernal, R.M. de Gutiérrez, A.L. Pedraza, J.L. Provis, E.D. Rodriguez, S. Delvasto, Effect of binder content on the performance of alkali-activated slag concretes, Cem Concr Res. 41 **(2011)** 1–8.

[29] K.H. Mo, H.J. Lee, M.Y.J. Liu, T.-C. Ling, Incorporation of expanded vermiculite lightweight aggregate in cement mortar, Constr Build Mater. 179 **(2018)** 302–306.

[30] H.-K. Kim, J.H. Jeon, H.-K. Lee, Workability, and mechanical, acoustic and thermal properties of lightweight aggregate concrete with a high volume of entrained air, Constr Build Mater. 29 **(2012)** 193–200.

[31] O. Ünal, T. Uygunoğlu, A. Yildiz, Investigation of properties of low-strength lightweight concrete for thermal insulation, Build Environ. 42 **(2007)** 584–590.

[32] A.M. Rashad, Possibility of producing thermal insulation materials from cementitious materials without foaming agent or lightweight aggregate, Environmental Science and Pollution Research. 29 **(2022)** 3784–3793.

[33] J. Davidovits, Geopolymers: inorganic polymeric new materials, J Therm Anal Calorim. 37 **(1991)** 1633–1656.

[34] J. Davidovits, Geopolymer, green chemistry and sustainable development solutions: proceedings of the world congress geopolymer 2005, Geopolymer Institute, **2005**.

[35] I. Giannopoulou, D. Panias, Structure, design and applications of geopolymeric materials, in: Proceedings of the 3rd International Conference on Deformation Processing and Structure of Materials, **2007**: pp. 20–22.

[36] P. Cong, Y. Cheng, Advances in geopolymer materials: A comprehensive review, Journal of Traffic and Transportation Engineering (English Edition). 8 **(2021)** 283–314.

[37] F.A. Shilar, S. V Ganachari, V.B. Patil, N. Almakayeel, T.M.Y. Khan, Development and optimization of an eco-friendly geopolymer brick production process for sustainable masonry construction, Case Studies in Construction Materials. 18 **(2023)** e02133.

[38] J. Tan, Ö. Cizer, B. Vandevyvere, J. De Vlieger, H. Dan, J. Li, Efflorescence mitigation in construction and demolition waste (CDW) based geopolymer, Journal of Building Engineering. 58 **(2022)** 105001.

[39] A. Vásquez, V. Cárdenas, R.A. Robayo, R.M. de Gutiérrez, Geopolymer based on concrete demolition waste, Advanced Powder Technology. 27 **(2016)** 1173–1179.

[40] M. Vafaei, A. Allahverdi, High strength geopolymer binder based on waste-glass powder, Advanced Powder Technology. 28 **(2017)** 215–222.

[41] M. Tuyan, Ö. Andiç-Çakir, K. Ramyar, Effect of alkali activator concentration and curing condition on strength and microstructure of waste clay brick powder-based geopolymer, Compos B Eng. 135 **(2018)** 242–252.

[42] P. Rovnaník, P. Rovnanikova, M. Vyšvařil, S. Grzeszczyk, E. Janowska-Renkas, Rheological properties and microstructure of binary waste red brick powder/metakaolin geopolymer, Constr Build Mater. 188 **(2018)** 924–933.

[43] N. Sedira, J. Castro-Gomes, M. Magrinho, Red clay brick and tungsten mining waste-based alkali-activated binder: Microstructural and mechanical properties, Constr Build Mater. 190 **(2018)** 1034–1048.

[44] P. Shoaei, H.R. Musaeei, F. Mirlohi, F. Ameri, N. Bahrami, Waste ceramic powder-based geopolymer mortars: Effect of curing temperature and alkaline solution-to-binder ratio, Constr Build Mater. 227 **(2019)** 116686.

[45] C.-L. Hwang, M.D. Yehualaw, D.-H. Vo, T.-P. Huynh, Development of high-strength alkali-activated pastes containing high volumes of waste brick and ceramic powders, Constr Build Mater. 218 **(2019)** 519–529.

[46] C.L. Wong, K.H. Mo, U.J. Alengaram, S.P. Yap, Mechanical strength and permeation properties of high calcium fly ash-based geopolymer containing recycled brick powder, Journal of Building Engineering. 32 **(2020)** 101655.

[47] R. Xiao, Y. Ma, X. Jiang, M. Zhang, Y. Zhang, Y. Wang, B. Huang, Q. He, Strength, microstructure, efflorescence behavior and environmental impacts of waste glass geopolymers cured at ambient temperature, J Clean Prod. 252 **(2020)** 119610.

[48] O. Mahmoodi, H. Siad, M. Lachemi, S. Dadsetan, M. Sahmaran, Optimization of brick waste-based geopolymer binders at ambient temperature and pre-targeted chemical parameters, J Clean Prod. 268 **(2020)** 122285.

[49] A.S. Ouda, M. Gharieb, Development the properties of brick geopolymer pastes using concrete waste incorporating dolomite aggregate, Journal of Building Engineering. 27 **(2020)** 100919.

[50] T. Tho-In, V. Sata, K. Boonserm, P. Chindaprasirt, Compressive strength and microstructure analysis of geopolymer paste using waste glass powder and fly ash, J Clean Prod. 172 **(2018)** 2892–2898.

[51] S. Dadsetan, H. Siad, M. Lachemi, M. Sahmaran, Extensive evaluation on the effect of glass powder on the rheology, strength, and microstructure of metakaolin-based geopolymer binders, Constr Build Mater. 268 **(2021)** 121168.

[52] G. Yıldırım, A. Kul, E. Özçelikci, M. Şahmaran, A. Aldemir, D. Figueira, A. Ashour, Development of alkali-activated binders from recycled mixed masonry-originated waste, Journal of Building Engineering. 33 **(2021)** 101690.

[53] H. Ulugöl, A. Kul, G. Yıldırım, M. Şahmaran, A. Aldemir, D. Figueira, A. Ashour, Mechanical and microstructural characterization of geopolymers from assorted construction and demolition waste-based masonry and glass, J Clean Prod. 280 **(2021)** 124358.

[54] H. Ilcan, O. Sahin, A. Kul, E. Ozcelikci, M. Sahmaran, Rheological property and extrudability performance assessment of construction and demolition waste-based geopolymer mortars with varied testing protocols, Cem Concr Compos. 136 **(2023)** 104891.

[55] E. Ozcelikci, A. Kul, M.F. Gunal, B.F. Ozel, G. Yildirim, A. Ashour, M. Sahmaran, A comprehensive study on the compressive strength, durability-related parameters and microstructure of geopolymer mortars based on mixed construction and demolition waste, J Clean Prod. 396 **(2023)** 136522.

[56] I. International, ISO/ASTM 52900–Additive manufacturing–general principles–terminology, Int Stand. 5 **(2015)** 1–26.

[57] D.L. Bourell, Perspectives on additive manufacturing, Annu Rev Mater Res. 46 **(2016)**.

[58] A. Savini, G.G. Savini, A short history of 3D printing, a technological revolution just started, in: Proceedings of the 2015 ICOHTEC/IEEE International History of High-Technologies and Their Socio-Cultural Contexts Conference, HISTELCON 2015: The 4th IEEE Region 8 Conference on the History of Electrotechnologies, Institute of Electrical and Electronics Engineers Inc., **2015**.

[59] M.A. Alzarrad, S. Elhouar, 3D Printing Applications in Construction from the Past and into the Future, in: Periodica Polytechnica Budapest University of Technology and Economics, **2019**: pp. 754–760.

[60] Z. Malaeb, F. AlSakka, F. Hamzeh, 3D Concrete Printing, in: 3D Concrete Printing Technology, Elsevier, **2019**: pp. 115–136.

[61] C.W. Hull, The birth of 3D printing, Research Technology Management. 58 **(2015)** 25–29.

[62] H. Quan, T. Zhang, H. Xu, S. Luo, J. Nie, X. Zhu, Photo-curing 3D printing technique and its challenges, Bioact Mater. 5 **(2020)** 110–115.

[63] J. Graham, Three-dimensional printing technology, JCO ·, **2014**. www.jco-online.com.

[64] A. Su, S.J. Al'Aref, History of 3D printing, in: 3D Printing Applications in Cardiovascular Medicine, Elsevier, 2018: pp. 1–10.

[65] R.A. Buswell, R.C. Soar, A.G.F. Gibb, A. Thorpe, Freeform Construction: Mega-scale Rapid Manufacturing for construction, Autom Constr. 16 **(2007)** 224–231.

[66] A. Pandian, C. Belavek, A review of recent trends and challenges in 3D printing, **2016**.

[67] A. Pîrjan, D.-M. Petroşanu, The impact of 3D printing technology on the society and economy, **2013**.

[68] C. Hinczewski, S. Corbel, T. Chartier, Stereolithography for the fabrication of ceramic three-dimensional parts, Rapid Prototyp J. 4 **(1998)** 104–111.

[69] B. Khoshnevis, S. Bukkapatnam, H. Kwon, J. Saito, Experimental investigation of contour crafting using ceramics materials, Rapid Prototyp J. **(2001)**.

[70] S. Lim, T. Le, J. Webster, R. Buswell, A. Austin, A. Gibb, T. Thorpe, Fabricating construction components using layered manufacturing technology, in: Global Innovation in Construction Conference, Loughborough University Leicestershire, UK, **2009**: pp. 512–520.

[71] G. Cesaretti, E. Dini, X. De Kestelier, V. Colla, L. Pambaguian, Building components for an outpost on the Lunar soil by means of a novel 3D printing technology, Acta Astronaut. 93 **(2014)** 430–450.

[72] D. Zarubin, Building a house with a 3D printer, Moohii. **(2023)**. https://moohii.com/blog/d-shape (accessed May 18, **2023**).

[73] S. Lim, R.A. Buswell, T.T. Le, S.A. Austin, A.G.F. Gibb, T. Thorpe, Developments in construction-scale additive manufacturing processes, Autom Constr. 21 **(2012)** 262–268.

[74] D. Hwang, B. Khoshnevis, E. Daniel, Concrete wall fabrication by contour crafting, in: 21st International Symposium on Automation and Robotics in Construction (ISARC 2004), Jeju, South Korea, Citeseer, **2004**: pp. 301–307.

[75] B. Khoshnevis, D. Hwang, K.-T. Yao, Z. Yeh, Mega-scale fabrication by contour crafting, International Journal of Industrial and Systems Engineering. 1 **(2006)** 301–320.

[76] C. Gosselin, R. Duballet, Ph. Roux, N. Gaudillière, J. Dirrenberger, Ph. Morel, Large-scale 3D printing of ultra-high performance concrete – a new processing route for architects and builders, Mater Des. 100 **(2016)** 102–109.

[77] K. Kuzmenko, N. Gaudillière, A. Feraille, J. Dirrenberger, O. Baverel, Assessing the Environmental Viability of 3D Concrete Printing Technology, in: C. Gengnagel, O. Baverel, J. Burry, M. Ramsgaard Thomsen, S. Weinzierl (Eds.), Impact: Design With All Senses, Springer International Publishing, Cham, **2020**: pp. 517–528.

[78] N. Lecoq, Democrite Wall, Xtreee. (2023). https://xtreee.com/en/project/mur-democrite/ (accessed May 5, **2023**).

[79] M. Zastrow, 3D printing gets bigger, faster and stronger, Nature, 578(7793). **(2020)** 20–23.

[80] O. Pons-Valladares, M. del M. Casanovas-Rubio, J. Armengou, A. de la Fuente, Approach for sustainability assessment for footbridge construction technologies: Application to the first world D-shape 3D-Printed fiber-reinforced mortar footbridge in Madrid, J Clean Prod. 394 **(2023)** 136369.

[81] A. de la Fuente, A. Blanco, E. Galeote, S. Cavalaro, Structural fibre-reinforced cement-based composite designed for particle bed 3D printing systems. Case study Parque de Castilla Footbridge in Madrid, Cem Concr Res. 157 **(2022)** 106801.

[82] 3D printed bridge, (2023). https://iaac.net/project/3d-printed-bridge/ (accessed May 20, **2023**).

[83] F. Craveiro, J.P. Duarte, H. Bartolo, P.J. Bartolo, Additive manufacturing as an enabling technology for digital construction: A perspective on Construction 4.0, Autom Constr. 103 **(2019)** 251–267.

[84] L.D. Evjemo, S. Moe, J.T. Gravdahl, O. Roulet-Dubonnet, L.T. Gellein, V. Br⊘tan, Additive manufacturing by robot manipulator: An overview of the state-of-the-art and proof-of-concept results, in: 2017 22nd IEEE International Conference on Emerging Technologies and Factory Automation (ETFA), **2017**: pp. 1–8.

[85] A. Lanko, Additive Technologies in Construction of Temporary Housing for Victims of Natural Disasters and Other Emergencies, in: V. Murgul, Z. Popovic (Eds.), International Scientific Conference Energy Management of Municipal Transportation Facilities and Transport EMMFT 2017, Springer International Publishing, Cham, **2018**: pp. 1102–1108.

[86] Apis Cor, A 3D printer designed by Apis Cor, **(2023)**. https://apis-cor.com/technologies/ (accessed June 1, 2023).

[87] S.H. Ghaffar, J. Corker, P. Mullett, The potential for additive manufacturing to transform the construction industry, in: Construction 4.0, Routledge, **2020**: pp. 155–187.

[88] M. Valente, A. Sibai, M. Sambucci, Extrusion-based additive manufacturing of concrete products: revolutionizing and remodeling the construction industry, Journal of Composites Science. 3 **(2019)** 88.

[89] R. Morton, 3D-printed house in Austin, Texas, M3design. (n.d.). https://www.m3design.com/case-study/3d-concrete-printer-design/ (accessed June 10, **2023**).

[90] O. Sai Saran, A. Prudhvidhar Reddy, L. Chaturya, M. Pavan Kumar, 3D printing of composite materials: A short review, Mater Today Proc. 64 **(2022)** 615–619.

[91] N.D. Bello, A.M. Memari, Comparative Review of the Technology and Case Studies of 3D Concrete Printing of Buildings by Several Companies, Buildings. 13 **(2022)** 106.

[92] F.P. Bos, C. Menna, M. Pradena, E. Kreiger, W.R.L. da Silva, A.U. Rehman, D. Weger, R.J.M. Wolfs, Y. Zhang, L. Ferrara, V. Mechtcherine, The realities of additively manufactured concrete structures in practice, Cem Concr Res. 156 **(2022)** 106746.

[93] 3D printing of house, Peri3dconstruction. (n.d.). https://www.peri3dconstruction.com/en/tempe (accessed June 18, **2023**).

[94] Y. Pan, Y. Zhang, D. Zhang, Y. Song, 3D printing in construction: state of the art and applications, The International Journal of Advanced Manufacturing Technology. 115 (2021) 1329–1348.

[95] S.C. Paul, Y.W.D. Tay, B. Panda, M.J. Tan, Fresh and hardened properties of 3D printable cementitious materials for building and construction. Arch Civ Mech Eng 18 (1): 311–319, **(2018)**.

[96] Office of the Future, Archello. (n.d.). https://archello.com/project/office-of-the-future-future-foundation-pavillion (accessed April 13, **2023**).

[97] World's Largest 3D-Printed Building, Dwell. (n.d.). https://www.dwell.com/article/worlds-largest-3d-printed-building-apis-cor-6a4b7f45 (accessed June 5, **2023**).

[98] R. Morton, Sustainable Housing Neighborhood, Iconbuild. (n.d.). https://www.iconbuild.com/projects/east-17th-street-residences (accessed June 5, **2023**).

[99] Two Story 3D-Printed House, Cobod. (n.d.). https://cobod.com/the-us-largest-3d-printed-building-project/ (accessed June 10, **2023**).

[100] Low Carbon 3D Housing, 3dwasp. (n.d.). https://www.3dwasp.com/en/3d-printed-house-tecla/ (accessed June 16, **2023**).

[101] Two Story Single 3D-Printed Family House, Peri. (n.d.). https://www.peri.com/en/company/press-releases/germanys-first-printed-house-officially-openend.html (accessed June 14, **2023**).

[102] P. Bedarf, A. Dutto, M. Zanini, B. Dillenburger, Foam 3D printing for construction: A review of applications, materials, and processes, Autom Constr. 130 **(2021)** 103861.

[103] B. García de Soto, I. Agustí-Juan, J. Hunhevicz, S. Joss, K. Graser, G. Habert, B.T. Adey, Productivity of digital fabrication in construction: Cost and time analysis of a robotically built wall, Autom Constr. 92 **(2018)** 297–311.

[104] N. Van Tam, T. Watanabe, N.L. Hai, Importance of Autonomous Motivation in Construction Labor Productivity Improvement in Vietnam: A Self-Determination Theory Perspective, Buildings. 12 **(2022)** 763.

[105] K.K. P, M. Nirajan, R.E. M, F.E. Terence, Optimal Productivity in Labor-Intensive Construction Operations: Pilot Study, J Constr Eng Manag. 143 **(2017)** 04016107.

[106] Z. Malaeb, F. AlSakka, F. Hamzeh, Chapter 6 - 3D Concrete Printing: Machine Design, Mix Proportioning, and Mix Comparison Between Different Machine Setups, in: J.G. Sanjayan, A. Nazari, B. Nematollahi (Eds.), 3D Concrete Printing Technology, Butterworth-Heinemann, **2019**: pp. 115–136.

[107] C.M. Rouhana, M.S. Aoun, F.S. Faek, M.S. Eljazzar, F.R. Hamzeh, The Reduction of Construction Duration by Implementing Contour Crafting (3D Printing), in: B.T.

Kalsaas, L. Koskela, T.A. Saurin (Eds.), 22nd Annual Conference of the International Group for Lean Construction, Oslo, Norway, **2014**: pp. 1031–1042.

[108] K. Kim, S. Park, W. Kim, Y. Jeong, J. Lee, Evaluation of shear strength of RC beams with multiple interfaces formed before initial setting using 3D printing technology, Materials. 10 **(2017)** 1349.

[109] B. Panda, S.C. Paul, L.J. Hui, Y.W.D. Tay, M.J. Tan, Additive manufacturing of geopolymer for sustainable built environment, J Clean Prod. 167 **(2017)** 281–288.

[110] M. Xia, J.G. Sanjayan, Methods of enhancing strength of geopolymer produced from powder-based 3D printing process, Mater Lett. 227 **(2018)** 281–283.

[111] B. Panda, S.C. Paul, N.A.N. Mohamed, Y.W.D. Tay, M.J. Tan, Measurement of tensile bond strength of 3D printed geopolymer mortar, Measurement. 113 **(2018)** 108–116.

[112] D.-W. Zhang, D. Wang, X.-Q. Lin, T. Zhang, The study of the structure rebuilding and yield stress of 3D printing geopolymer pastes, Constr Build Mater. 184 **(2018)** 575–580.

[113] B. Panda, M.J. Tan, Experimental study on mix proportion and fresh properties of fly ash based geopolymer for 3D concrete printing, Ceram Int. 44 **(2018)** 10258–10265.

[114] C. Sun, J. Xiang, M. Xu, Y. He, Z. Tong, X. Cui, 3D extrusion free forming of geopolymer composites: Materials modification and processing optimization, J Clean Prod. 258 **(2020)** 120986.

[115] B. Panda, C. Unluer, M.J. Tan, Extrusion and rheology characterization of geopolymer nanocomposites used in 3D printing, Compos B Eng. 176 **(2019)** 107290.

[116] S.H. Bong, B. Nematollahi, A. Nazari, M. Xia, J.G. Sanjayan, Fresh and Hardened Properties of 3D Printable Geopolymer Cured in Ambient Temperature, in: T. Wangler, R.J. Flatt (Eds.), First RILEM International Conference on Concrete and Digital Fabrication – Digital Concrete 2018, Springer International Publishing, Cham, **2019**: pp. 3–11.

[117] O. Şahin, H. İlcan, A.T. Ateşli, A. Kul, G. Yıldırım, M. Şahmaran, Construction and demolition waste-based geopolymers suited for use in 3-dimensional additive manufacturing, Cem Concr Compos. 121 **(2021)** 104088.

[118] H. Ilcan, O. Sahin, A. Kul, G. Yildirim, M. Sahmaran, Rheological properties and compressive strength of construction and demolition waste-based geopolymer mortars for 3D-Printing, Constr Build Mater. 328 **(2022)** 127114.

[119] N.C. Demiral, M. Ozkan Ekinci, O. Sahin, H. Ilcan, A. Kul, G. Yildirim, M. Sahmaran, Mechanical anisotropy evaluation and bonding properties of 3D-printable construction and demolition waste-based geopolymer mortars, Cem Concr Compos. 134 **(2022)** 104814.

[120] M. Lahoti, K.H. Tan, E.-H. Yang, A critical review of geopolymer properties for structural fire-resistance applications, Constr Build Mater. 221 **(2019)** 514–526.

[121] S. Top, H. Vapur, M. Altiner, D. Kaya, A. Ekicibil, Properties of fly ash-based lightweight geopolymer concrete prepared using pumice and expanded perlite as aggregates, J Mol Struct. 1202 **(2020)** 127236.

[122] Z. Safari, R. Kurda, B. Al-Hadad, F. Mahmood, M. Tapan, Mechanical characteristics of pumice-based geopolymer paste, Resour Conserv Recycl. 162 **(2020)** 105055.

[123] Z. Wang, H. Su, S. Zhao, N. Zhao, Influence of phase change material on mechanical and thermal properties of clay geopolymer mortar, Constr Build Mater. 120 **(2016)** 329–334.

[124] A. Wongsa, V. Sata, P. Nuaklong, P. Chindaprasirt, Use of crushed clay brick and pumice aggregates in lightweight geopolymer concrete, Constr Build Mater. 188 **(2018)** 1025–1034.

[125] Z. Su, L. Guo, Z. Zhang, P. Duan, Influence of different fibers on properties of thermal insulation composites based on geopolymer blended with glazed hollow bead, Constr Build Mater. 203 **(2019)** 525–540.

[126] K. Pasupathy, S. Ramakrishnan, J. Sanjayan, Enhancing the mechanical and thermal properties of aerated geopolymer concrete using porous lightweight aggregates, Constr Build Mater. 264 **(2020)** 120713.

[127] H. Gao, L. Liao, Y. Liang, X. Tang, H. Liu, L. Mei, G. Lv, L. Wang, Improvement of durability of porous perlite geopolymer-based thermal insulation material under hot and humid environment, Constr Build Mater. 313 **(2021)** 125417.

[128] M. Łach, K. Korniejenko, J. Mikuła, Thermal Insulation and Thermally Resistant Materials Made of Geopolymer Foams, Procedia Eng. 151 **(2016)** 410–416.

[129] N. Kabay, M. Mert, N. Miyan, T. Omur, Pumice as precursor in geopolymer paste and mortar, Journal of Civil Engineering and Construction. 10 **(2021)** 225–236.

[130] G. Kakali, D. Kioupis, A. Skaropoulou, S. Tsivilis, Lightweight geopolymer composites as structural elements with improved insulation capacity, in: MATEC Web of Conferences, EDP Sciences, **2018**: p. 01042.

[131] W.I. Wan Mastura, A. Romisuhani, A.M. Mustafa Al Bakri, M. Faheem Mohd Tahir, S. Ahmad Syauqi, N. Aida Mohd Mortar, Correlation between Thermal Insulation Properties with Compressive Strength and Density of Lightweight Geopolymer, IOP Conf Ser Mater Sci Eng. 864 **(2020)** 012040.

[132] P. Posi, C. Teerachanwit, C. Tanutong, S. Limkamoltip, S. Lertnimoolchai, V. Sata, P. Chindaprasirt, Lightweight geopolymer concrete containing aggregate from recycle lightweight block, Materials & Design (1980-2015). 52 **(2013)** 580–586.

[133] L.Y. Ming, A.V. Sandu, H.C. Yong, Y. Tajunnisa, S.F. Azzahran, R. Bayuji, M. Abdullah, P. Vizureanu, K. Hussin, T.S. Jin, Compressive strength and thermal conductivity of fly ash geopolymer concrete incorporated with lightweight aggregate, expanded clay aggregate and foaming agent, Revista de Chimie. 70 **(2019)** 4021–4028.

[134] N.F. Shahedan, M.M.A.B. Abdullah, N. Mahmed, A. Kusbiantoro, S. Tammas-Williams, L.-Y. Li, I.H. Aziz, P. Vizureanu, J.J. Wysłocki, K. Błoch, Properties of a new insulation material glass bubble in geopolymer concrete, Materials. 14 **(2021)** 809.

[135] K. Komnitsas, D. Zaharaki, Geopolymerisation: A review and prospects for the minerals industry, Miner Eng. 20 **(2007)** 1261–1277.

[136] R.C. Kaze, L.M. Beleuk à Moungam, M. Cannio, R. Rosa, E. Kamseu, U.C. Melo, C. Leonelli, Microstructure and engineering properties of Fe2O3(FeO)-Al2O3-SiO2 based geopolymer composites, J Clean Prod. 199 **(2018)** 849–859.

[137] P. De Silva, K. Sagoe-Crenstil, V. Sirivivatnanon, Kinetics of geopolymerization: Role of Al2O3 and SiO2, Cem Concr Res. 37 **(2007)** 512–518.

[138] S. Panda, Molecular interaction of polymer dextran in sodium hydroxide through evaluation of thermo acoustic parameters, Ind J Pharma Edu Res. 54 **(2020)** 630–636.

[139] F. Pacheco-Torgal, J. Castro-Gomes, S. Jalali, Alkali-activated binders: A review: Part 1. Historical background, terminology, reaction mechanisms and hydration products, Constr Build Mater. 22 **(2008)** 1305–1314.

[140] K. Somna, C. Jaturapitakkul, P. Kajitvichyanukul, P. Chindaprasirt, NaOH-activated ground fly ash geopolymer cured at ambient temperature, Fuel. 90 **(2011)** 2118–2124.

[141] S. Alonso, A. Palomo, Alkaline activation of metakaolin and calcium hydroxide mixtures: influence of temperature, activator concentration and solids ratio, Mater Lett. 47 **(2001)** 55–62.

[142] B. Ma, Y. Luo, L. Zhou, Z. Shao, R. Liang, J. Fu, J. Wang, J. Zang, Y. Hu, L. Wang, The influence of calcium hydroxide on the performance of MK-based geopolymer, Constr Build Mater. 329 **(2022)** 127224.

[143] J. Moreno-Juez, I.J. Vegas, M. Frías Rojas, R. Vigil de la Villa, E. Guede-Vázquez, Laboratory-scale study and semi-industrial validation of viability of inorganic CDW fine fractions as SCMs in blended cements, Constr Build Mater. 271 **(2021)** 121823.

[144] E. ASTM, 8/E 8M Annual book of ASTM standards, ASTM. **(2007)**.

[145] S. Muthukrishnan, S. Ramakrishnan, J. Sanjayan, Technologies for improving buildability in 3D concrete printing, Cem Concr Compos. 122 **(2021)** 104144.

[146] B. Nematollahi, P. Vijay, J. Sanjayan, A. Nazari, M. Xia, V. Naidu Nerella, V. Mechtcherine, Effect of polypropylene fibre addition on properties of geopolymers made by 3D printing for digital construction, Materials. 11 **(2018)** 2352.

[147] ASTM, C518 - Standard test method for steady-state thermal transmission properties by means of the heat flow meter apparatus, ASTM International. **(2017)**.

[148] P. Ren, B. Li, J.-G. Yu, T.-C. Ling, Utilization of recycled concrete fines and powders to produce alkali-activated slag concrete blocks, J Clean Prod. 267 **(2020)** 122115.

[149] O. Sengul, S. Azizi, F. Karaosmanoglu, M.A. Tasdemir, Effect of expanded perlite on the mechanical properties and thermal conductivity of lightweight concrete, Energy Build. 43 **(2011)** 671–676.

[150] A.M. Rashad, A synopsis about perlite as building material – A best practice guide for Civil Engineer, Constr Build Mater. 121 **(2016)** 338–353.

[151] B. Işıkdağ, Characterization of lightweight ferrocement panels containing expanded perlite-based mortar, Constr Build Mater. 81 **(2015)** 15–23.

[152] T.S. Tie, K.H. Mo, U.J. Alengaram, S.K. Kaliyavaradhan, T.-C. Ling, Study on the use of lightweight expanded perlite and vermiculite aggregates in blended cement mortars, European Journal of Environmental and Civil Engineering. 26 **(2022)** 3612–3631.

[153] M. Gürsoy, M. Karaman, Improvement of wetting properties of expanded perlite particles by an organic conformal coating, Prog Org Coat. 120 **(2018)** 190–197.

[154] L.Y.W.D. Stefan, A. Farhad, M. Guowei, Lightweight Self-Compacting Concrete Incorporating Perlite, Scoria, and Polystyrene Aggregates, Journal of Materials in Civil Engineering. 30 **(2018)** 04018178.

[155] P. Torkittikul, T. Nochaiya, W. Wongkeo, A. Chaipanich, Utilization of coal bottom ash to improve thermal insulation of construction material, J Mater Cycles Waste Manag. 19 **(2017)** 305–317.

[156] ACI Committee 213, Guide for Structural Lightweight-Aggregate Concrete, 2014.

[157] A. Benk, A. Coban, Possibility of producing lightweight, heat insulating bricks from pumice and H3PO4- or NH4NO3-hardened molasses binder, Ceram Int. 38 **(2012)** 2283–2293.

[158] S. Verma, A. Sara, H. Singh, Why and which opacifier for perlite based vacuum insulation panels (VIPs) in the average temperature range of 10–70 °C, International Journal of Thermal Sciences. 186 **(2023)** 108136.

[159] M. Arifuzzaman, H.S. Kim, Novel mechanical behaviour of perlite/sodium silicate composites, Constr Build Mater. 93 **(2015)** 230–240.

[160] M.D. Arifuzzaman, H.S. Kim, Development of new perlite/sodium silicate composites, in: International Conference on Mechanical, Industrial and Energy Engineering (ICMIEE), Khulna University of Engineering & Technology, Khulna, Bangladesh, **2014**: pp. 26–27.

[161] V. Akyuncu, F. Sanliturk, Investigation of physical and mechanical properties of mortars produced by polymer coated perlite aggregate, Journal of Building Engineering. 38 **(2021)** 102182.

[162] M.L. Torres, P.A. García-Ruiz, Lightweight pozzolanic materials used in mortars: Evaluation of their influence on density, mechanical strength and water absorption, Cem Concr Compos. 31 **(2009)** 114–119.

[163] H. Karakaş, S. İlkentapar, U. Durak, E. Örklemez, S. Özuzun, O. Karahan, C.D. Atiş, Properties of fly ash-based lightweight-geopolymer mortars containing perlite aggregates: Mechanical, microstructure, and thermal conductivity coefficient, Constr Build Mater. 362 **(2023)** 129717.

[164] L. Wang, P. Liu, Q. Jing, Y. Liu, W. Wang, Y. Zhang, Z. Li, Strength properties and thermal conductivity of concrete with the addition of expanded perlite filled with aerogel, Constr Build Mater. 188 **(2018)** 747–757.

[165] TBEC, Turkish Seismic Earthquake Code, **(2018)** 1–146.

[166] IBC, International Building Code, **(2015)**.

[167] J.L. Noland, An Overview of the US Coordinated Program for Masonry Building Research, in: Structural Design, Analysis and Testing, ASCE, **1987**: pp. 949–958.

[168] M. Davraz, M. Koru, A.E. Akdağ, The Effect of Physical Properties on Thermal Conductivity of Lightweight Aggregate, Procedia Earth and Planetary Science. 15 **(2015)** 85–92.

[169] A.A. Alghamdi, H.A. Alharthi, Multiscale 3D finite-element modelling of the thermal conductivity of clay brick walls, Constr Build Mater. 157 **(2017)** 1–9.

[170] Á. Lakatos, F. Kalmár, Investigation of thickness and density dependence of thermal conductivity of expanded polystyrene insulation materials, Mater Struct. 46 **(2013)** 1101–1105.

[171] H. Uysal, R. Demirboğa, R. Şahin, R. Gül, The effects of different cement dosages, slumps, and pumice aggregate ratios on the thermal conductivity and density of concrete, Cem Concr Res. 34 **(2004)** 845–848.

[172] I. Asadi, P. Shafigh, Z.F. Bin Abu Hassan, N.B. Mahyuddin, Thermal conductivity of concrete – A review, Journal of Building Engineering. 20 **(2018)** 81–93.

[173] A.G. de Oliveira, J.C. Jandorno, E.B.D. da Rocha, A.M.F. de Sousa, A.L.N. da Silva, Evaluation of expanded perlite behavior in PS/Perlite composites, Appl Clay Sci. 181 **(2019)** 105223.

[174] A. Hassan, M. Arif, M. Shariq, T. Alomayri, S. Pereira, Fire resistance characteristics of geopolymer concrete for environmental sustainability: a review of thermal, mechanical and microstructure properties, Environ Dev Sustain. **(2022)**.

[175] M. Lahoti, K.K. Wong, E.-H. Yang, K.H. Tan, Effects of Si/Al molar ratio on strength endurance and volume stability of metakaolin geopolymers subject to elevated temperature, Ceram Int. 44 **(2018)** 5726–5734.

[176] D.L.Y. Kong, J.G. Sanjayan, Effect of elevated temperatures on geopolymer paste, mortar and concrete, Cem Concr Res. 40 **(2010)** 334–339.

[177] O.A. Abdulkareem, A.M. Mustafa Al Bakri, H. Kamarudin, I. Khairul Nizar, A.A. Saif, Effects of elevated temperatures on the thermal behavior and mechanical performance of fly ash geopolymer paste, mortar and lightweight concrete, Constr Build Mater. 50 **(2014)** 377–387.

[178] L. Zongjin, Z. Xiangming, S. Bin, Fiber-Cement Extrudates with Perlite Subjected to High Temperatures, Journal of Materials in Civil Engineering. 16 **(2004)** 221–229.